Charting the Uncharted: The (Un)Intended Consequences of Oil Sanctions and Dark Shipping*

Jesús Fernández-Villaverde† Yiliang Li§

Le Xu◊ Francesco Zanetti¶

June 30, 2025

Abstract

We examine the global macroeconomic consequences of dark shipping —oil tankers disabling AIS transceivers to evade detection— in the context of Western sanctions on Iran, Syria, North Korea, Venezuela, and Russia. Using a machine learning–based clustering model, we track worldwide crude oil flows carried by dark ships. From 2017 to 2023, these vessels transported an estimated 9.3 million metric tons of crude oil per month, nearly half of global seaborne exports, with China absorbing 15%. We show that dark shipping rebalances oil markets by mitigating sanction-induced supply shocks through segmented markets and costly cross-market reallocations. These adjustments propagate through global value chains, yielding divergent effects. In the U.S., a net oil exporter, lower oil prices dampen producer revenues but are offset by cheaper Chinese inputs, fostering deflationary, supply-driven growth. The EU, a net importer, confronts higher energy costs yet benefits from reduced import prices and stronger Chinese demand, leading to robust output growth and moderate inflation. China, as the primary recipient of discounted oil and a central hub in global supply chains, expands industrial production and amplifies these effects abroad. Our findings underscore the broad unintended consequences of oil sanctions.

JEL Classification: C32, C38, E32, Q43, R40.
Keywords: Dark shipping, oil sanction, global supply chain, satellite data, clustering analysis, LP.

*We are grateful to Xiwen Bai for her invaluable help, and to Robert Barro, Hilde Bjørnland, Emily Blanchard, Craig Burnside, Charles Calomiris, Kerem Coşar, Steven Davis, Diego Känzig, Lutz Kilian, Matteo Maggiori, and Tony Venables, as well as participants at the SED Annual Meeting, BSE Summer Forum, Reykjavík Economic Conference, CEPR-JHU Geoeconomics Conference, AMLEDS webinar, and seminars at the University of Oxford, the Heritage Foundation, UC Santa Barbara, Shanghai University of Finance and Economics, and Peking University for their insightful comments and suggestions.
† Fernández-Villaverde: University of Pennsylvania, U.S. jesusfv@econ.upenn.edu. § Li: University of International Business and Economics, China. yiliang_li@uibe.edu.cn. ◊ Xu: Shanghai Jiao Tong University, China. lexu1@sjtu.edu.cn. ¶ Zanetti: University of Oxford, U.K. francesco.zanetti@economics.ox.ac.uk.

1. Introduction

Dark shipping —the deliberate deactivation of mandated AIS (Automatic Identification System) transceivers, which broadcast a vessel's location, heading, and speed— has surged in recent years, driven by Western sanctions targeting oil transport from or to Iran, Syria, North Korea, Venezuela, and Russia. Aimed at curbing these regimes' oil revenues (or restricting imports, in North Korea's case), the sanctions have prompted producers to offer premiums to tanker operators willing to transport oil covertly, fueling the rise of dark shipping. Although seaborne transport accounts for over three-quarters of global crude oil trade (U.S. Energy Information Administration, 2024), the absence of systematic monitoring has left the broader economic impact of this practice poorly understood.

We address this knowledge gap by making three contributions. First, we develop a machine learning–based ship clustering model to track dark shipping in real time, mapping its practices, key features, and global geographic concentration. Second, we present new empirical evidence and a parsimonious theoretical framework that highlight the role of dark shipping in rebalancing oil markets. Third, we examine how these oil market adjustments propagate through global supply chains, shaping aggregate outcomes in both sanctioning and non-sanctioning economies.

Tracking dark shipping is challenging. When a vessel disables its AIS transceiver, its location, heading, and speed become invisible to global tracking systems. Dark ships often exploit these gaps to transport oil from sanctioned countries or to conduct unauthorized ship-to-ship transfers in maritime areas with weak regulatory oversight, such as international waters in the Persian Gulf, off the coast of Gibraltar, and in West Africa.[1] Consequently, identifying dark ships requires more than monitoring AIS data; it demands integrating vessel-specific suspicious characteristics, the likelihood of evasive activity during data gaps, and anomalies in navigational patterns.

While various attempts have been made to identify dark ships, many fall short. Existing methods often rely on incomplete data, lack clear criteria to distinguish dark shipping from routine maritime operations, or focus on individual ships or small vessel groups, failing to capture the broader tanker fleet.[2] Additionally, some methods rely heavily on external sources, such as

[1] A ship-to-ship transfer is the process of transferring cargo, such as oil, between two vessels positioned alongside each other.

[2] The terms "dark ships" and "shadow fleet" are often used interchangeably but denote distinct phenomena. While "shadow fleet" typically refers to vessels bypassing the $60-per-barrel price cap on Russian oil exports, these ships operate within alternative systems without technically violating sanctions and may still broadcast AIS signals

satellite imagery and proprietary data on ownership and insurance status, which may be costly or inaccessible. The lack of fleet-wide approaches to identifying dark ships creates significant gaps in understanding the full scale of this covert activity and its broader economic implications.

We address these challenges by introducing a multi-attribute ship clustering model that uses a three-level trip classification process to identify dark ships. The model combines vessel traits, movement dynamics, and trip-level AIS data, enabling fleet-wide analysis of dark shipping. A key contribution is the construction of two measures that estimate the likelihood that a vessel is either transporting oil from sanctioned countries or engaging in suspicious ship-to-ship transfers. The first measure captures proximity to sanctioned ports during AIS gaps; the second identifies likely transfers based on overlapping AIS gaps and spatial proximity between two vessels. To detect such transfers, we propose a novel method that uses historical AIS data —coordinates, headings, and timestamps— even when AIS transceivers are off. By analyzing vessel proximity and movement patterns during AIS gaps, our approach offers an alternative to external sources like satellite imagery, although we use satellite data to audit and validate selected findings.

Our results reveal notable differences in vessel characteristics, travel patterns, and movement dynamics between tankers likely engaged in suspicious activities ("dark") and those less likely to do so ("white"). Compared to white ships, dark ships are older, operated by firms with smaller fleets, and registered under more obscure flags. They show higher suspicion scores and more erratic behavior, including increased idling, greater speed variability, and frequent route deviations. From 2017 to 2023, the dark fleet averaged 555 tankers, about one-fourth of the global crude oil tanker fleet. Its size closely mirrors major geopolitical shifts during the sample period.

Leveraging our findings, we quantify the exports and imports of dark-shipped oil from sanctioned countries. Between 2017 and 2023, an average of 9.3 million metric tons of crude oil per month was exported via dark ships from Iran, Syria, Venezuela, and Russia —nearly half of global seaborne crude oil exports and 7% of total global crude exports recorded in UN Comtrade data. Iran and Russia dominate this trade, with unauthorized shipments surging after key Western sanctions, including the U.S. withdrawal from the JCPOA in 2018 and the oil embargoes and price caps imposed on Russia in late 2022. China is the largest importer, receiving over 117 million metric tons between 2017 and 2023, or 15% of total dark-shipped exports. Other notable

(Johnson et al., 2023a). In contrast, "dark ships" encompass a broader range of sanction evasion tactics at the behavioral level and also include vessels linked to Iran, Syria, North Korea, and Venezuela, thereby enabling us to investigate a more comprehensive set of sanctions beyond the case of Russia.

importers include South Korea, the UAE, and India. The intensity of dark shipping activity declines with geographic distance, in line with the predictions of a standard gravity model in international trade.

Having charted dark shipping worldwide, we assess its impact on oil markets using local projections (LPs) (Jordà, 2005; Barnichon and Brownlees, 2019) and interpret the results through a parsimonious theoretical model of global oil markets. Our empirical findings show that although intensifying oil sanctions reduce seaborne exports recorded in official data, a concurrent surge in dark-shipped oil largely offsets this decline, putting downward pressure on global oil prices.

To explain the empirical regularities and the otherwise counterintuitive, muted response of global oil prices to sanctions, we develop a model featuring segmented oil markets and the endogenous, costly reallocation of oil supply. The model is calibrated using oil export and price data from Russia and OPEC. Simulation results underscore the central role of cross-market oil reallocation via dark shipping and OPEC's limited ability to adjust in shaping global export and price dynamics. When sanctions on Russian oil in the EU intensify, Russia redirects exports to China via dark shipping, while OPEC reallocates sluggishly. The resulting influx of Russian oil creates an oversupply in China, which in turn pushes down its oil import prices. This decline largely offsets the inflationary pressure from reduced oil supply in the EU, producing an almost flat response of global oil prices, consistent with our LP findings.

Our account aligns with a classical insight from international trade: when the international flow of factors (such as oil) is restricted by sanctions, trade in goods embodying those factors can circumvent the barriers. Dark shipping and the global supply chain —particularly China's central role— enable this circumvention. Accordingly, the effects of oil sanctions must be assessed in the broader context of global oil markets and supply chains, rather than through narrow bilateral lenses like Russia vs. the EU. These insights are valuable for understanding the unintended consequences of sanctions as they reveal a mechanism operating through both oil reallocation and global value chains that has received relatively little attention in prior work.

To further investigate these broader effects, we analyze the impact of Western sanctions on the U.S., the EU, and China using local projections. We find that post-sanction shifts in oil supply via dark shipping generate distinct economic outcomes for the U.S. and the EU, shaped by their respective oil trade positions and, more importantly, by their input-output relationships with China within the global supply chain.

For the U.S., a net oil exporter, the increased supply of dark-shipped oil and the associated decline in domestic oil prices cause a short-run production slowdown in both energy and non-energy sectors. At the same time, the U.S. benefits from lower import prices for intermediate inputs from China, where production costs fall due to discounted dark-shipped oil. These lower input prices foster supply-driven growth characterized by deflationary output expansion. In contrast, the EU, a net oil importer, faces higher oil import prices due to sanctions and supply shortages. Yet the combined effects of cheaper Chinese inputs and rising demand from China (where output expands thanks to lower oil prices) offset the direct impact of higher energy costs. As a result, dark shipping supports economic growth in the EU while mitigating inflationary pressures.

China benefits directly from discounted oil, which significantly boosts its industrial production. More importantly, its central role in global supply chains —as both an upstream input supplier to the U.S. and EU and a downstream importer of EU goods— allows it to transmit the effects of lower costs and increased output to sanctioning economies.

By contrast, we do not assess the impact of sanctions on the sanctioned countries, where data are either nonexistent (e.g., Syria) or extremely poor (e.g., Venezuela). We conjecture that the lower oil prices received —as these countries must compensate dark fleet operators and offer discounts to buyers— have significantly negative effects on their economies.

Importance of our results. Our study charts the vast flows of dark-shipped oil under Western sanctions, highlighting its role in stabilizing global oil markets and its considerable impact on inflation and output. The segmentation of oil markets, the costly cross-market reallocation of supply, and China's pivotal role in global input-output linkages enable dark shipping to rebalance markets, curb expected oil price increases, and raise output in the U.S., EU, and China in unexpected ways. These findings may help explain why sanctioning countries have not enforced sanctions more vigorously or curbed the dark fleet more aggressively.

These insights are crucial, though often overlooked, for evaluating sanctions (on oil and other goods and services). Policymakers must consider not only the intended effects but also the broader general equilibrium consequences that emerge through dark shipping and global supply chains.

Related literature. Our analysis relates to several strands of research. First, it builds on recent work using high-frequency satellite data to examine global trade and transport, including port call behavior (Cerdeiro et al., 2020; Komaromi et al., 2022; Brancaccio et al., 2024), maritime

flows (Prochazka et al., 2019; Brancaccio et al., 2020; Li et al., 2022), and responses to supply chain shocks and geopolitical events (Bai et al., 2024). Recent studies have also used deep learning and satellite imagery to detect unauthorized ship-to-ship transfers. However, these methods often struggle with data gaps or rely on costly proprietary imagery (Bernabé et al., 2024). In contrast, we introduce a multi-attribute ship clustering model that uses only AIS data, enabling fleet-wide detection of dark ships and measurement of sanctioned oil trade flows.

Second, our work connects to the literature on oil markets and macroeconomic dynamics, which uses structural vector autoregressions (SVARs) to estimate the effects of demand and supply shocks on oil prices and the real economy (Kilian, 2009; Kilian and Murphy, 2012, 2014; Baumeister and Hamilton, 2019; Känzig, 2021; Kilian et al., 2024; Verduzco-Bustos and Zanetti, 2025), microdata to study industry developments and their aggregate implications (Bjørnland et al., 2021; Bornstein et al., 2023), and structural models to trace how oil shocks propagate (Lippi and Nobili, 2012; Melek et al., 2017). Our contribution lies in quantifying sanctioned oil exports moved by dark ships and identifying the dynamic causal effects of dark shipping on prices and production in the U.S. and EU.

Third, we contribute to the literature on international trade and aggregate dynamics triggered by sanctions, particularly those imposed on Russia after its invasion of Ukraine (Itskhoki and Mukhin, 2022; Ghironi et al., 2024).[3] While existing studies acknowledge that dark shipping helps sustain Russia's economy by preserving oil revenues despite Western sanctions (Hilgenstock et al., 2023; Johnson et al., 2023b; Kilian et al., 2024), the opacity of sanctioned oil trade has limited quantitative assessments of its impact on global oil trade, prices, and output. We develop a scalable framework that detects dark shipping across fleets and quantifies sanctioned oil exports and imports, offering policymakers a tool to evaluate the broader economic effects of sanctions.

The remainder of the paper is structured as follows. Section 2 introduces our multi-attribute ship clustering model. Section 3 presents identification results. Section 4 quantifies dark-shipped oil exports and imports. Section 5 examines the effects of sanctions and dark shipping on global oil markets using data and a parsimonious model, while Section 6 analyzes aggregate impacts on the U.S., EU, and China. Section 7 concludes. An online appendix presents additional details.

[3] Felbermayr et al. (2024) review recent research on the economics of sanctions.

2. A Clustering Model for Dark Ship Identification

This section presents a multi-attribute ship clustering model to identify vessels likely involved in transporting sanctioned oil for Iran, Syria, North Korea, Venezuela, and Russia between 2017 and 2023.

2.1. Background

In recent years, dark shipping has become a covert way to evade Western oil sanctions on Iran, Syria, North Korea, Venezuela, and Russia. A major challenge in assessing the scale and impact of these sanctions is the lack of reliable oil export data from the sanctioned nations. For example, Russia stopped publishing detailed oil export figures after its 2022 invasion of Ukraine. Similarly, countries importing sanctioned oil often withhold accurate data on their imports.

Identifying vessels engaged in dark shipping is difficult. These ships do not report covert activity, and before satellite-based AIS data became available (described shortly), real-time tracking was nearly impossible. Even with AIS, dark ships often disable their transceivers. These frequent, unexplained gaps—along with intentional AIS manipulation or "spoofing," make tracking and identifying violations hard.

For example, Figure 1 shows frequent AIS transmission gaps in 2023 for the anonymously owned crude oil tanker *Roma* (IMO: 9182291), later classified as a dark ship by our algorithm. *Roma* mainly operated in international waters between the Strait of Hormuz near Iran and Southeast Asia, with AIS data missing for over 40% of the time.

Existing research has relied on alternative data sources —such as satellite imagery (Bernabé et al., 2024) and proprietary information on vessel ownership and insurance— to identify individual vessels or small groups involved in dark shipping. For example, anonymous ownership or opaque corporate structures often signal possible dark activity (S&P Global Market Intelligence, 2023). Likewise, the absence of known protection and indemnity (P&I) insurance, or coverage outside the International Group of 12 P&I clubs (e.g., the American Club), which insures 95% of the global tanker fleet, is another red flag (Lloyd's List Intelligence, 2023). But these external sources are often restricted, expensive, and not publicly available. And while identifying individual ships helps, it does not show the broader scale of the clandestine oil trade or its aggregate economic impact on sanctioning economies.

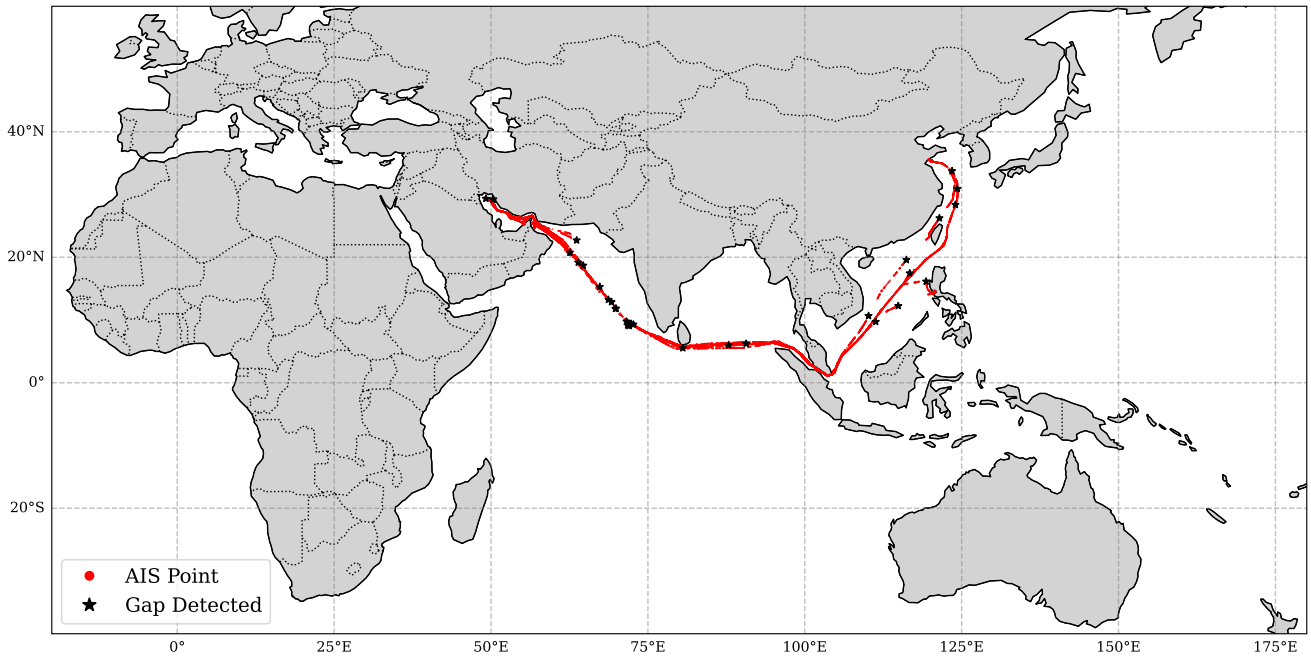


Figure 1: Illustrative example of AIS transmission gaps: *Roma* (IMO: 9182291)

Notes. AIS observations (red points) of *Roma* recorded in 2023, along with the first positions after each 10-hour AIS gap when *Roma* disabled its transceiver (asterisks).

2.2. AIS Data

To construct indicators for dark shipping, we use over 330 million crude oil tanker records from satellite-based AIS data.[4] From this dataset, we curate an annual sample of around 2,160 tankers for detailed analysis.[5] We focus on crude oil tankers rather than petroleum product carriers because the latter handle varied cargoes, complicating trade volume estimates. Unlike crude oil tankers, which only transport crude oil, product tankers have specialized features (e.g., internal coatings) and can opportunistically switch to crude (Li et al., 2022), complicating product-specific flow calculations. While dark ships also transport sanctioned petroleum products, identifying them is left to future work. In any case, including these ships (or those without any AIS data whatsoever) would only strengthen our central argument: the critical role of the dark fleet in transporting sanctioned oil and its broader economic significance.

[4]These data, decoded from satellite tracking systems on vessels, cover tankers over 300 gross tons on international voyages, as mandated by the International Maritime Organization (IMO) (Heiland et al., 2019; Bai et al., 2024).

[5]Beyond these, an annual average of 700 crude oil tankers do not broadcast AIS signals, according to Lloyd's List Intelligence. These vessels are either decommissioned, laid up, or deliberately operating without AIS to obscure movements. This last group likely belongs to the global dark fleet but cannot be identified by our algorithm due to missing trip-level data, making our three-level trip classification (described below) inapplicable. We leave their analysis to future research.

The AIS system processes over 2,000 reports per minute and updates as frequently as every two seconds, providing comprehensive global coverage of crude oil tanker movements from 2017 to 2023. Each AIS entry includes the vessel's IMO identification number, timestamp, draft, speed, heading, and coordinates. These data let us track ship movements and detect AIS deactivations —key signs of potential dark shipping, such as transporting or transferring sanctioned oil.

2.3. The Challenges of Labeling Ships

Identifying dark ships is a labeling problem: Is ship x dark or white? The sheer volume of AIS records, numbering in the millions, naturally lends itself to machine learning methods for automating this classification.

Designing a machine learning algorithm for this task faces a key challenge: no training set exists for classifying dark ships. By nature, these vessels conceal their identities, and commercial firms do not disclose their methodology to label ships. Moreover, dark ships can sometimes behave like "white ships," reducing detection risk during periods of scrutiny. These factors make supervised and semi-supervised models unsuitable. Furthermore, our goal goes beyond identifying individual non-compliant vessels. We aim to label the global dark ship fleet and estimate sanctioned crude oil exports and imports based on their trips worldwide.

This requires a computationally efficient algorithm that can group data without labeled examples. As we will show, the K-means clustering algorithm fits the task well due to its simplicity and effectiveness (MacQueen, 1967). It relies solely on AIS data, thereby avoiding the high cost and complexity associated with satellite imagery (although we use this imagery to audit a selected set of our results). Appendix A details our methodology, but we summarize the key ideas next.

2.4. Overview of the Algorithm

Our starting point is the domain knowledge that dark ships display similar behavioral patterns. The U.S. Department of State (2020) highlights two key indicators of deceptive shipping. First, disabling or manipulating AIS transceivers to hide movements. Second, conducting ship-to-ship transfers, particularly in areas prone to sanction violations or unauthorized activity.

Using this domain knowledge, we develop a three-level trip classification process. We combine (i) direct involvement in sanctioned oil trade (e.g., calls at sanctioned ports), (ii) AIS gaps that

may conceal suspicious activity, and (iii) anomalies in kinematic movements (e.g., high speed variability or frequent detours). This multi-level method avoids labeling a vessel "dark" solely for calling at a sanctioned port. Instead, we distinguish between ships that may lawfully transport sanctioned cargo (e.g., Russian crude priced under the G7/EU cap) and those showing deceptive behavior, such as AIS deactivation near sanctioned ports or suspicious transfers. Similarly, this approach extends beyond estimating "dark" status based solely on suspicious traits (e.g., vessel age or use of flags of convenience).[6]

Level 1 (sanctioned port calls). In the first step, we flag trips that start or end at a port in one of five sanctioned countries (Iran, Syria, North Korea, Venezuela, or Russia), but only if they occur after sanctions were imposed on that country. These trips are high-risk due to their direct involvement in the potential transportation of sanctioned oil. We exclude trips before the relevant sanction dates, as there is no reason to suspect evasion prior to the restrictions.[7]

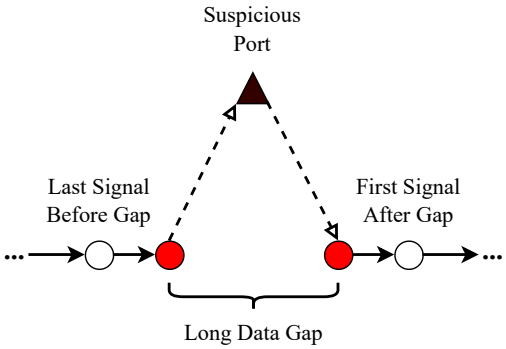
Level 2 (AIS data gaps). Next, we examine prolonged gaps in a vessel's AIS transmissions —defined as those exceeding the vessel-specific 99th percentile of time gaps between consecutive signals— and analyze their start and end locations. While such gaps may indicate suspicious behavior, their frequency alone is not a reliable signal. As shown in Figure A.2, both white and dark ships (as classified by our algorithm) show similar shares of trips with prolonged gaps in some years, underscoring the need to consider geographical context, such as where the gap occurs.

One type of suspicious trips occurs when a vessel is near a port in one of the five sanctioned countries and may call there during a prolonged AIS data gap. Panel 2a in Figure 2 illustrates this mechanism, while Panel 2b shows satellite imagery of such a case. It captures *Roma* (IMO: 9182291), previously identified by our algorithm as a dark ship, loading crude oil at Kharg Island, Iran, on August 20, 2022, with its AIS transceiver turned off. More concretely, our algorithm flags *Roma* as dark in 2022; then we verify the classification by searching the satellite imagery.

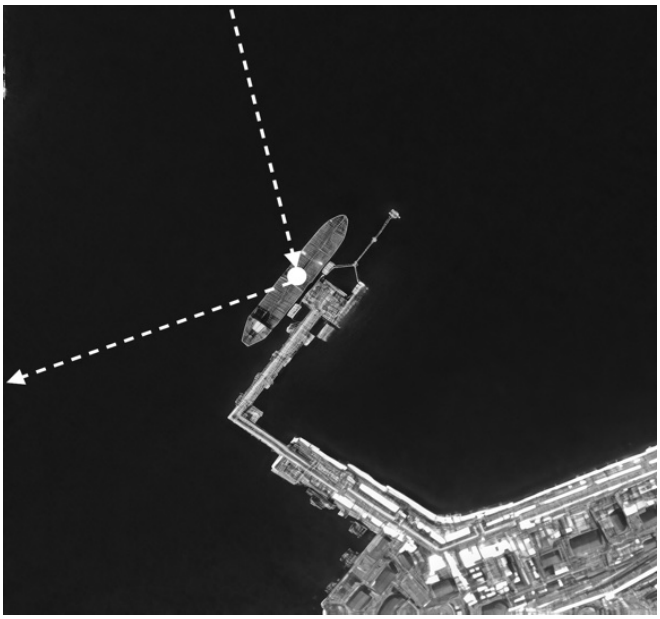
The second type of suspicious trips involves ship-to-ship transfers. We identify such trips by analyzing the geographical coordinates and timestamps of two vessels before and after their

[6] As noted by Lloyd's List Intelligence (2023), dark ships are often older and sail under high-risk flags of convenience. These flags, such as Panama, Liberia, and the Marshall Islands, offer weak oversight. In 2022, they covered 44.3% of global cargo capacity (UNCTAD, 2022).

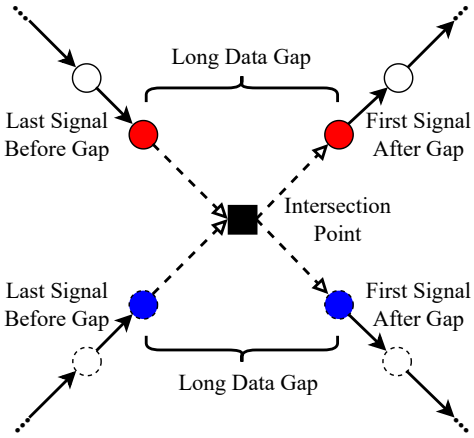
[7] This principle also applies in the second step of our classification. A vessel's proximity to a not-yet-sanctioned country's port is not treated as suspicious, even if AIS is disabled.



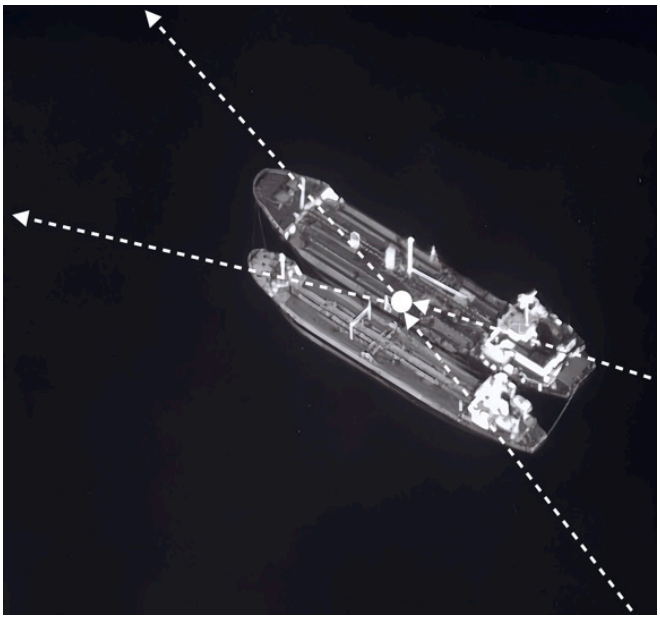
(a) Direct port visit: Mechanism



(b) Direct port visit: Satellite imagery



(c) Ship-to-ship transfer: Mechanism



(d) Ship-to-ship transfer: Satellite imagery

Figure 2: Deceptive shipping practices during prolonged AIS data gaps

Notes. Panel 2a shows a vessel returning to a nearby port in a sanctioned country during a prolonged AIS data gap. Panel 2b provides satellite imagery of such a visit by the dark ship *Roma* (IMO: 9182291), with dashed white arrows marking its trajectory during the gap. Panel 2c depicts a ship-to-ship transfer where both vessels disable their AIS, creating overlapping data gaps. The intersection point is estimated from the last known positions and headings. Panel 2d shows satellite imagery of a dark ship-to-ship transfer involving *Abyss* (IMO: 9157765) and *Shanaye Queen* (IMO: 9242118), with dashed arrows tracing their movements.

respective data gaps, particularly when these gaps overlap. This case is depicted in Panel 2c and illustrated with satellite imagery in Panel 2d. The latter reveals that *Abyss* (IMO: 9157765) engaged in an unauthorized ship-to-ship transfer with *Shanaye Queen* (IMO: 9242118) on January 28, 2022, in the Persian Gulf. Both vessels were identified as dark ships by our algorithm and were alleged to have actively participated in loading and transferring sanctioned Iranian oil.[8]

Level 3 (kinematic anomalies). In the final step, we assess each trip's speed and route irregularities by computing the vessel's average speed, speed standard deviation, and a detour factor comparing the actual to the direct route. Trips with low speeds, high speed variability, or circuitous paths receive higher suspicion scores, as such patterns often indicate deceptive maneuvers or AIS spoofing.

After classifying each trip across three levels, we assign a categorical suspicion score (0, 0.5, or 1) based on whether it triggers flags for sanctioned port calls, AIS gaps, or kinematic anomalies. A trip scores 1 if it starts or ends at a sanctioned port (Level 1). If not, it scores 1 if both Levels 2 and 3 indicate suspicious behavior, 0.5 if only one does, and 0 if neither does. We then calculate each vessel's average suspicion score by averaging its trip-level scores.

Next, we combine this average trip suspicion score with four additional vessel-level attributes: (i) vessel age (older vessels pose lower financial risks if seized), (ii) operator size (smaller operators face less scrutiny and have limited compliance resources), (iii) the flag state risk ranking from the annually updated Paris MoU list, and (iv) the idle trip ratio, defined as the fraction of trips where a vessel operates at 1 knot or less for 14 consecutive days.[9]

Finally, we input these vessel-level metrics into a K-means clustering model, which classifies vessels as dark (high suspicion) or white (low suspicion) each year.

[8]Figure C.1 in Appendix C presents additional satellite imagery capturing dark ships —identified by our ship clustering algorithm— either visiting ports in sanctioned countries or conducting unauthorized ship-to-ship transfers during extended AIS data gaps. As mentioned above, we use this imagery to validate a selected subset of our findings, with the scope of validation limited only by the monetary cost of acquiring such imagery.

[9]Larger commercial operators typically have stronger compliance departments and face higher reputational costs if involved in sanction violations, making them less likely to engage in unauthorized activities. The Paris Memorandum of Understanding (MoU) on Port State Control categorizes flag states into White, Gray, and Black lists based on vessel inspections and detentions, provided the flag state has undergone at least 30 inspections in the past three years. The Black list indicates the highest risk.

3. Charting Dark Shipping

This section presents the results of our ship clustering model. We begin by comparing vessel characteristics, travel patterns, and movement dynamics between dark and white ships. We then examine the size and composition of the dark fleet and its evolution over the sample period. Finally, we analyze the geographical concentration of dark shipping, demonstrating that our results align with externally documented locations and reflect shifts in sanction regimes over time.

3.1. Fleet Characteristics and Temporal Dynamics of Dark Ships

Our first check tests whether dark and white ships identified by our clustering model differ in vessel characteristics, travel patterns, and movement dynamics from 2017 to 2023. We also assess whether our K-means clusters are well-separated, characterized by high internal cohesion (within-cluster similarity) and strong separation (between-cluster dissimilarity).

Figure 3 shows that, on average, dark ships are older, operated by smaller entities, flagged by higher-risk states, and have higher trip suspicion scores and idle trip ratios. Most differences are statistically significant, though some features do not vary in certain years. These patterns match prior findings.[10]

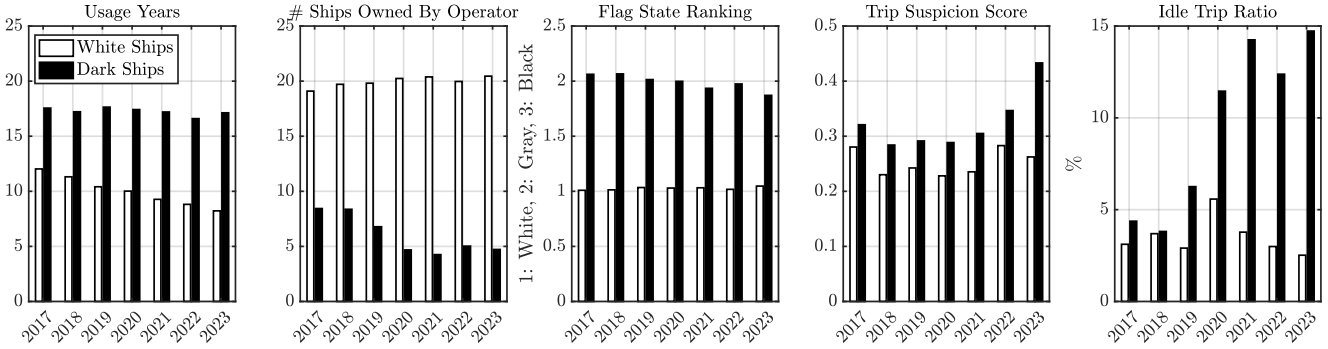


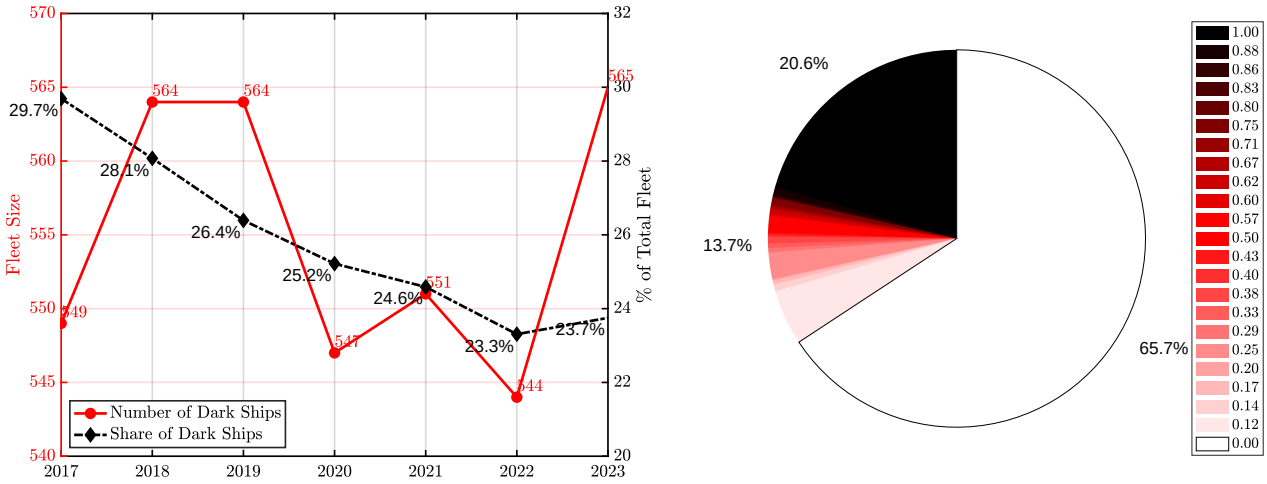
Figure 3: White vs. dark ships

Notes. Average values of usage years, number of vessels owned by the ship's commercial operator, flag state risk ranking, trip suspicion score, and idle trip ratio for white and dark ships.

Figure 4a shows the estimated dark ship fleet size, both in absolute terms and as a share of the global crude oil tanker fleet from 2017 to 2023. The fleet experienced sharp growth in

[10] Appendix B evaluates predictive performance by comparing our results to external classifications and an alternative method based only on vessel characteristics. We find that incorporating trip-level AIS data significantly enhances model accuracy.

2018, reaching a peak of 564 vessels. This rise followed the U.S. exit from the JCPOA and the reimposition of sanctions on Iranian oil exports (U.S. Department of State, 2018; Laudati and Pesaran, 2023). With crude prices rising, these sanctions made unauthorized Iranian oil trade highly profitable, prompting many tankers to go dark.



(a) Fleet size **(b)** Composition

Figure 4: Overview of the dark ship fleet

Notes. Figure 4a shows the number and share of dark ships in the global crude oil tanker fleet from 2017 to 2023. Figure 4b reports how often each tanker is identified as dark, calculated as the share of years with AIS data in which the vessel is classified as dark. A frequency of 1 means the ship is always dark; 0 means it is never dark during the sample.

Dark shipping remained high in 2019 as the U.S. expanded sanctions on Venezuela, targeting its state oil firm PDVSA to cut off crude export revenues (U.S. Department of the Treasury, 2019). In contrast, the COVID-19 pandemic triggered a global downturn in 2020, resulting in lower oil demand and a shrinking oil shipping market. With reduced profits, fewer tankers went dark. But the drop was brief: economic reopening in 2021, especially in China, revived oil demand and dark shipping activity.

By 2022, the fleet shrank due to a global slowdown caused by contractionary monetary policies aimed at fighting inflation and the lasting impact of China's zero-COVID policy (International Monetary Fund, 2022; Bai et al., 2025). But in late 2022 and through 2023, sanctions on Russia after its invasion of Ukraine —including oil price caps and export bans— created strong incentives for dark shipping (Hilgenstock et al., 2023; U.S. Department of the Treasury, 2023; Kilian et al., 2024). Buyers from non-sanctioning countries continued to import Russian oil, fueling another surge in the dark fleet, which reached 565 vessels by the end of 2023.

Despite fluctuations in the absolute size of the dark ship fleet, its share of the global crude oil tanker fleet steadily declined from 29.7% in 2017 to 23.7% in 2023. This decline was largely driven by the continuous addition of new white tankers (Kalouptsidi, 2014; Greenwood and Hanson, 2015; Dunn and Leibovici, 2023), the slow scrapping of older vessels, and increased scrutiny of unauthorized oil shipping.

Figure 4b shows how often a tanker was classified as a dark ship during its AIS operational years. We find that 65.7% of tankers were never labeled as dark, 20.6% were consistently classified as dark every year, and 13.7% only in some years. This suggests a relatively stable dark fleet, with most dark ships remaining dark and few white ships temporarily switching to dark status.

3.2. Geographical Concentration of Dark Shipping

Next, we examine the areas where dark shipping is concentrated, focusing on locations where vessels often disable AIS transceivers to transport oil for sanctioned countries or conduct suspicious ship-to-ship transfers. We first identify geographical hotspots by mapping the last recorded positions of vessels before AIS deactivation near ports in sanctioned countries. These points, combined with port-based trip suspicion scores, reveal areas of heightened suspicious activity.[11]

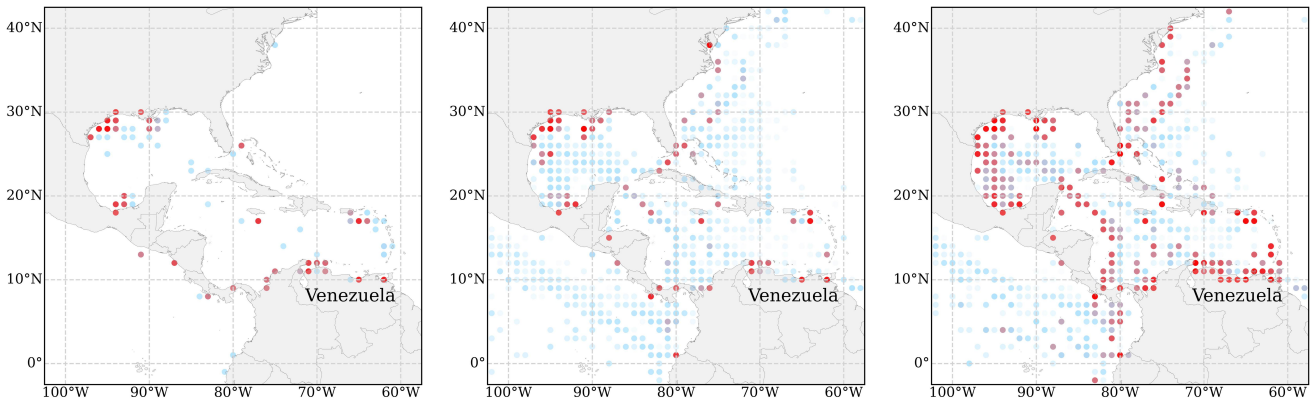
The estimated dark shipping hotspots align with locations frequently reported by external sources, and their variations over time correspond to changes in sanction regimes. For instance, Figure 5 shows dark shipping activity near Venezuela from 2017 to 2019. Both the number of trips with AIS gaps (colored points) and the associated suspicion scores (chromatic intensity) increased sharply in 2019, coinciding with U.S. sanctions on PDVSA, which severely restricted Venezuela's oil exports. This forced Venezuela to seek alternative buyers (e.g., China, India), often resorting to dark shipping. This pattern persisted through 2023, as shown in Figure C.2 in Appendix C.

Next, we analyze the dark shipping of Russian oil by examining activity in the vicinity of the Black Sea and Baltic Sea. Rather than aggregating data into geographic squares, we classify trips by AIS gap length and plot lines between the last and first AIS signals surrounding each gap. This offers a clearer view of dark ship movements, revealing specific routes and evasive maneuvers.

Figure 6 shows direct vessel visits to suspicious Russian ports near the Black Sea from 2021 to 2023.[12] The top row shows short AIS gaps (under 10 hours), the middle row medium gaps

[11] For details on the calculation of the port-based trip suspicion score, see Algorithm A.1 in Appendix A.3.

[12] For comparison, see Figures C.3 and C.4 in Appendix C, which show port visits in the Black and Baltic Seas from 2017 to 2020.



(a) 2017 **(b)** 2018 **(c)** 2019

Figure 5: Geographical concentration of dark shipping activities near Venezuela: 2017–2019

Notes. Each colored point marks a 1-degree geographic square containing at least one final AIS signal before a vessel disables its transceiver. Chromatic intensity reflects the sum of associated port-based trip suspicion scores, which estimate the likelihood that the vessel visited a nearby sanctioned-country port during the AIS gap.

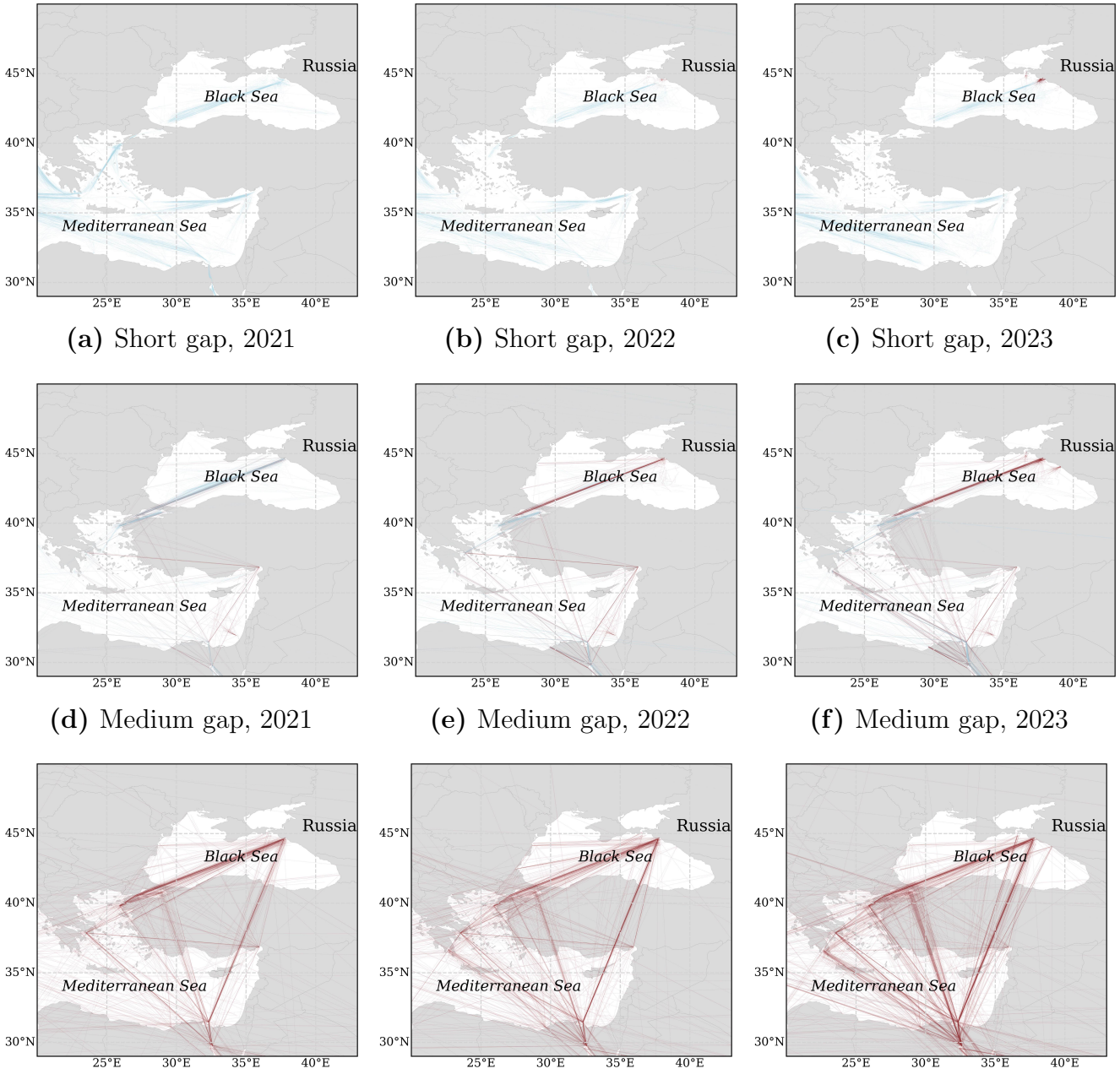
(10–120 hours), and the bottom row long gaps (over 120 hours). Chromatic intensity reflects the port-based trip suspicion score for each gap.

Following Western sanctions on Russian oil in late 2022, the scale and intensity of dark shipping increased near the Russian ports of Novorossiysk, Taman, and Tuapse, particularly for short and medium AIS gaps. For long gaps, intensity remained stable, but activity spread, as shown by denser lines in later years relative to 2021.[13]

Figure 7 shows the concentration of dark ship visits to Russian Baltic ports from 2021 to 2023. As in the Black Sea, both the scale and intensity of dark shipping rose near Primorsk, Ust-Luga, Vysotsk, and St. Petersburg, especially for medium and long AIS gaps. This rise coincided with a drop in dark shipping near Iran. As shown in Figure C.5 (Appendix C), AIS gap trips near the Strait of Hormuz fell sharply after 2021. This shift reflects tankers moving from Iranian to Russian oil, driven by premiums that compensate for the G7/EU price caps.

The surge in dark shipping near Russian ports in the Black Sea and Baltic Sea highlights the unintended effects of Western oil sanctions. Designed to limit Russia's oil revenue, these measures instead spurred evasion tactics, reflected in longer AIS gaps and more frequent visits to sanctioned ports.

[13]Trips with longer AIS gaps tend to have higher port-based trip suspicion scores due to lower required average speeds to reach a suspicious port. Since the score in Algorithm A.1 (Appendix A) is inversely related to speed, lower speeds raise suspicion.



(a) Short gap, 2021 **(b)** Short gap, 2022 **(c)** Short gap, 2023

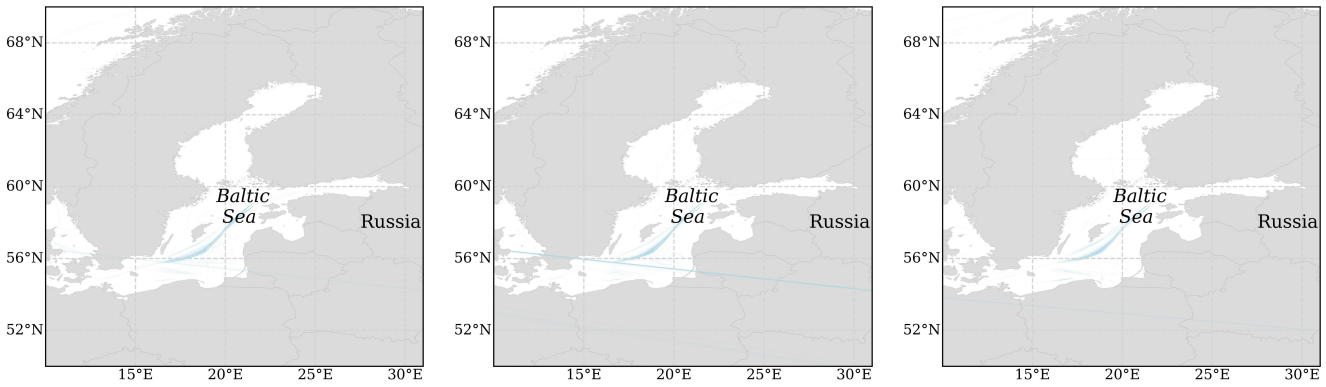
(d) Medium gap, 2021 **(e)** Medium gap, 2022 **(f)** Medium gap, 2023

(g) Long gap, 2021 **(h)** Long gap, 2022 **(i)** Long gap, 2023

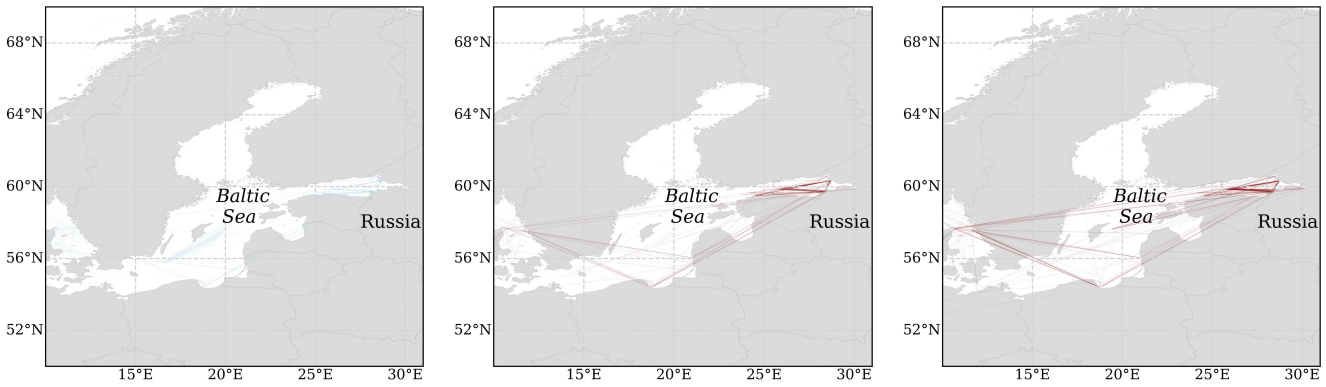
Figure 6: Geographical concentration of dark shipping activities in the Black Sea: 2021–2023

Notes. Each line connects the two data points recorded before and after an AIS gap during a trip. Chromatic intensity reflects the port-based trip suspicion score. To highlight variation in vessel travel patterns by gap duration, we classify AIS gaps as short (under 10 hours), medium (10–120 hours), or long (over 120 hours).

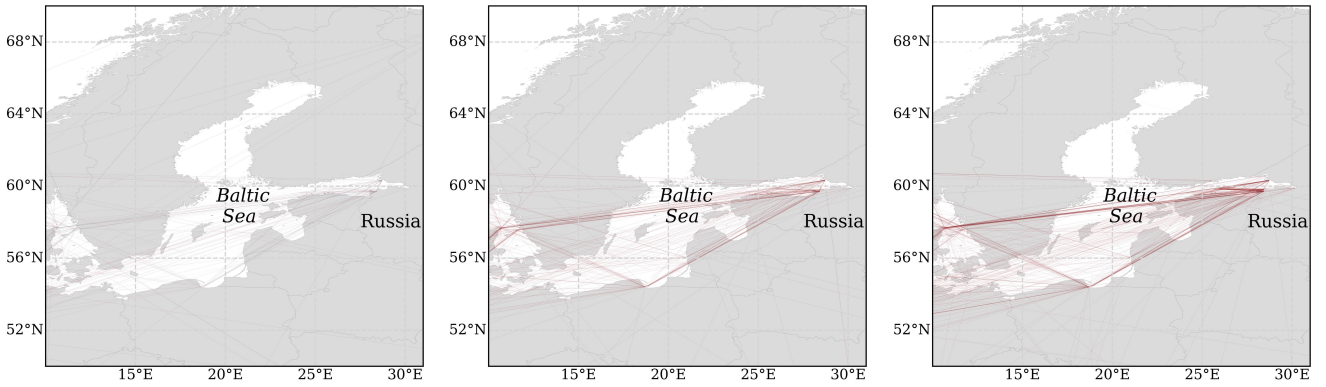
Finally, we identify hotspots for suspicious ship-to-ship transfers by aggregating the last AIS signals before tankers go dark into small geographical squares. We sum the corresponding ship-to-ship transfer suspicion scores, with chromatic intensity reflecting the overall suspicion level in each square (see Appendix A.3 for more details).



(a) Short gap, 2021 **(b)** Short gap, 2022 **(c)** Short gap, 2023



(d) Medium gap, 2021 **(e)** Medium gap, 2022 **(f)** Medium gap, 2023



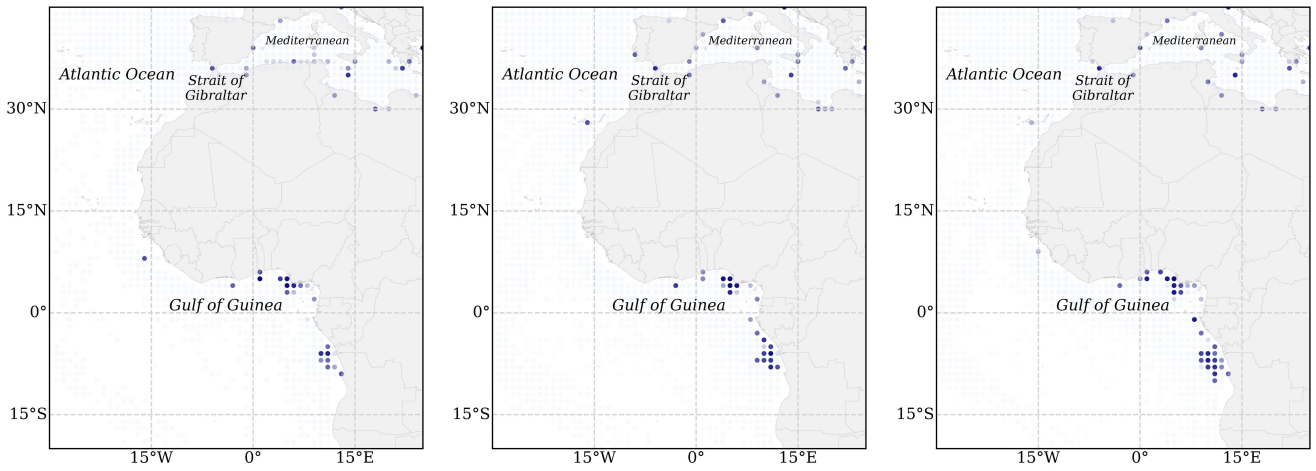
(g) Long gap, 2021 **(h)** Long gap, 2022 **(i)** Long gap, 2023

Figure 7: Geographical concentration of dark shipping activities in the Baltic Sea: 2021–2023

Notes. Colored lines and chromatic intensity are represented as in Figure 6.

Figure 8 shows suspicious ship-to-ship transfers near the Strait of Gibraltar and the Gulf of Guinea from 2021 to 2023.[14] Our results align with reports by Lloyd's List Intelligence (2023) and S&P Global Market Intelligence (2023), which identify Ceuta near Gibraltar and West Africa

[14] As seen in Figure C.6 in Appendix C, these hotspots have persisted since 2017, suggesting that increased sanctions and enforcement have not deterred unauthorized transfers.



(a) 2021 **(b)** 2022 **(c)** 2023

Figure 8: Geographical concentration of dark shipping activities near the Strait of Gibraltar and the Gulf of Guinea: 2021–2023

Notes. Each colored point marks a 1-degree square containing at least one last recorded AIS signal before a vessel disables its transceiver. Chromatic intensity reflects the sum of ship-to-ship transfer-based suspicion scores tied to these points. These scores estimate the likelihood of a transfer when two vessels are nearby and have overlapping AIS gaps.

as key sites for transfers involving U.S.-sanctioned Venezuelan, Iranian, or Russian oil.[15]

4. Oil Trade via Dark Shipping

Next, we quantify the volume of dark-shipped oil exports and analyze its evolution relative to officially recorded global seaborne oil exports. We also identify China as the largest importer of dark-shipped oil —making it a central player in shaping the aggregate effects of oil sanctions and dark shipping on sanctioning economies.

4.1. Quantifying Dark-Shipped Oil Exports

Using our identification of dark ships, we estimate monthly crude oil exports transported by these vessels from Iran, Syria, Venezuela, and Russia between 2017 and 2023. The estimation process consists of several steps.

First, we compile a comprehensive set of trips undertaken by dark ships for each sample year. For trips without significant AIS gaps (i.e., those with gaps not exceeding the 99th percentile

[15]Other hotspots include the Strait of Malacca, South China Sea, Yellow Sea (off northern China), and Arabian Sea (off Oman and the UAE). Results are available upon request.

of time differences between consecutive AIS signals per vessel), we count those originating from ports in each of the four sanctioned countries.

For trips with at least one prolonged AIS gap, we first identify the geographically closest port to each long gap. We then determine the gap with the highest port-based trip suspicion score and attribute the trip to the corresponding sanctioned country.[16] The total number of trips is allocated across months based on each trip's start date.

Finally, we estimate dark-shipped crude oil exports, $X_{c,t}$, in month t from each sanctioned country $c \in \{\text{Iran}, \text{Syria}, \text{Venezuela}, \text{Russia}\}$ as:

$$X_{c,t} = \sum_{i \in \mathcal{N}_{c,t}^{\text{EXP}}} \text{DWT}_i,$$

where $\mathcal{N}_{c,t}^{\text{EXP}}$ is the set of qualifying trips for country c and DWT_i is the deadweight tonnage of the vessel on trip i. We assume each dark ship is fully loaded to its deadweight tonnage capacity (a likely event, as it maximizes the profit from the covert trip).

Figure 9 displays the monthly time series of crude oil exports transported by dark ships from the four sanctioned countries (stacked bars in varying shades of red). For comparison, it also shows recorded global seaborne crude oil exports (solid blue line) and a monthly index of oil-related sanctions imposed by Western authorities (dashed black line with diamond markers) from January 2017 to December 2023. None of the series is seasonally adjusted.

Data on global seaborne crude oil exports are sourced from the UN Comtrade database and identified using the HS code 2709, which corresponds to petroleum oils and oils from bituminous minerals, crude. The sanction intensity index is constructed from a manually curated dataset covering every new oil-related sanction imposed by Western authorities on Iran, Syria, Venezuela, and Russia between 2017 and 2023.[17]

This intensity index is defined as:

$$SANCTION_t = \begin{cases} \sum_{s=1}^{N_t} n_{s,t}, & \text{if } N_t > 0; \\ 0, & \text{if } N_t = 0, \end{cases} \tag{1}$$

[16] A dark ship may transport oil for multiple sanctioned economies within a single trip. Thus, attributing oil exports based solely on the highest port-based trip suspicion score may underestimate sanctioned oil trade.

[17] Table D.1 in Appendix D lists each measure with its date, parties, and description. North Korea is excluded because the relevant restrictions target imports rather than exports, and smaller producers such as Libya and Cuba are omitted to avoid introducing noise.

where N_t is the number of new sanctions imposed in month t and $n_{s,t}$ is the number of participating countries for sanction s. Hence, $SANCTION_t$ measures monthly innovations in sanction intensity rather than stocks.[18] A higher monthly value indicates stronger incremental constraints on the crude oil export capacity of the targeted countries.

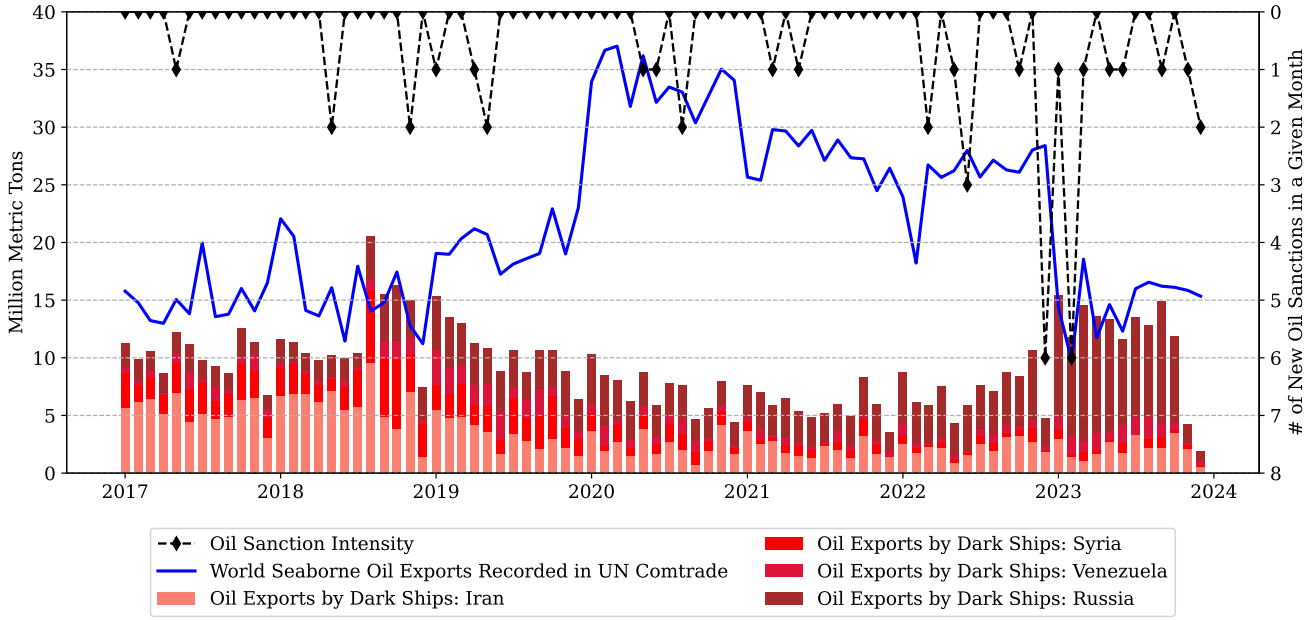


Figure 9: Oil exports of sanctioned countries by dark ships, world seaborne oil exports on record, and oil sanction intensity: 2017M1–2023M12

Notes. The stacked bars depict estimated monthly crude oil exports transported by dark ships from Iran, Syria, Venezuela, and Russia. The solid blue line represents global seaborne crude oil exports, sourced from the UN Comtrade database (HS code 2709: petroleum oils and oils from bituminous minerals, crude). Both series are measured in million metric tons and plotted on the left vertical axis. The dashed black line plots the monthly oil sanction intensity index defined in Equation (1). This index is plotted on the right vertical axis. All time series remain unadjusted for seasonal variation.

Figure 9 highlights three key observations on oil exports by dark ships from sanctioned countries, global seaborne oil exports, and oil sanction intensity from January 2017 to December 2023. First, dark-shipped oil exports account for a significant share of the global seaborne crude oil trade, averaging 9.3 million metric tons per month (about half of global seaborne crude oil exports and 7% of total global crude oil exports reported in UN Comtrade data).[19] This underscores the pivotal role of dark shipping in the global oil trade, particularly for sanctioned nations.

[18]For example, $SANCTION_t = 6$ in December 2022, when the EU, Canada, Japan, the U.K., the U.S., and Australia jointly imposed the $60-per-barrel price cap on Russian crude exports. None of the sanctions in our sample window were fully revoked (see Table D.2), so the index is unaffected by deletions.

[19]Many dark-shipped oil exports (especially those involving prolonged data gaps) may go unrecorded due to the covert nature of such trade after sanctions. Thus, actual global oil trade volumes could exceed official estimates.

Second, Iran and Russia are the primary contributors to crude oil exports via dark ships, with their shares fluctuating over time. From 2017 to 2019, Iran dominated sanctioned oil exports through dark shipping, coinciding with the reimposition of Western nuclear-related sanctions. However, following the oil embargoes and price caps introduced in response to Russia's invasion of Ukraine in late 2022, Russia overtook Iran as the largest exporter of sanctioned oil via dark shipping.

Third, periods of heightened oil sanction intensity (especially in 2022-2023) show that such measures reduced recorded global seaborne oil exports but also triggered a surge in dark-shipped crude oil, as sanctioned trade became more profitable. After the implementation of the $60-per-barrel price cap on Russian crude in December 2022, recorded global seaborne oil exports fell by nearly 50% in January 2023. At the same time, sanctioned oil exports via dark shipping more than doubled, offsetting much of the direct supply reduction caused by the price cap.[20]

4.2. Imports of Dark-Shipped Oil

Our trip-level identification of dark shipping pinpoints the main importers of discounted sanctioned oil. As shown in the following sections, these countries benefit from lower prices, which enhance domestic production and reduce costs for energy-intensive sectors (Bornstein et al., 2023; Bjørnland and Skretting, 2024). Countries trading with these importers may also benefit indirectly through global value chains, as they face higher demand for their exports and/or cheaper intermediate goods.

To estimate monthly crude oil imports from Iran, Syria, Venezuela, and Russia via dark ships, we analyze the annual set of trips by these vessels. For trips without major AIS gaps that originate in the four sanctioned countries, we track their destinations and count those that terminate in each importing country. For trips with prolonged AIS gaps, we identify the most likely origin by selecting the sanctioned country with the highest port-based trip suspicion score during any long gap. Then, we trace the destination and assign the trip to the relevant importer.

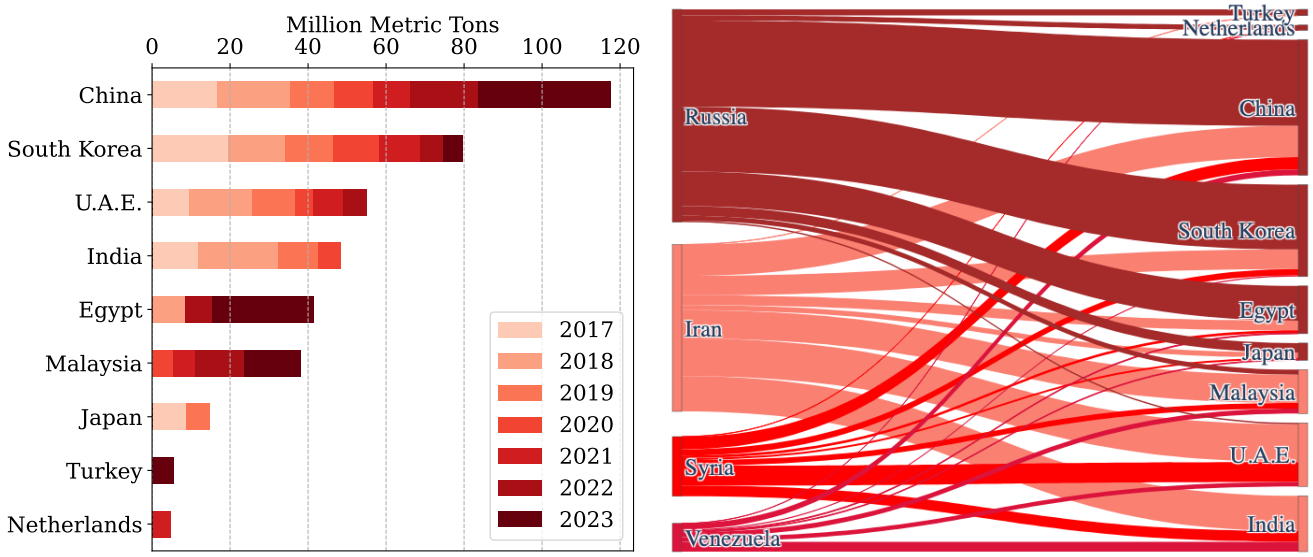
Finally, we estimate $M_{c,t}$, the volume of crude oil delivered by dark ships to country c in month

[20] Although the price cap was technically non-binding in the first half of 2023 (as the Free on Board, FOB, price of Russian Urals crude remained below $60; see Kilian et al., 2024), the use of Western shipping and insurance still required formal price attestation (Office of Foreign Assets Control, 2023). To avoid this compliance burden and regulatory scrutiny, many Russian exporters and intermediaries turned to dark shipping practices, contributing to the surge in such activity from early 2023.

t, as:

$$M_{c,t} = \sum_{i \in \mathcal{N}_{c,t}^{\text{IMP}}} \text{DWT}_i, \tag{2}$$

where $\mathcal{N}_{c,t}^{\text{IMP}}$ is the set of qualifying trips arriving in c during t, and DWT_i is the deadweight tonnage of the vessel on trip i.



(a) Major importers **(b)** Dark-shipped oil flows

Figure 10: Major importers of dark-shipped oil from sanctioned countries: 2017–2023

Notes. Figure 10a shows the top importers of crude oil from Iran, Syria, Venezuela, and Russia transported via dark ships from 2017 to 2023, with import volumes in million metric tons. Varying shades of red indicate annual imports. Volumes are estimated using Equation (2). Figure 10b displays the corresponding trade flows, with link widths proportional to volume.

Figure 10 shows the top importers of crude oil exported via dark ships from the four sanctioned countries between 2017 and 2023. Each country's total was computed using the methodology described above. We identified the five largest importers each year based on annual volumes and aggregated their imports over the full period.

China is the largest importer of crude oil from sanctioned countries via dark shipping, with over 117 million metric tons imported during the sample period, about 15% of total crude oil exports from the four sanctioned nations (Figure 10a). A large share of these imports occurred after the imposition of sanctions on Russian oil in 2022 (Figure 10b).

Interestingly, dark shipping intensity declines with geographic distance, consistent with the gravity model of trade (e.g., Anderson and van Wincoop 2003; Helpman et al. 2008). Substantial crude oil imports via dark shipping were traced to South Korea, the United Arab Emirates, and

India. In 2017–2018, these countries, along with China, were the main importers of crude oil from sanctioned nations. From 2021 onward, China, Egypt, and Malaysia sharply increased their imports of dark-shipped oil.[21]

5. Propagation of Sanctions in Segmented Oil Markets

This section examines how sanctions propagate through global oil markets and assesses the impact of dark shipping, using both empirical local projections and a model of the global oil economy.

5.1. Empirical Evidence

We begin by using LPs to examine the dynamic causal effects of unexpected oil sanction intensity shocks on global oil markets. LPs provide a flexible framework that mitigates the curse of dimensionality, making them well-suited to capture time-varying responses (Fernández-Villaverde et al., 2025; Bai et al., 2025).

Our assessment of causality relies on identifying an unexpected oil sanction intensity shock using the local projection specification:

$$y_{i,t+k} = \beta_{i,k,0} \cdot SANCTION_t + \sum_{l=1}^{L} \boldsymbol{\beta}'_{i,k,l} \boldsymbol{y}_{t-l} + \alpha_k + u_{i,k,t}, \tag{3}$$

where $1 \leq i \leq n$, $0 \leq k \leq K$, $\boldsymbol{y}_t$ is an $n \times 1$ vector of endogenous variables, and $SANCTION_t$ denotes the sanction intensity index defined in Equation (1). The vector $\boldsymbol{y}_{t+k}$ contains the k-step-ahead forecasts, with $y_{i,t+k}$ representing the i-th component. The regressors include L lags of the endogenous variables, α_k is a horizon-specific constant, and $u_{i,k,t}$ is the prediction error. The coefficients of interest, $\beta_{i,k,0}$ for $k = 0, \ldots, K$, trace the dynamic response of the i-th variable to a one-standard-deviation oil sanction intensity shock at time t.

For the baseline estimation, we use a 4-variable LP model with monthly time series for: (i) the sanction intensity index, (ii) world seaborne crude oil exports from UN Comtrade, (iii) crude oil exports via dark ships from Iran, Syria, Venezuela, and Russia, and (iv) the Brent spot price, spanning January 2017 to December 2023. All series except the sanction intensity index

[21] Our results do not identify India as a major importer of Russian oil. This likely reflects India's reliance on re-exports from intermediaries (e.g., Egypt), while our method captures only direct shipments from sanctioned nations. See https://www.bloomberg.com/news/articles/2022-08-03/russia-finds-a-new-route-to-oil-market-via-a-tiny-egyptian-port (Accessed February 25, 2025) for further coverage.

are seasonally adjusted. The sanction intensity index is standardized and enters the LP model in standard deviations; the remaining endogenous variables enter in log percent. Appendix E provides further details.

We estimate the LP model (3) using the least squares method (Jordà, 2005), applying Newey-West standard errors (Newey and West, 1987) to quantify the uncertainty around the impulse response functions (IRFs) for $\beta_{i,k,0}$. As the forecast horizon k increases, the variance of $\beta_{i,k,0}$ estimates tends to rise, especially given the limited sample size.

To address this concern, here and throughout the paper, we apply the smooth local projections (SLP) method in Barnichon and Brownlees (2019), approximating $\beta_{i,k,0}$ using a linear B-spline basis function expansion at horizon k:

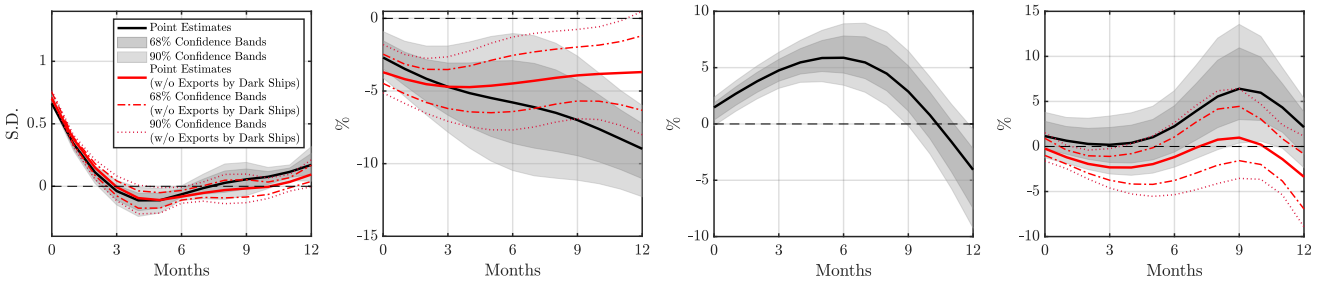
$$\beta_{i,k,0} \approx \sum_{m=1}^{M} b_{i,m} B_{i,m}(k), \tag{4}$$

where $B_{i,m}(k) : \mathbb{R} \to \mathbb{R}$ for $m = 1, \ldots, M$ is a set of B-spline basis functions and $b_{i,m}$ are scalar parameters. These parameters are estimated using a penalized estimator that shrinks Equation (4) toward a quadratic polynomial in k.

We identify an oil sanction intensity shock by controlling only for the lagged endogenous variables $\boldsymbol{y}_{t-l}$ (i.e., no contemporaneous values of other endogenous variables are included as controls) and by estimating the LP model (3) starting from horizon $k = 0$. This approach is equivalent to placing the sanction intensity index first in a recursive ordering, allowing all other endogenous variables to respond contemporaneously to the oil sanction intensity shock. We include three lags of the endogenous variables in the LP model (i.e., $L = 3$) based on the Hannan–Quinn Information Criterion (HQIC).

Figure 11 presents IRFs to an unexpected oil sanction intensity shock using the 4-variable LP model. Black solid lines denote point estimates, while gray-shaded areas represent 68% and 90% confidence bands. An unexpected shock raises the sanction intensity index by 0.66 standard deviations, equivalent to approximately 0.73 additional oil-related sanctions (Panel 11a). This shock triggers an immediate and sustained decline in global seaborne oil exports recorded in UN Comtrade data, lasting up to a year post-impact (Panel 11b). While this contraction reduces global oil supply, its effect is largely offset in the first six months by a surge in dark-shipped oil exports (Panel 11c), which peak around the sixth month before falling sharply.

More importantly, as discounted dark-shipped oil enters global markets in the months following



(a) Sanction intensity **(b)** Recorded seaborne exports **(c)** Exports by dark ships **(d)** Brent spot price

Figure 11: IRFs to a one-standard-deviation oil sanction intensity shock for global oil exports and prices

Notes. The IRFs are computed using both a 4-variable LP model and a counterfactual 3-variable LP model that excludes crude oil exports from Iran, Syria, Venezuela, and Russia via dark ships. The black solid lines represent the responses estimated from the 4-variable LP model, with gray-shaded areas indicating the corresponding 68% and 90% confidence bands. The red solid lines show the responses estimated from the counterfactual 3-variable LP model, while the red dash-dotted and dotted lines indicate the respective 68% and 90% confidence bands.

the shock, the Brent spot price (the global oil price benchmark) remains muted. It is only when dark-shipped oil exports decline that sanctions drive significant price increases. This effect is even more pronounced when estimating a counterfactual 3-variable LP model (excluding dark-shipped crude oil exports from Iran, Syria, Venezuela, and Russia) and comparing the resulting IRFs of the Brent spot price to the baseline. As shown in Panel 11d, the counterfactual point estimates, plotted as a red solid line, consistently fall below those from the 4-variable LP model, even dipping beneath the lower bound of the 68% confidence bands associated with the baseline estimation.

This finding suggests the presence of a negative omitted variable bias, wherein dark-shipped oil exports exert downward pressure on global oil prices. As illustrated in Appendix F.1, this result remains robust to (i) extending the lag length ($L = 4$); (ii) including a linear trend in the LP model (3); (iii) replacing the Brent spot price with the West Texas Intermediate (WTI) spot price; (iv) restricting the sample to the period from January 2017 to November 2022, ending just before the $60-per-barrel price cap on Russian oil exports took effect; and (v) using a simplified sanction intensity index that equals one if Western authorities imposed new oil-related sanctions on Iran, Syria, Venezuela, or Russia in a given month, and zero otherwise.[22]

[22]The fourth robustness check aims to isolate the effects of earlier oil-related sanctions (e.g., embargoes) from those of the $60-per-barrel price cap on Russian oil exports, which has been the subject of extensive analysis in the literature (e.g., Kilian et al., 2024).

5.2. A Model With Segmented Oil Markets and Costly Shift of Supply

Unlike other energy markets characterized by homogeneous and easily transportable products, the oil market is highly segmented, comprising various types and qualities of oil, a diverse set of suppliers, and multiple destinations. As a result, short-run adjustments in oil supply across markets are complex and costly. For instance, Russian seaborne crude oil primarily consists of Urals and Eastern Siberia–Pacific Ocean (ESPO), which are exported from Black Sea and Baltic Sea ports to the EU, and from Pacific ports to Asia, respectively. After the EU and other countries imposed sanctions and restricted Russian oil imports, Russia was forced to sell its crude to more distant buyers, resulting in both increased insurance and transportation costs (Kilian et al., 2024).

Thus, the propagation of sanction shocks in global oil markets encompasses *endogenous* and *costly* shifts in oil supply across segmented markets by different suppliers. To study this process, we outline a simple model with segmented markets and costly cross-market shifts in oil supply, examining the critical role of dark shipping in rebalancing the global oil market after sanctions. The model replicates the observed dynamics of oil exports and prices shown in Figure 11.

The static global oil market consists of two segmented regions, Europe and China, indexed by $k \in \{E, C\}$, each with a representative oil buyer (the U.S. is a net oil exporter, so we exclude it for simplicity of exposition). Two oil suppliers —sanctioned (S) and non-sanctioned (NS)— export to both markets and can reallocate oil across them at a cost, depending on the exogenous state of sanctions.

Oil suppliers. Each oil supplier $s \in \{S, NS\}$, taking as given the FOB prices received in different markets ($\{P_{k,s}\}_k$), maximizes profit subject to a CES cost function over the quantities of oil supplied to these markets ($\{Q_{k,s}\}_k$):

$$\pi_s\left(\{Q_{k,s}\}_k\right) = \max_{\{Q_{k,s}\}_k} \sum_{k\in\{E,C\}} P_{k,s}Q_{k,s} - C_{OS,s}\left(\{Q_{k,s}\}_k\right), \tag{5}$$

$$\text{s.t.} \quad C_s\left(\{Q_{k,s}\}_k\right) = a_s Q_s + b_s \frac{Q_s^2}{2}, \tag{6}$$

$$Q_s \equiv \left(\sum_k \Omega_{k,s}^{1-\rho_s} Q_{k,s}^{\rho_s}\right)^{\frac{1}{\rho_s}},$$

where $\Omega_{k,s}$ represents the steady-state share of supplier s' oil revenue from market k in its total oil revenue. The parameter $\rho_s \in (1, +\infty)$ defines a cost function that comprises a strictly convex

combination of oil supply across different markets, indicating higher costs for reallocating oil supply between them.

The first-order condition for the oil supplier's problem (5) is:

$$Q_{k,s} = \left(\frac{P_{k,s}}{\Phi_s}\right)^{\frac{1}{\rho_s - 1}} \Omega_{k,s} Q_s, \tag{7}$$

where $\Phi_s = a_s + b_s Q_s$ is the supplier s' marginal cost of total oil supply. Equation (7) implies that the amount of oil supplied to market k increases with the supplier s' FOB price in that market. A decline in $P_{k,s}$ due to a sanction imposed on supplier s in market k will prompt s to shift its oil supply away from the sanctioning market to others.

Importantly, Equation (7) shows that the elasticity of cross-market oil supply reallocation to relative oil prices declines with the convexity parameter ρ_s. Thus, ρ_s captures short-run rigidity in reallocating oil supply across markets, which can arise from the costly redeployment of oil tankers servicing different markets or coordination failures among various parties within the supplier coalition. For instance, stricter regulation of dark shipping increases ρ_S for the sanctioned country.

Oil prices and demand. In each market, the two suppliers engage in Bertrand competition based on the Cost, Insurance, and Freight (CIF) price, determining the oil price P_k in market k, which incorporates the impact of sanctions, $P_k = P_{k,s} + \delta_{k,s}$, where the intensity of oil sanctions is modeled as a positive trade margin above supplier s' FOB price, i.e., $\delta_{k,s} > 0$.[23]

The representative oil buyer in market k has the demand curve:

$$d_k\left(P_k\right) = \exp\left(\alpha_k - \beta_k \ln\left(P_k\right)\right). \tag{8}$$

Hence, the equilibrium of the global oil market is defined as follows:

Definition 1. *An equilibrium is a set of allocations and prices such that, for any realized state* $\boldsymbol{\delta} \equiv \{\delta_{k,s}\}_{k\in\{E,C\},s\in\{S,NS\}}$*:*

(i) Each oil supplier optimally chooses its supply in each market given the oil prices; and

(ii) Oil prices clear each segmented oil market k, i.e., $\sum_{s\in\{S,NS\}} Q_{k,s}(\boldsymbol{\delta}) = d_k\left(P_k(\boldsymbol{\delta})\right)$.

[23] Our modeling of the oil supplier's problem, particularly the CES cost function for oil supply and the treatment of sanctions as a trade margin above the FOB price, incorporates the (market-specific) oil embargo as a special case when $P_{k,s} < a_s$, preventing supplier s from selling oil to market k.

5.3. Data and Calibration

Our calibration of the model focuses on Russia and OPEC as the sanctioned and non-sanctioned suppliers, denoted by the subscripts S and NS, respectively. We use monthly price and volume data on crude oil exports from Russia and OPEC to the EU and China from March 2022 to December 2023, sourced directly from Kpler and the China National Petroleum Corporation, respectively.[24]

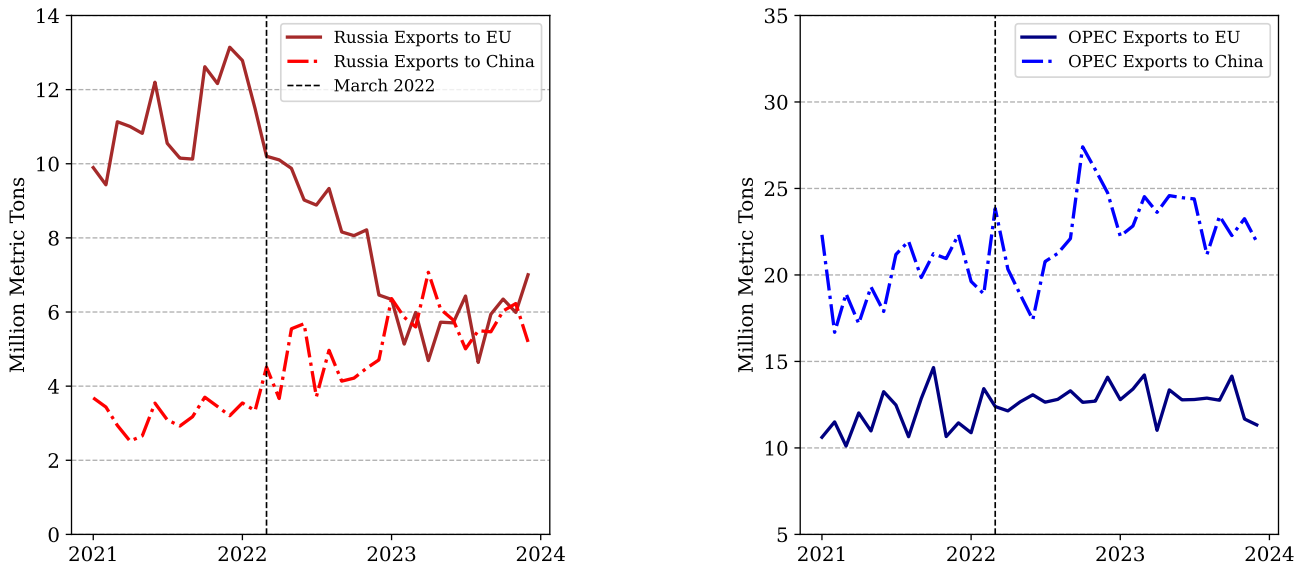
We normalize the steady-state values of all prices to one. The total volume of oil exports by market and supplier during the sample period is summed and normalized by the corresponding global volume, denoted as $\overline{Q}_{k,s}$. We calibrate α_k and β_k in the demand function (8) to equal $\sum_s \overline{Q}_{k,s}$ and one, respectively, for each market k. The steady-state share of supplier s' oil supply to different markets, $\Omega_{k,s}$, is calibrated as $\overline{Q}_{k,s} / \sum_k \overline{Q}_{k,s}$.

We estimate the parameter a_s in the supplier's cost function (6) as -9.5 for Russia and -13.3 for OPEC by regressing each supplier's HP-filtered log total export volume on its average price across markets. The parameter b_s is calibrated as $(1 - a_s) / \sum_k \overline{Q}_{k,s}$.

Furthermore, we calibrate the convexity parameter ρ_s in each supplier s' cost function by regressing the monthly year-over-year growth rates of its relative oil supply volume on its relative prices in the two markets during the sanctioning period from March 2022 to December 2023. The estimated values of ρ_s are 1.3 for Russia and 1.8 for OPEC, indicating more rigid reallocation of oil supply for OPEC than for Russia, potentially due to OPEC's institutional constraints (Behar and Ritz, 2016).

This is also evident in the comparison of Russia's and OPEC's oil exports to the EU and China (Figure 12). While OPEC's exports to both markets have remained relatively stable since the imposition of the first oil-related sanction on Russia in March 2022, Russian exports to the EU have plummeted, whereas exports to China have risen steadily. Since our model nests a non-segmented oil market as a special case when $\rho_S = \rho_{NS} = 1$, estimates of ρ_s significantly above one validate our specification of segmented oil markets.

[24] The calibration window is restricted to March 2022-December 2023 because the G7/EU sanctions and price-cap regime on Russian crude took effect during this interval, prompting the steepest surge in dark shipping activity and the largest observable reallocation of seaborne supply (see Figures 4a and 9). OPEC is chosen as the non-sanctioned benchmark because, taken as a bloc, it supplies more than one-third of global crude output and remains the dominant source of China's imports during the sample, while most of its members were not themselves subject to the sanctions that constrained Russian exports. Appendix G provides further details.



(a) Russia **(b)** OPEC

Figure 12: Crude oil exports to the EU and China: Russia vs. OPEC, 2021-2023

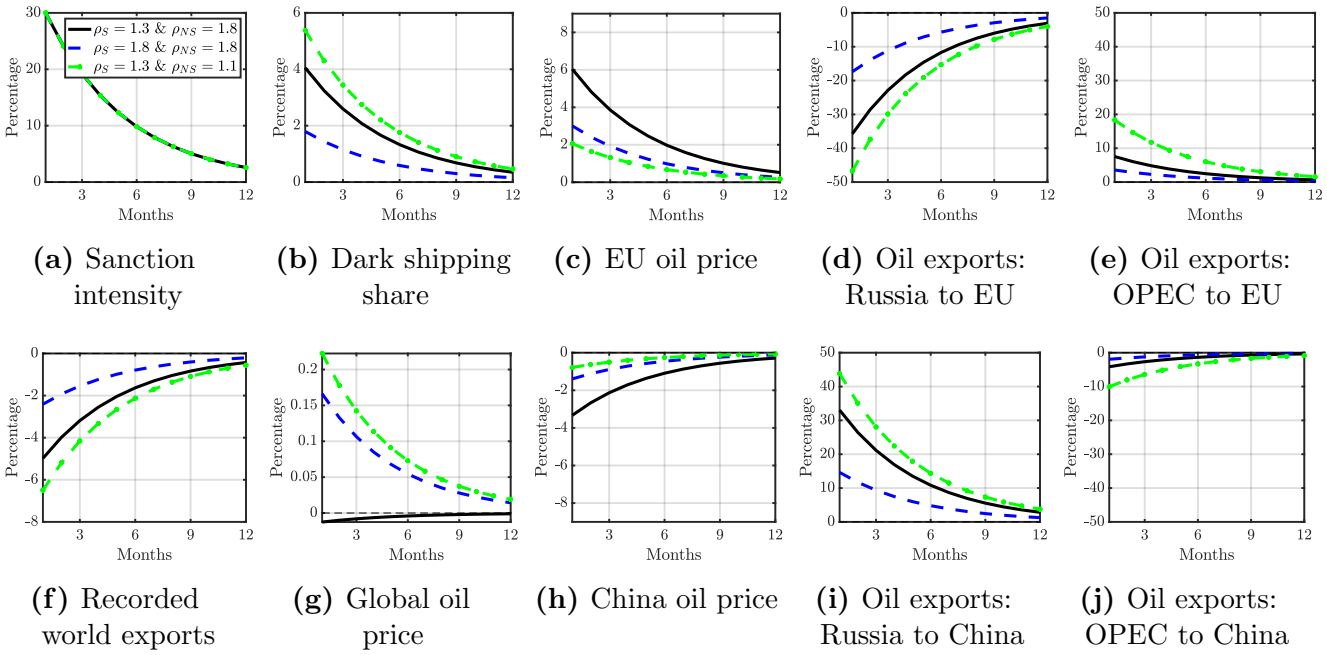
Notes. All series are measured in million metric tons, sourced directly from Kpler, and are not seasonally adjusted. The vertical dashed line marks March 2022, when the first oil-related sanction on Russia was imposed.

5.4. Simulation Results

Figure 13 plots the IRFs of oil exports and prices to a 30% increase in sanction intensity on Russia in the EU market. In the baseline case ($\rho_S = 1.3$ and $\rho_{NS} = 1.8$, solid black lines), the share of dark-shipped oil in global exports increases, reducing recorded world oil exports (proxied by the sum of Russia's oil exports to the EU and OPEC's total oil exports) by approximately 5% in response to the rise in sanction intensity (Panels 13b and 13f). The global oil price (proxied by OPEC's average FOB price) remains flat (Panel 13g), consistent with the LP results in Figure 11.

The impulse responses of market-specific oil prices and the endogenous reallocation of oil exports across markets illustrate the propagation mechanism behind the stable global oil price. In response to intensified sanctions on its exports to the EU, Russia reallocates more than 30% of its oil supply from the EU to China via dark shipping (Panels 13d and 13i), leading to an oversupply and a corresponding 3.3% decline in China's oil price (Panel 13h).

This price drop is so substantial that, although the resulting oil supply shortage in the EU is only partially offset by OPEC increasing its exports to the region —by less than 10%, a much smaller magnitude than Russia's reduction (Panel 13e)— the rise in the EU's oil price (Panel 13c) does not trigger a significant increase in the global oil price.



(a) Sanction intensity **(b)** Dark shipping share **(c)** EU oil price **(d)** Oil exports: Russia to EU **(e)** Oil exports: OPEC to EU

(f) Recorded world exports **(g)** Global oil price **(h)** China oil price **(i)** Oil exports: Russia to China **(j)** Oil exports: OPEC to China

Figure 13: Model IRFs to an oil sanction intensity shock for oil exports and prices

Notes. IRFs of oil exports and prices to a 30% increase in sanction intensity on Russia in the EU market (i.e., $\delta_{E,S} = 0.3$) for the baseline case ($\rho_S = 1.3$ and $\rho_{NS} = 1.8$, solid black lines) and two counterfactual cases: strict enforcement of dark shipping ($\rho_S = \rho_{NS} = 1.8$, dashed blue lines) and costless reallocation of OPEC's oil supply ($\rho_S = 1.3$ and $\rho_{NS} = 1.1$, dash-dotted green lines). The dark shipping share is measured as the percentage deviation of dark-shipped oil's share in global oil exports from its steady-state value. Recorded world exports are defined as the sum of Russia's oil exports to the EU and OPEC's total oil exports. The global oil price is represented by OPEC's average FOB price, computed as the weighted average of its FOB prices across the two markets.

To highlight the two key factors contributing to the stable global oil price (dark shipping and OPEC's limited ability to reallocate oil supply across markets), we consider two counterfactual scenarios. First, we eliminate dark shipping (as if sanctions were strictly enforced), making it equally costly for Russia to reallocate oil across markets ($\rho_S = \rho_{NS} = 1.8$). As shown in Figure 13 (dashed blue lines), Russia reallocates significantly less oil from the EU to China (under 20%), resulting in a much smaller drop in recorded world oil exports. The decline in China's oil price is also smaller, at under 2%, leading to a significant increase in the global oil price. Intuitively, when dark shipping is restricted, Russia's inability to reallocate oil traps a large share of global oil in the sanctioned EU market and hence increases the global oil price.

Second, OPEC's inability to swiftly reallocate oil supply to the EU during a shortage also contributes to the flat global oil price. When we allow OPEC to shift oil more freely than Russia ($\rho_S = 1.3$ and $\rho_{NS} = 1.1$), as shown in Figure 13 (dash-dotted green lines), it effectively swaps

markets with Russia, reallocating a much larger share of its oil from the oversupplied Chinese market to the under-supplied EU market. Consequently, the decline in China's oil price is much less pronounced, causing an even larger increase in the global oil price.

6. Broader Macroeconomic Effects of Dark Shipping

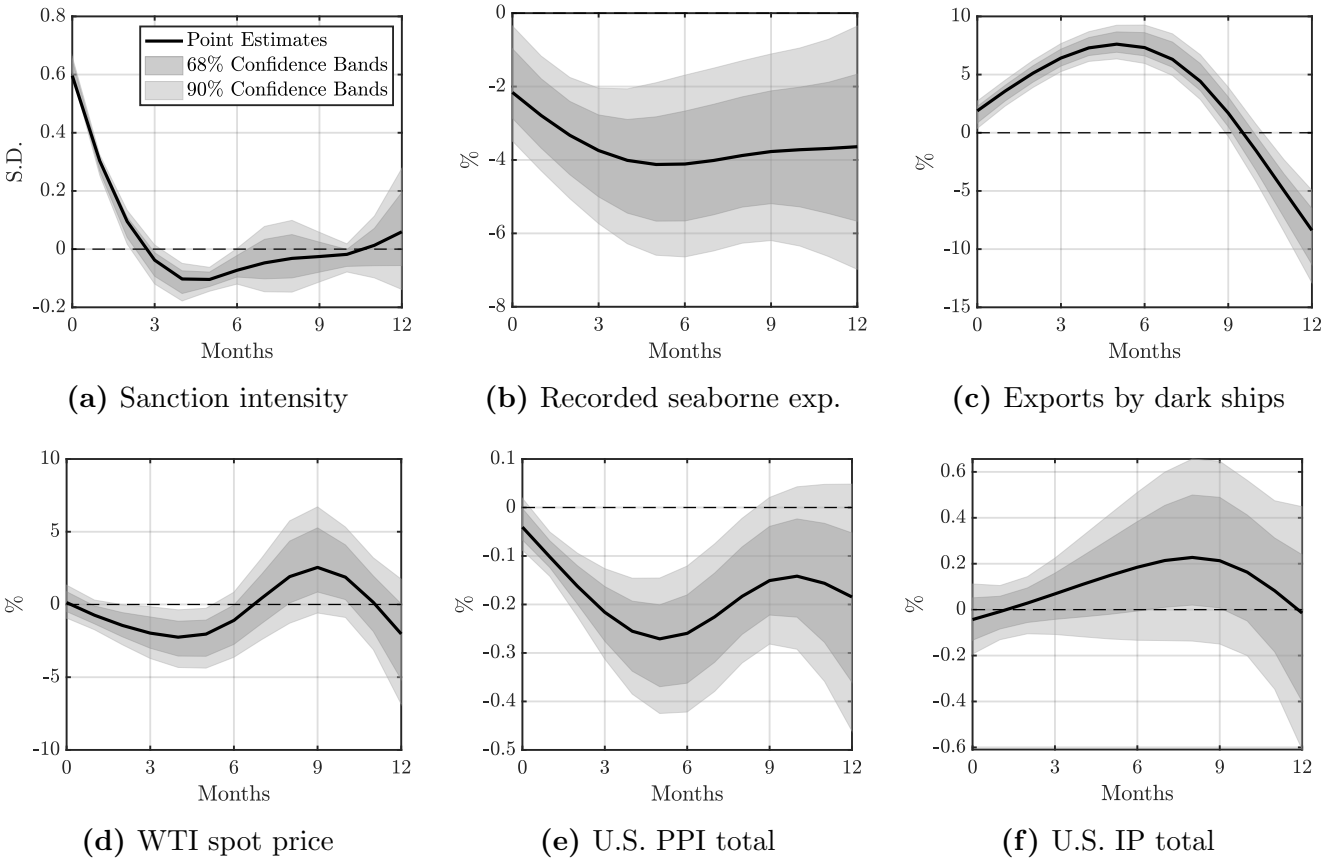
The previous section highlighted the role of dark shipping's endogenous response to sanctions in reallocating the global oil supply. Now, we examine the dynamic causal effects of unexpected oil sanction intensity shocks on inflation and production in the U.S. and the EU, again leveraging LPs. We identify the propagation of oil sanction shocks along the global supply chain as the key mechanism driving aggregate dynamics in these economies. As the largest importer of discounted dark-shipped oil, China plays a central role in this transmission.

6.1. Aggregate Dynamics

To assess the aggregate effects on the U.S. and the EU, we build on the oil market LP model developed in Section 5.1 by incorporating additional variables. The U.S. model includes monthly time series for: (i) the sanction intensity index, (ii) world seaborne crude oil exports recorded in UN Comtrade data, (iii) crude oil exports from Iran, Syria, Venezuela, and Russia via dark ships, (iv) the WTI spot price (while Brent serves as the global benchmark, WTI is more relevant for U.S. oil prices), (v) the U.S. producer price index (PPI), and (vi) U.S. industrial production (IP), covering the period from January 2017 to December 2023. In the EU model, we replace the WTI spot price with Brent and substitute U.S. PPI and IP with their EU equivalents. Like the oil market variables, the PPI and IP series are seasonally adjusted and enter the LP model (3) in log percent. Appendix E provides further details.

Following Barnichon and Brownlees (2019), we identify an oil sanction intensity shock by controlling solely for lagged endogenous variables, $\boldsymbol{y}_{t-l}$, without incorporating contemporaneous values of other endogenous variables as controls. The LP model (3) is estimated from horizon $k = 0$. Based on the HQIC criterion, we include three lags of the endogenous variables ($L = 3$), and our results remain robust when accounting for longer lag specifications.

Figures 14 and 15 present the IRFs of the endogenous variables to an unexpected oil sanction intensity shock in the U.S. and EU economies, respectively. The black solid lines denote point



(a) Sanction intensity **(b)** Recorded seaborne exp. **(c)** Exports by dark ships

(d) WTI spot price **(e)** U.S. PPI total **(f)** U.S. IP total

Figure 14: IRFs to a one-standard-deviation unexpected oil sanction intensity shock for the U.S. economy: Aggregate dynamics

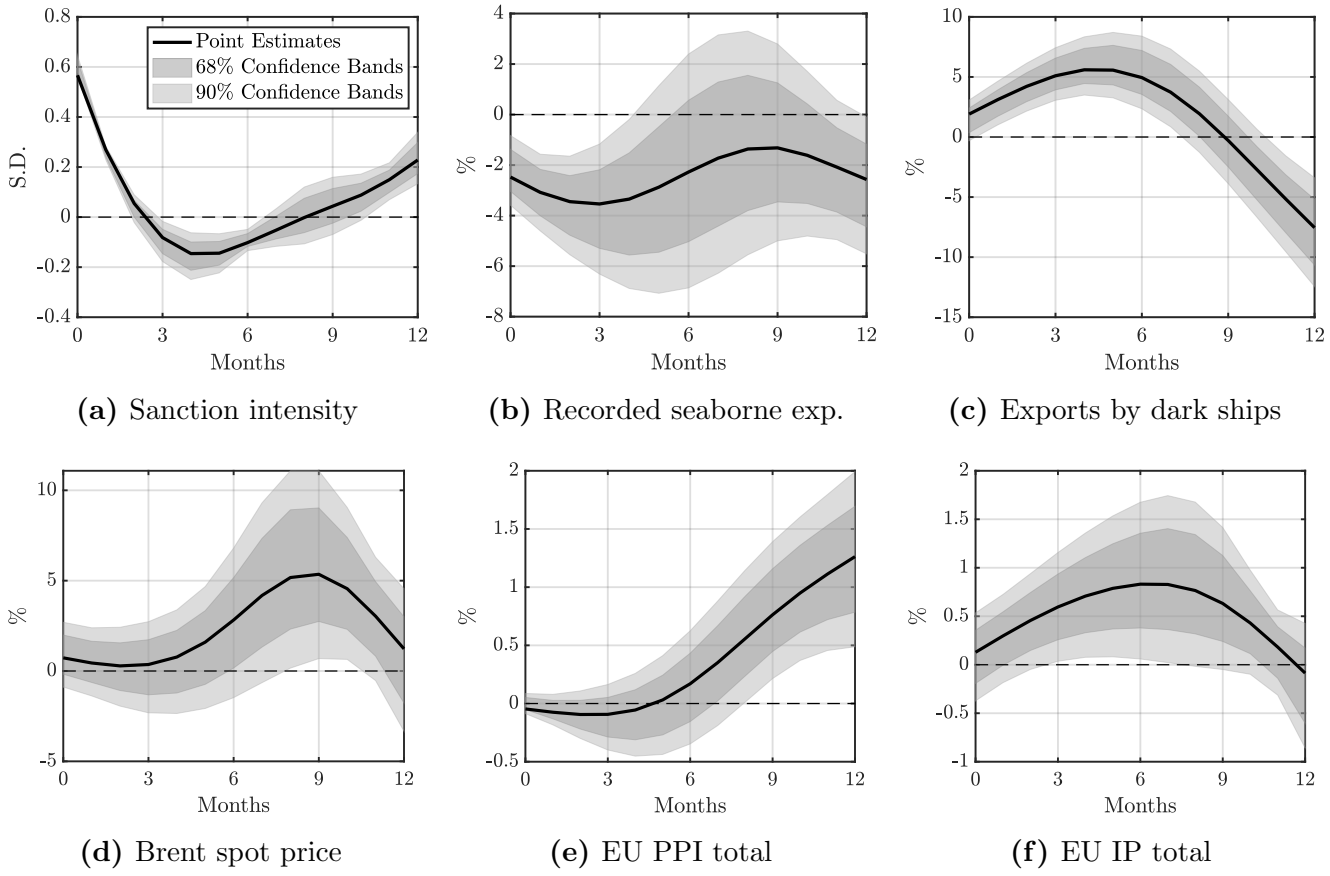
Notes. Black solid lines represent point estimates, while gray-shaded areas indicate the 68% and 90% confidence bands.

estimates, while the gray-shaded areas represent the 68% and 90% confidence bands.

The responses of oil market variables to the sanction intensity shock resemble those in Figure 11. The shock triggers an immediate and persistent drop in recorded global seaborne oil exports (Panels 14b and 15b). However, rising dark-shipped exports in the first six months largely offset the supply contraction (Panels 14c and 15c), pushing WTI prices down and preventing a Brent price increase (Panels 14d and 15d).

Distinct inflation and production responses in the U.S. and EU. Reflecting the post-impact responses of WTI and Brent spot prices, the U.S. and EU economies display distinct patterns in PPI and IP, differing in both shape and magnitude.

In the U.S., a net oil exporter, the initial decline in WTI prices reduces revenues for domestic oil producers as importers shift to discounted dark-shipped oil, contributing to a drop in PPI



(a) Sanction intensity **(b)** Recorded seaborne exp. **(c)** Exports by dark ships

(d) Brent spot price **(e)** EU PPI total **(f)** EU IP total

Figure 15: IRFs to a one-standard-deviation unexpected oil sanction intensity shock for the EU economy: Aggregate dynamics

Notes. Black solid lines show point estimates; gray-shaded areas indicate the 68% and 90% confidence bands.

during the first six months (Panel 14e). However, the decline in U.S. PPI is sharper than that of WTI, and when WTI prices rebound after six months, PPI remains below the zero-response line. This suggests additional supply-side effects through which escalating oil sanctions and increased dark shipping continue to suppress PPI. A similar pattern appears in U.S. IP, which shows a mild but sustained positive impact throughout the year following the shock (Panel 14f). While lower oil prices would typically dampen demand in both energy and non-energy sectors —potentially leading to a demand-driven decline in industrial production— the observed increase in IP suggests the presence of offsetting forces.

In contrast, as a net oil importer, the EU shows only a marginally negative PPI response in the first six months following the oil sanction intensity shock, with confidence bands indicating limited statistical significance (Panel 15e). Since oil supply to the EU contracts as sanctioned exporters reallocate shipments to non-sanctioning buyers via dark shipping —as shown in Figure 13— one

would expect upward pressure on EU oil import prices and PPI. Yet the muted PPI response suggests the presence of additional supply-side forces that offset this inflationary pressure.

Furthermore, compared to the U.S. IP response (Panel 14f), the EU response is not only statistically significant —as indicated by the lower bound of the 90% confidence band reaching the zero-response line at its peak (Panel 15f)— but also substantially larger (approximately 0.83% for the EU vs. 0.22% for the U.S.). This suggests that, beyond supply-side factors potentially common to both regions, additional demand-side forces contribute to the stronger increase in EU industrial production. The presence of such forces is further supported by the sustained expansion of EU IP over longer forecast horizons. As Brent prices rise sharply following a steep drop in dark-shipped oil exports after the first quarter —and as PPI begins to increase significantly— EU IP continues to grow, peaking beyond the six-month mark.

To assess robustness, we modify the baseline specification in four ways: (i) extending the lag length ($L = 4$); (ii) including a linear trend; (iii) restricting the estimation sample to January 2017–November 2022 (the pre–price cap period); and (iv) using the simplified sanction intensity index introduced in Section 5.1. As shown in Figures F.6 to F.13 in Appendix F, the results remain largely unchanged. Additionally, we conduct a robustness check using a Cholesky-ordered structural vector autoregression (SVAR) model for both the U.S. and the EU. Figures F.14 and F.15 present quantitatively similar SVAR results, further confirming the robustness of our findings.

6.2. Propagation Channels

The missing propagation channels needed to explain the divergent PPI inflation and production responses in the U.S. and EU prompt us to look beyond the direct impacts of oil sanctions and dark shipping, and to examine their general equilibrium effects transmitted through the global supply chain. China is the primary recipient of discounted dark-shipped oil —as shown in Figure 10— and a key trading partner for both the U.S. and the EU. This positions China as a central node in the transmission of these shocks.

To explore this idea, we expand the U.S. LP model by adding two endogenous variables: China's crude oil import price and the U.S. import price for Chinese-manufactured goods, averaged across NAICS sectors 31–33. For the EU LP model, we include the EU import price for Chinese goods, China's total IP, and its total import value from the EU. Additionally, we differentiate between energy and non-energy sectors by replacing the total PPI and IP for the U.S. and EU

with sector-specific counterparts. All additional series are seasonally adjusted and expressed in log percent. Appendix E provides data sources for these variables.

The estimation specifications remain consistent with those in Figures 14 and 15. We include only lagged endogenous variables and estimate the augmented LP models from horizon $k = 0$, maintaining a lag length of three ($L = 3$). In the discussion that follows, we highlight key panels illustrating the propagation channels, while additional panels are provided in Figures F.16 and F.17 in Appendix F for completeness.

Decline in oil import prices and increased production in China. As the leading importer of discounted dark-shipped oil, China experiences an immediate and sharp decline in its oil import price following an unexpected oil sanction intensity shock (Panel 16e).[25] The decline in oil prices propagates downstream through domestic input–output linkages, lowering production costs and stimulating China's industrial production (Panel 17f).[26] However, starting in the ninth month post-impact, a rebound in oil import prices, driven by the rapid decline in dark-shipped oil exports (Panel 14c), triggers a contraction in Chinese production.

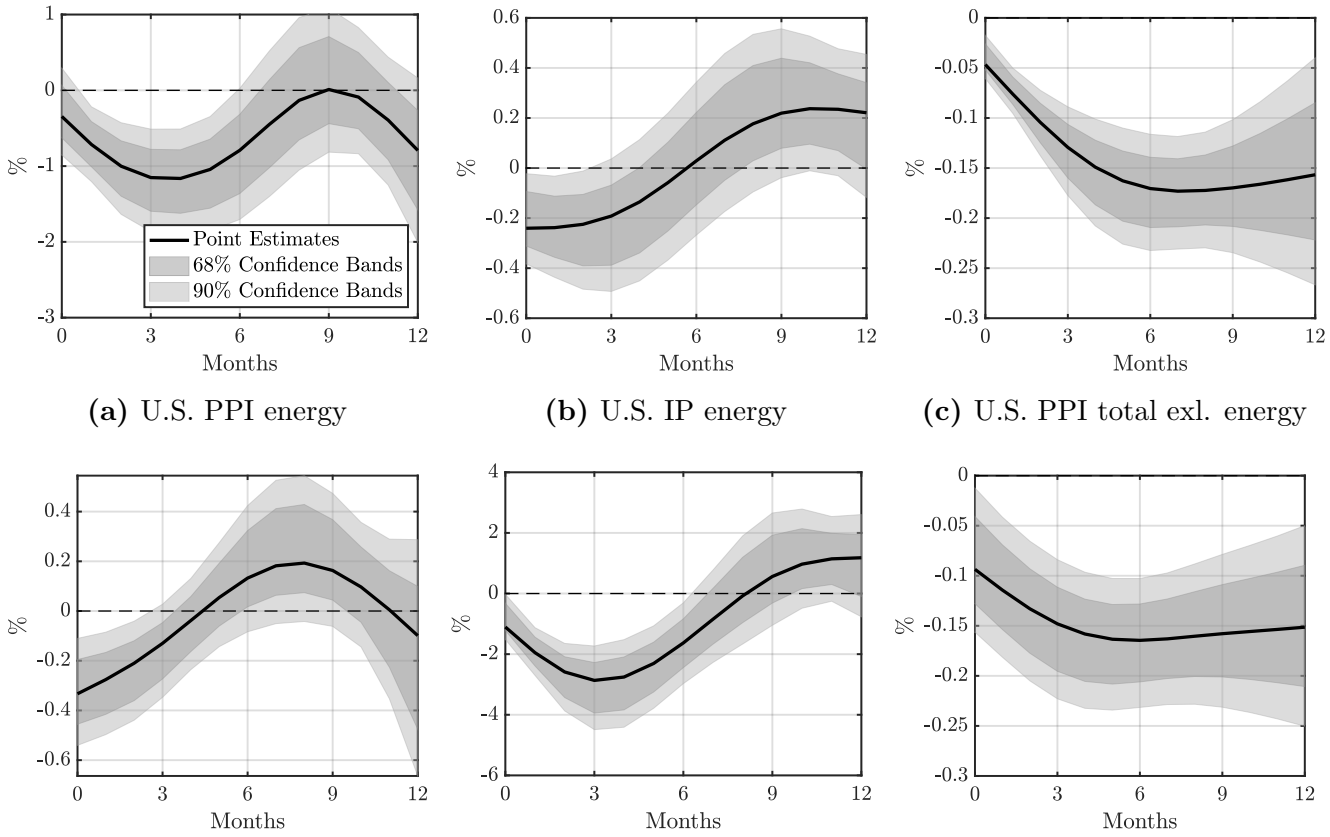
The role of China in propagating oil sanction shocks. The decline in oil import prices and the resulting rise in China's industrial production affect the U.S. and EU differently, reflecting their distinct input–output linkages with China in global production networks and varying exposure to energy prices.

For the U.S., as shown in Figure 14d, the decline in the WTI spot price and lower oil export revenues for domestic producers reduce PPI (Panels 16a and 16c) and IP (Panels 16b and 16d) across both sectors. The decline in U.S. oil export volumes during the first six months post-impact reinforces this, as shown in Figure F.20 in Appendix F. Both reduced volumes and lower prices lower oil export revenues.

Lower production costs in China reduce the U.S. import price of Chinese-manufactured goods (Panel 16f), driving cost-saving growth that amplifies PPI deflation, partially offsetting initial production declines. This effect is clearer when excluding China-related variables and re-estimating

[25] This decline aligns with our model simulation results in Figure 13, where the reallocation of Russian oil from the EU to China (triggered by intensified sanctions on exports to the EU) creates an oil oversupply in China, leading to a corresponding drop in China's oil import price.

[26] Figure F.18 in Appendix F further confirms the reduction in production costs, showing a significant drop in China's total PPI. This also contributes to a sharp decline in the U.S. import price for Chinese goods, including manufactured products, as seen in Figures F.19 and 16f.



(a) U.S. PPI energy **(b)** U.S. IP energy **(c)** U.S. PPI total exl. energy

(d) U.S. IP total exl. energy **(e)** China oil import price **(f)** U.S. import price China mfg.

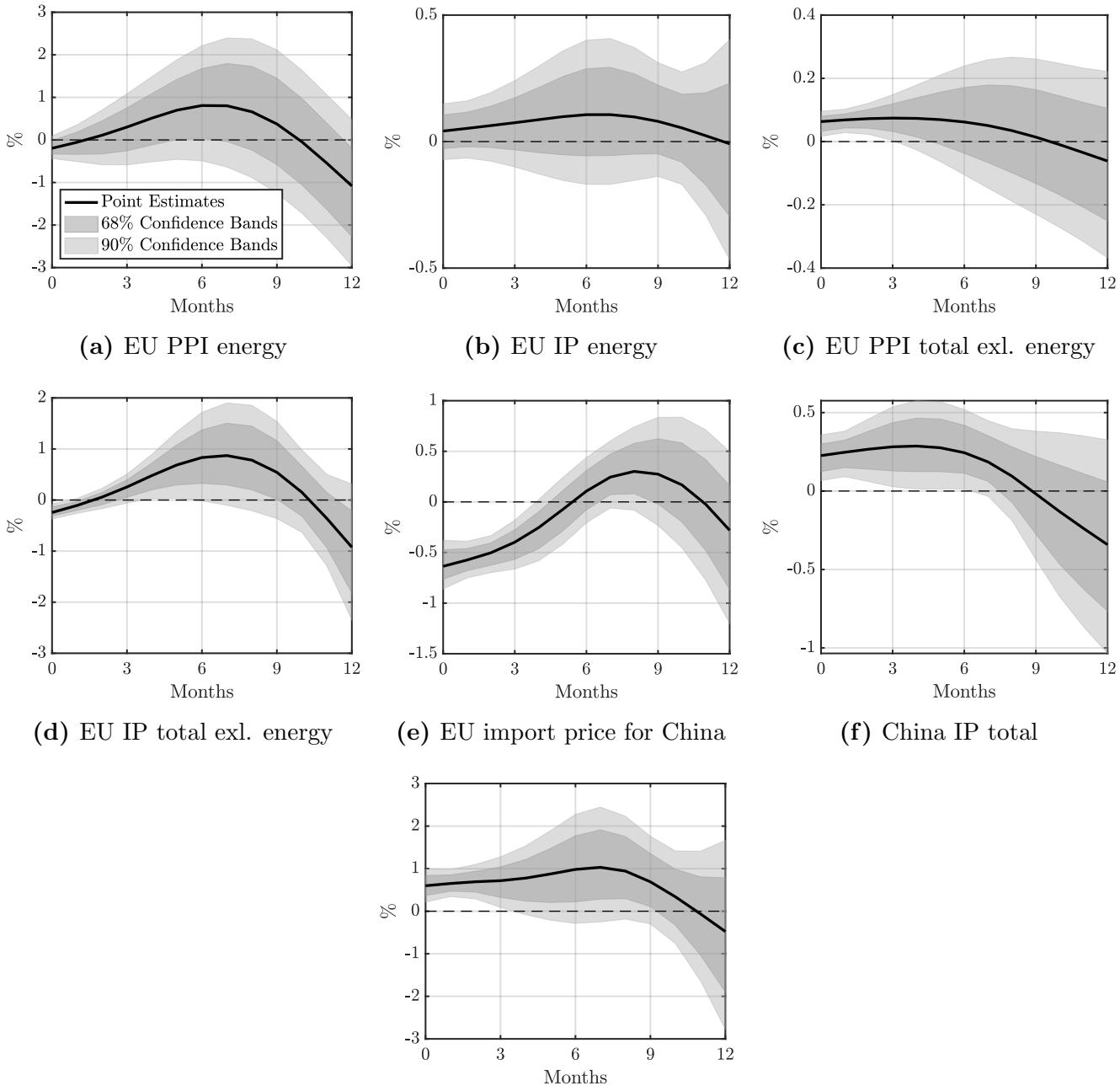
Figure 16: IRFs to a one-standard-deviation unexpected oil sanction intensity shock for the U.S. Economy: Propagation channels

Notes. The specifications follow the LP model outlined in Section 6.1, with two modifications: (i) two additional variables —China's crude oil import price and the U.S. import price for manufactured goods from China, averaged across NAICS sectors 31 to 33— are included, and (ii) total PPI and IP for the U.S. economy are replaced by PPI and IP for the energy and non-energy sectors. Black solid lines represent point estimates, and gray-shaded areas indicate the 68% and 90% confidence bands.

the LP model. As shown in Figure F.21 of Appendix F, during the first three months post-impact, the responses of IP for U.S. energy and non-energy sectors are closer to zero-response lines than in Panels 16b and 16d. This suggests the presence of a positive omitted variable bias, wherein lower import prices of Chinese inputs help attenuate short-term contractions in U.S. production.

In the medium term, as oil prices rebound (Panel 14d), the U.S. energy sector recovers sharply, reflected in rising IP after six months and mean-reverting PPI. Non-energy sectors also experience production gains, though PPI continues to decline due to sustained cost reductions from cheaper Chinese inputs (Panels 16c and 16f).

For the EU, the impact unfolds through two distinct channels. On one hand, rising Chinese demand for intermediate goods from the EU (Panel 17g), driven by expanding Chinese industrial



(a) EU PPI energy **(b)** EU IP energy **(c)** EU PPI total exl. energy

(d) EU IP total exl. energy **(e)** EU import price for China **(f)** China IP total

(g) China imports from EU

Figure 17: IRFs to a one-standard-deviation unexpected oil sanction intensity shock for the EU economy: Propagation channels

Notes. The specifications follow the LP model outlined in Section 6.1, with two modifications: (i) three additional variables —the EU import price for Chinese goods, China's total IP, and its total import value from the EU— are included, and (ii) total PPI and IP for the EU economy are replaced by PPI and IP for the energy and non-energy sectors. Black solid lines represent point estimates, and gray-shaded areas indicate the 68% and 90% confidence bands.

production (Panel 17f), supports strong demand-driven growth in the EU, creating inflationary pressure on PPI in non-energy sectors while stimulating production. On the other hand, lower

import prices for Chinese products (Panel 17e), resulting from declining oil prices and production costs in China (Panel 16e and Figure F.18 in Appendix F), generate strong supply-driven growth in the EU, exerting downward pressure on PPI in non-energy sectors while further boosting production. As a result, non-energy sectors experience moderate PPI increases (Panel 17c) alongside robust production growth (Panel 17d).

This growth in the EU non-energy sector propagates upstream, increasing energy demand and subsequently raising PPI (Panel 17a) and production (Panel 17b) in the EU energy sector despite rising energy costs.

In the medium term, as China's expansion slows down and production costs rebound, the EU faces reduced Chinese demand and loses the advantage of cheap intermediate inputs from China. Consequently, production in EU sectors contracts, and their prices revert to pre-impact levels.

Takeaways. Our results highlight that, in response to oil sanctions, the endogenous rise in dark shipping reallocates oil from sanctioning to non-sanctioning economies, limiting global oil price increases. This mechanism propagates through the global supply chain, boosting output in the EU, U.S., and China.

The key point is that China —whose input costs and production benefit from discounted dark-shipped oil— plays a pivotal role due to its central position in the global supply chain, acting both as an upstream supplier of inputs to the U.S. and EU and as a downstream importer of EU products. Dark-shipped oil fosters a supply-side, deflationary expansion in the U.S. by lowering the cost of intermediate inputs imported from China. Meanwhile, the EU experiences both supply- and demand-driven growth, benefiting from cheaper imported inputs and increased demand from China. This China-driven growth offsets the negative effects of constrained oil supply and rising oil prices, ultimately enabling dark shipping to generate an economic expansion in the EU.

7. Conclusion

This paper presents a novel multi-attribute ship clustering model for detecting dark shipping activities associated with sanctioned oil transport. The model allows us to document the distinctive features of dark shipping, identify geographical hotspots, and reveal systematic patterns of evasive behavior. Our findings indicate that dark ships comprise a substantial portion of the fleet, facilitating large-scale trade in sanctioned oil. From 2017 to 2023, an average of 9.3 million

metric tons of crude oil per month —about half of officially recorded global seaborne exports— was transported via dark ships. Our empirical analysis shows that increased exports of discounted dark-shipped oil offset the upward pressure on global oil prices stemming from the sanction-driven decline in recorded exports. We also develop a parsimonious theoretical framework to rationalize this finding.

Next, we link dark shipping to broader macroeconomic dynamics and changes in output and inflation across sanctioning and non-sanctioning economies. As a net oil exporter, the U.S. benefits from lower Chinese import prices, which create deflationary pressure and supply-driven growth, despite lower revenues for domestic producers. In contrast, the EU —an oil importer— faces higher energy costs but gains from rising Chinese demand and cheaper Chinese goods, fostering both demand- and supply-driven growth, with strong output and moderate inflation. China's access to discounted oil boosts its industrial production, amplifying the macroeconomic effects of sanctions and shaping outcomes in both the U.S. and the EU.

Several promising avenues for future research remain. First, modeling the global economy with input–output linkages and a micro-founded international oil market could shed further light on the differing responses of the U.S. and the EU to oil sanction shocks. Extending the analysis to production networks (as in Ghassibe, 2024 or Qiu et al., 2025) could clarify whether variations in sanction impacts stem mainly from spatial proximity (Redding and Sturm, 2008), higher trading costs (Xu et al., 2025), or production synergies (Fernández-Villaverde et al., 2021, 2024, 2025). Second, policy counterfactuals could help guide responses to the (un)intended effects of current sanction regimes, such as the EU's inflationary pressures from higher energy costs and rising Chinese demand. Finally, deeper integration of satellite imagery could improve validation — especially in identifying ship-to-ship transfers— and boost model accuracy. We plan to explore some of these directions in future work.

References

Anderson, J. E. and van Wincoop, E. (2003). Gravity With Gravitas: A Solution to the Border Puzzle. *American Economic Review*, 93(1):170—-192.

Bai, X., Fernández-Villaverde, J., Li, Y., and Zanetti, F. (2024). The Causal Effects of Global Supply Chain Disruptions on Macroeconomic Outcomes: Evidence and Theory. Working Paper 32098, National Bureau of Economic Research.

Bai, X., Fernández-Villaverde, J., Li, Y., and Zanetti, F. (2025). State Dependence of Monetary Policy During Global Supply Chain Disruptions. Working paper, University of Pennsylvania.

Barnichon, R. and Brownlees, C. (2019). Impulse Response Estimation by Smooth Local Projections. *Review of Economics and Statistics*, 101(3):522–530.

Baumeister, C. and Hamilton, J. D. (2019). Structural Interpretation of Vector Autoregressions with Incomplete Identification: Revisiting the Role of Oil Supply and Demand Shocks. *American Economic Review*, 109(5):1873–1910.

Behar, A. and Ritz, R. A. (2016). An Analysis of OPEC's Strategic Actions, US Shale Growth and the 2014 Oil Price Crash. Working Paper 2016/131, International Monetary Fund.

Bernabé, P., Gotlieb, A., Legeard, B., Marijan, D., Sem-Jacobsen, F. O., and Spieker, H. (2024). Detecting Intentional AIS Shutdown in Open Sea Maritime Surveillance Using Self-Supervised Deep Learning. *IEEE Transactions on Intelligent Transportation Systems*, 25(2):1166–1177.

Bjørnland, H. C., Nordvik, F. M., and Rohrer, M. (2021). Supply Flexibility in the Shale Patch: Evidence From North Dakota. *Journal of Applied Econometrics*, 36(3):273–292.

Bjørnland, H. C. and Skretting, J. (2024). The Shale Oil Boom and the US Economy: Spillovers and Time-Varying Effects. *Journal of Applied Econometrics*, 39(6):1000–1020.

Bornstein, G., Krusell, P., and Rebelo, S. (2023). A World Equilibrium Model of the Oil Market. *Review of Economic Studies*, 90(1):132–164.

Brancaccio, G., Kalouptsidi, M., and Papageorgiou, T. (2020). Geography, Transportation, and Endogenous Trade Costs. *Econometrica*, 88(2):657–691.

Brancaccio, G., Kalouptsidi, M., and Papageorgiou, T. (2024). Investment in Infrastructure and Trade: The Case of Ports. Working Paper 32503, National Bureau of Economic Research.

Cerdeiro, D. A., Komaromi, A., Liu, Y., and Saeed, M. (2020). World Seaborne Trade in Real Time: A Proof of Concept for Building AIS-Based Nowcasts From Scratch. Working Paper 2020/57, International Monetary Fund.

Dunn, J. and Leibovici, F. (2023). Navigating the Waves of Global Shipping: Drivers and Aggregate Implications. Working Paper 2023-002, Federal Reserve Bank of St. Louis.

Felbermayr, G., Morgan, T. C., Syropoulos, C., and Yotov, Y. V. (2024). Economic Sanctions: Stylized Facts and Quantitative Evidence. *Annual Review of Economics*. forthcoming.

Fernández-Villaverde, J., Mandelman, F., Yu, Y., and Zanetti, F. (2021). The "Matthew Effect" and Market Concentration: Search Complementarities and Monopsony Power. *Journal of Monetary Economics*, 121:62–90.

Fernández-Villaverde, J., Mandelman, F., Yu, Y., and Zanetti, F. (2025). Search Complementarities, Aggregate Fluctuations, and Fiscal Policy. *Review of Economic Studies*, page rdae053.

Fernández-Villaverde, J., Mineyama, T., and Song, D. (2025). Are We Fragmented Yet? Measuring Geopolitical Fragmentation and Its Causal Effect. Working Paper 32638, National Bureau of Economic Research.

Fernández-Villaverde, J., Yu, Y., and Zanetti, F. (2024). Technological Synergies, Heterogeneous Firms, and Idiosyncratic Volatility. Working Paper 32247, National Bureau of Economic Research.

Ghassibe, M. (2024). Endogenous Production Networks and Non-Linear Monetary Transmission. Working paper, CREi.

Ghironi, F., Kim, D., and Ozhan, G. K. (2024). International Economic Sanctions and Third-Country Effects. *IMF Economic Review*, 72(2):611–652.

Greenwood, R. and Hanson, S. G. (2015). Waves in Ship Prices and Investment. *Quarterly Journal of Economics*, 130(1):55–109.

Heiland, I., Moxnes, A., Ulltveit-Moe, K. H., and Zi, Y. (2019). Trade From Space: Shipping Networks and the Global Implications of Local Shocks. Discussion Paper 14193, Centre for Economic Policy Research.

Helpman, E., Melitz, M., and Rubinstein, Y. (2008). Estimating Trade Flows: Trading Partners and Trading Volumes. *Quarterly Journal of Economics*, 123(2):441–487.

Hilgenstock, B., Ribakova, E., Shapoval, N., Babina, T., Itskhoki, O., and Mironov, M. (2023). Russian Oil Exports Under International Sanctions. Working Paper 4430053, SSRN.

International Monetary Fund (2022). World Economic Outlook Update: Rising Caseloads, A Disrupted Recovery, and Higher Inflation. World Economic Outlook, International Monetary Fund.

Itskhoki, O. and Mukhin, D. (2022). Sanctions and the Exchange Rate. Working Paper 32247, National Bureau of Economic Research.

Johnson, S., Rachel, L., and Wolfram, C. (2023a). A Theory of Price Caps on Non-Renewable Resources. Working Paper 31347, National Bureau of Economic Research.

Johnson, S., Rachel, L., and Wolfram, C. (2023b). Design and Implementation of the Price Cap on Russian Oil Exports. *Journal of Comparative Economics*, 51(4):1244–1252.

Jordà, O. (2005). Estimation and Inference of Impulse Responses by Local Projections. *American Economic Review*, 95(1):161–182.

Kalouptsidi, M. (2014). Time to Build and Fluctuations in Bulk Shipping. *American Economic Review*, 104(2):564–608.

Känzig, D. R. (2021). The Macroeconomic Effects of Oil Supply News: Evidence From OPEC Announcements. *American Economic Review*, 111:1092–1125.

Kilian, L. (2009). Not All Oil Price Shocks Are Alike: Disentangling Demand and Supply Shocks in the Crude Oil Market. *American Economic Review*, 99(3):1053–69.

Kilian, L. and Murphy, D. P. (2012). Why Agnostic Sign Restrictions Are Not Enough: Understanding the Dynamics of Oil Market VAR Models. *Journal of the European Economic Association*, 10(5):1166–1188.

Kilian, L. and Murphy, D. P. (2014). The Role of Inventories and Speculative Trading in the Global Market for Crude Oil. *Journal of Applied Econometrics*, 29(3):454–478.

Kilian, L., Rapson, D., and Schipper, B. (2024). The Impact of the 2022 Oil Embargo and Price Cap on Russian Oil Prices. Working Paper 2401, Federal Reserve Bank of Dallas.

Komaromi, A., Cerdeiro, D. A., and Liu, Y. (2022). Supply Chains and Port Congestion Around the World. Working Paper 2022/59, International Monetary Fund.

Laudati, D. and Pesaran, M. H. (2023). Identifying the Effects of Sanctions on the Iranian Economy Using Newspaper Coverage. *Journal of Applied Econometrics*, 38(3):271–294.

Li, Y., Bai, X., Wang, Q., and Ma, Z. (2022). A Big Data Approach to Cargo Type Prediction and Its Implications for Oil Trade Estimation. *Transportation Research Part E: Logistics and Transportation Review*, 165:102831.

Lippi, F. and Nobili, A. (2012). Oil and the Macroeconomy: A Quantitative Structural Analysis. *Journal of the European Economic Association*, 10(5):1059–1083.

Lloyd's List Intelligence (2023). Shifty Shades of Grey: The Different Risk Profiles of the Dark Fleet Explained. Technical report, Lloyd's List Intelligence.

MacQueen, J. B. (1967). Some Methods for Classification and Analysis of Multivariate Observations. In Cam, L. M. L. and Neyman, J., editors, *Proceedings of the Fifth Berkeley Symposium on Mathematical Statistics and Probability*, volume 1, pages 281–297. University of California Press.

Melek, N., Plante, M., and Yücel, M. K. (2017). The U.S. Shale Oil Boom, the Oil Export Ban, and the Economy: A General Equilibrium Analysis. Working Paper 23818, National Bureau of Economic Research.

Newey, W. K. and West, K. D. (1987). A Simple, Positive Semi-definite, Heteroskedasticity and Autocorrelation Consistent Covariance Matrix. *Econometrica*, 55(3):703–708.

Office of Foreign Assets Control (2023). OFAC Guidance on Implementation of the Price Cap Policy for Crude Oil and Petroleum Products of Russian Federation Origin. Technical report, U.S. Department of the Treasury.

Paris MoU (2018). Explanatory Note – "White," "Grey" and "Black List". Technical report, Paris Memorandum of Understanding on Port State Control.

Prochazka, V., Adland, R., and Wolff, F.-C. (2019). Contracting Decisions in the Crude Oil Transportation Market: Evidence From Fixtures Matched With AIS Data. *Transportation Research Part A: Policy and Practice*, 130:37–53.

Qiu, Z., Wang, Y., Xu, L., and Zanetti, F. (2025). Monetary Policy in Open Economies with Production Networks. Discussion Paper 19828, Centre for Economic Policy Research.

Redding, S. J. and Sturm, D. M. (2008). The Costs of Remoteness: Evidence From German Division and Reunification. *American Economic Review*, 98(5):1766–1797.

S&P Global Market Intelligence (2023). Russia's Shadow Fleet – Understanding Its Size, Activity and Relationships. Technical report, S&P Global Market Intelligence.

UNCTAD (2022). Review of Maritime Transport 2022. Technical report, United Nations Conference on Trade and Development.

U.S. Department of State (2018). Background Briefing on U.S. Withdrawal From the Joint Comprehensive Plan of Action (JCPOA). Foreign Press Centers Briefing.

U.S. Department of State (2020). Sanctions Advisory for the Maritime Industry, Energy and Metals Sectors, and Related Communities. Technical report, U.S. Department of State, U.S. Department of the Treasury's Office of Foreign Assets Control, and U.S. Coast Guard.

U.S. Department of the Treasury (2019). Treasury Sanctions Venezuela's State-Owned Oil Company Petroleos de Venezuela, S.A. Office of Foreign Assets Control.

U.S. Department of the Treasury (2023). With Over 300 Sanctions, U.S. Targets Russia's Circumvention and Evasion, Military-Industrial Supply Chains, and Future Energy Revenues. Office of Foreign Assets Control.

U.S. Energy Information Administration (2024). Country Analysis Brief: World Oil Transit Chokepoints. Technical report, U.S. Energy Information Administration.

Verduzco-Bustos, G. and Zanetti, F. (2025). The Effects of Geopolitical Oil Price Shocks. Working paper, University of Oxford.

Xu, L., Yu, Y., and Zanetti, F. (2025). The Adoption and Termination of Suppliers Over the Business Cycle. *Journal of Monetary Economics*, 151:103730.

Online Appendices

Charting the Uncharted:
The (Un)Intended Consequences of Oil Sanctions and Dark Shipping

Jesús Fernández-Villaverde[†], *Yiliang Li*[§], *Le Xu*[◊], *Francesco Zanetti*[¶]

Contents

A A Multi-Attribute Ship Clustering Model for Dark Ship Identification **A-2**

A.1 Additional Data Sources A-3

A.2 Data Preprocessing and Trip Construction A-3

A.3 Feature Extraction and Trip Classification A-5

A.4 Dark Ship Identification A-15

B Predictive Performance of the Ship Clustering Model **A-16**

C Additional Dark Ship Identification Results **A-18**

D Details of Oil Sanctions on Iran, Syria, Venezuela, and Russia in 2017–2023 **A-24**

E Data Sources for LP Estimation **A-26**

F Robustness of LP Results **A-27**

F.1 Oil Market Variables Only A-27

F.2 Aggregate Dynamics A-30

F.3 Propagation Channels A-36

G Further Details on the Oil Market Model **A-42**

References for Appendices **A-43**

† Fernández-Villaverde: University of Pennsylvania, U.S. jesusfv@econ.upenn.edu. § Li: University of International Business and Economics, China. yiliang_li@uibe.edu.cn. ◊ Xu: Shanghai Jiao Tong University, China. lexu1@sjtu.edu.cn. ¶ Zanetti: University of Oxford, U.K. francesco.zanetti@economics.ox.ac.uk.

A. A Multi-Attribute Ship Clustering Model for Dark Ship Identification

Before detailing our ship clustering model, we provide a high-level overview of its main components and their interactions, as shown in Figure A.1.

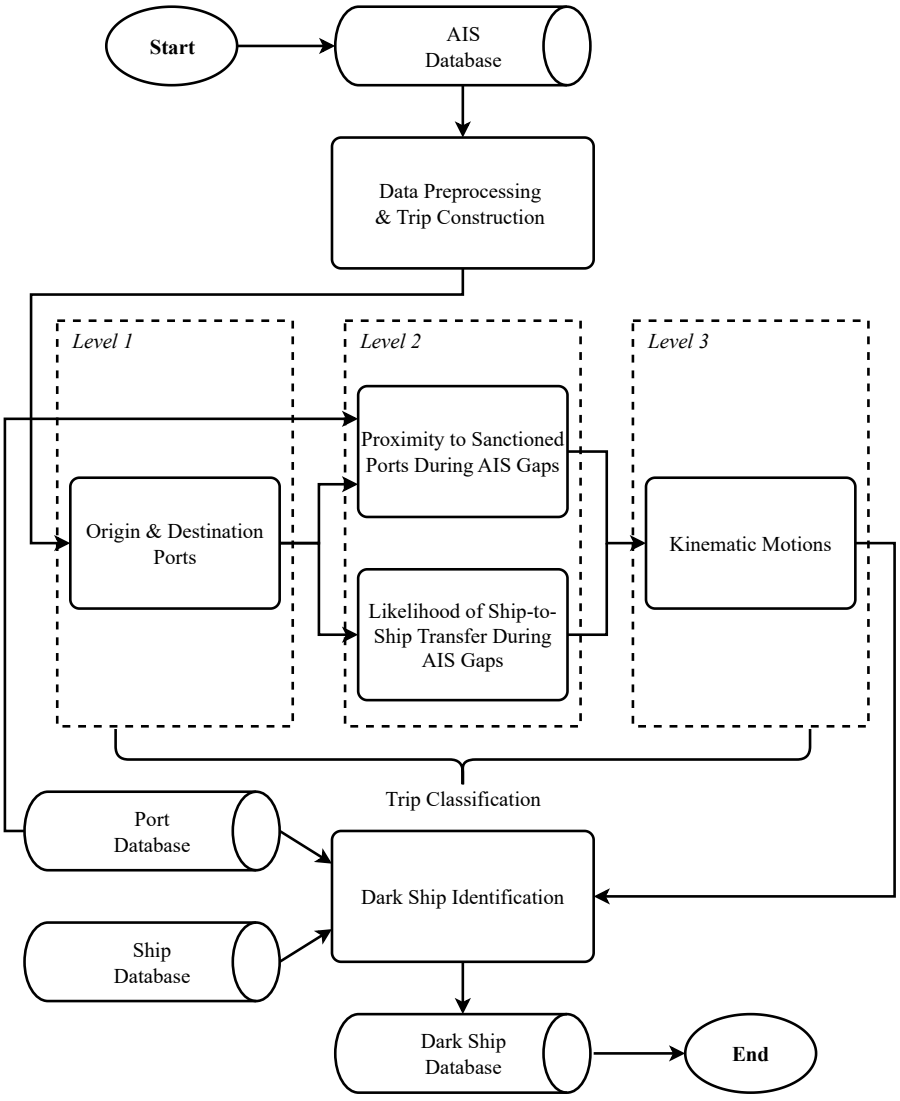


Figure A.1: Methodology overview

First, we preprocess the raw AIS data from the global crude oil tanker fleet (2017–2023) by removing anomalies and segmenting it into trips based on vessel position, speed, and port entry and exit patterns. This step also identifies trip start/end points, and idle trips.

Second, we apply a three-level trip classification process to assess: (i) whether the trip begins or ends at a sanctioned-country port; (ii) whether the vessel is near such a port during a prolonged AIS gap or near another ship with overlapping gaps, enabling potential unauthorized transfers; and (iii) whether its kinematic movements show abnormal patterns.

Third, we assign categorical suspicion scores to each trip and compute each vessel's average trip suspicion score and idle trip ratio. Combined with three features from ship and port databases —years of vessel usage, number of vessels owned by its operator, and flag state ranking— these metrics help identify dark oil tankers.

Finally, we estimate a k-means clustering model to classify ships as dark or white for each year in the sample period (MacQueen, 1967; Lloyd, 1982). The following sections provide further details.[1]

A.1. Additional Data Sources

Our algorithm analyzes four types of indicators: AIS signal gaps, vessel kinematics, vessel characteristics, and geographical information. AIS gaps and kinematics are derived from AIS data, our primary source (see Section 2.2). To improve robustness, we also include vessel-specific and geographical data.

Vessel data come mainly from the Seasearcher platform by Lloyd's List Intelligence. We focus on two attributes: vessel age and the number of ships owned by its commercial operator. We also use flag state rankings from the publicly available, annually updated Paris MoU List.[2]

Port data, sourced primarily from Lloyd's List, help segment continuous AIS records into trips for granular analysis. We use three port attributes: name, geographic coordinates (longitude and latitude), and country.

A.2. Data Preprocessing and Trip Construction

We begin by preprocessing AIS data and segmenting them into consecutive trips for each tanker, our basic unit of analysis. AIS data offer continuous vessel tracking but include noise from abnormal events, such as idling in port, repairs, and maintenance. Dividing AIS records into trip-

[1] Complete pseudocode and technical specifications for our multi-attribute ship clustering model are available upon request.

[2] See https://parismou.org/Statistics%26Current-Lists/white-grey-and-black-list (accessed July 3, 2024).

based units and extracting key features allow us to better capture vessel behavior and movement patterns (Yan et al., 2020; Li et al., 2022). This improves the distinction between normal and abnormal trips, providing more precise inputs for our clustering model.

Second, we filter out anomalous data by removing entries with draft values below zero or speeds above 20 knots. This threshold reflects normal tanker operations, as most vessels cruise well below this speed (Adland et al., 2020). Higher speeds usually signal AIS errors or abnormal events.[3]

Third, we identify port entries and exits by tracking changes in speed. A vessel enters a port if its speed drops from at least 1 knot to below 1 knot, and exits if it rises from below 1 knot to 1 knot or more. To retain only valid movements, we exclude cases near ports where speeds fluctuate due to congestion or cargo operations. We also drop port entries and exits separated by less than three hours, as these likely reflect noise rather than true port activity.

To identify entry and exit ports, our algorithm first locates ports geographically close to a vessel's entry point, defined by speed changes. It draws a 2-degree square (about 200 km) centered on the entry coordinates and selects ports within this area as candidates. The nearest port is then identified by calculating the distance (in kilometers) from the entry point to each candidate using the Haversine formula:

$$\begin{aligned} & D\left[\left(lon_{j,t}^{Ship}, lat_{j,t}^{Ship}\right), \left(lon_{p}^{Port}, lat_{p}^{Port}\right)\right] \\ & = 2R \arcsin\left[\sqrt{\sin^2\left(\frac{lat_{j,t}^{Ship} - lat_{p}^{Port}}{2}\right) + \cos\left(lat_{j,t}^{Ship}\right)\cos\left(lat_{p}^{Port}\right)\sin^2\left(\frac{lon_{j,t}^{Ship} - lon_{p}^{Port}}{2}\right)}\right], \end{aligned} \tag{A.1}$$

where $\left(lon_{j,t}^{Ship}, lat_{j,t}^{Ship}\right)$ and $\left(lon_{p}^{Port}, lat_{p}^{Port}\right)$ are the coordinates (in radians) of ship j at time t and port p, respectively, and $R = 6{,}371$ kilometers is Earth's radius.[4] The algorithm also removes repeated entries into the same port, keeping only the first, to eliminate redundancy and focus on meaningful movements.

Finally, the algorithm identifies and flags idle trips, defined as periods when a vessel's average speed stays at or below 1 knot for 14 consecutive days.[5]

[3]Some of these anomalous data points may reflect dark shipping behaviors. However, such suspicion is not grounded in widely accepted criteria used by authorities to identify dark shipping, such as those outlined in U.S. Department of State (2020). To ensure consistency and transparency, we adopt a presumption of innocence and rely exclusively on the explicit criteria outlined below to identify dark ships.

[4]If the nearest port is 50 kilometers or more from the entry point, the entry is deemed invalid.

[5]According to Clarksons' Shipping Intelligence Network, a vessel is considered idle if it maintains an average speed of 1 knot or less for at least 14 days, is not laid-up, under repair, or in storage, and undertakes no voyage

A.3. Feature Extraction and Trip Classification

Our next task is to distinguish between normal and abnormal trips, and then classify the abnormal ones. However, there is no standard definition of abnormality, as prior studies use different methods —such as detecting intentional AIS shutdowns (Bernabé et al., 2024) or identifying deviations in vessel movement patterns (Rong et al., 2024)— to capture suspicious ship behavior.

Thus, we develop a three-level trip classification process that extends features in the literature —such as direct involvement in transporting sanctioned oil via loading or unloading in sanctioned-country ports, and anomalies in vessel kinematics— while also leveraging AIS gap duration and transceiver-off locations. Specifically, we detect suspicious ship-to-ship transfers by analyzing the coordinates and timestamps of two vessels before and after overlapping AIS gaps. This approach relies solely on AIS data, avoiding the computational burden of methods that combine AIS with satellite imagery to detect unauthorized transfers (Rodger and Guida, 2022; Androjna et al., 2024; Ballinger, 2024).

With this trip classification process, we assign categorical suspicion scores to each trip and compute an average score for each vessel. The following sections provide a detailed examination of each level of the classification process.[6]

Level 1: Origin and Destination Ports

The first level of the trip classification process identifies trips directly linked to sanctioned countries by analyzing origin and destination ports. We focus on five oil-sanctioned nations: Iran, Syria, North Korea, Venezuela, and Russia. These countries were subject to major international sanctions restricting crude oil and petroleum trade during the 2017-2023 sample period. While four are oil exporters, we include North Korea due to Western sanctions on its oil imports. Table A.1 summarizes these sanctions.[7]

fixture activity. It must also avoid recording speeds above 1 knot for at least two consecutive days afterward. We apply only the first criterion, as the others require unavailable data. Results are robust to a 7-day threshold.

[6] We avoid inputting all features from the three levels into a single clustering model to prevent overfitting and preserve interpretability. Including too many diverse features at once could obscure the link between specific behaviors and their associated risks. By classifying trips at different levels, we gain a better understanding of the contribution of each feature set, enabling more targeted analysis of abnormal ship behavior.

[7] We exclude sanctions on Russia prior to 2022, as they mainly targeted specific companies and individuals, restricting access to Western technology, financing, and investment for oil exploration and production (Chupilkin et al., 2024). In contrast, post-2022 sanctions directly targeted Russian oil exports through import bans and price caps designed to reduce oil revenue. Table D.1 in Appendix D provides a detailed month-by-month breakdown of sanctions on Iran, Syria, Venezuela, and Russia.

Table A.1: Overview of oil export/import sanctions on key countries

Country	Sanctioning Parties	Timing	Details
Iran	U.S., European Union, Canada, etc.	Since 1995, intensified in 2012 and 2018	Sanctions targeting oil exports due to nuclear program
Syria	U.S., European Union, Canada, etc.	Since 2011	Prohibition on oil exports due to the Syrian civil war
North Korea	U.N. Security Council, U.S., European Union, etc.	Since 2017	Caps on oil and petroleum product imports due to nuclear program
Venezuela	U.S., European Union, Canada, etc.	Since 2019, intensified in 2020	Sanctions targeting PDVSA and oil embargo to pressure the government
Russia	U.S., European Union, U.K., Canada, etc.	Since 2022	Restrictions on oil exports due to the invasion of Ukraine

Our algorithm first flags trips departing from ports in sanctioned countries. If a trip originates at such a port, it is assigned a suspicion score (S^{Trip}) of 1 for its full duration. This flags high-risk trips early. Next, the algorithm checks for arrivals at ports in sanctioned countries. If a trip ends at such a port and has not already been flagged by origin, it also receives a score of 1. By analyzing both origin and destination, the algorithm captures all trips linked to sanctioned countries, regardless of direction.

We assess the suspicion level of each trip only after sanctions have been imposed on the relevant country, as there is no reason to suspect dark shipping of sanctioned oil before that point. For example, since Western sanctions on Venezuela began in 2019, trips to or from Venezuelan ports before then are not flagged as suspicious.[8]

While the first level of the trip classification process identifies trips linked to sanctioned countries, such trips are not necessarily conducted by dark ships. A white-listed vessel can legally transport oil for sanctioned countries if it complies with regulations. For instance, the tanker *Sino Star* (IMO: 9263693) called at St. Petersburg in early 2023 but complied with G7 price cap rules. Despite links to vessels engaged in dark shipping, *Sino Star* was not classified as part of the dark fleet, as there was no evidence of deceptive or evasive behavior (Lloyd's List Intelligence, 2023). This underscores the need for additional criteria —such as AIS data gaps and anomalies in kinematic movements— to assess trip suspicion more accurately.

[8]This condition also applies when calculating the port-based trip suspicion score in the second level of the trip classification process.

Level 2: AIS Data Gaps

The definition of dark ships varies across the literature, but two deceptive practices outlined by the U.S. Department of State (2020) are widely recognized: (i) disabling or manipulating a ship's AIS transceiver to obscure movements ("AIS spoofing"), and (ii) conducting ship-to-ship transfers, especially in high-risk zones for sanctions violations. Although AIS spoofing is hard to detect —a topic we examine later— our algorithm introduces a novel approach by assessing a vessel's proximity to suspicious ports during AIS gaps and evaluating the likelihood of unauthorized transfers when two ships are geographically close with overlapping gaps. By combining these indicators, our method improves the detection of potential sanctions evasion.

Direct visit to a suspicious port. We first analyze a vessel's proximity to ports in the five sanctioned countries during periods when its AIS transceiver is turned off. Such behavior often signals potential involvement in transporting oil for sanctioned nations. Our algorithm detects AIS data gaps by computing time differences between consecutive AIS observations for each vessel. To focus on suspicious rather than routine activity (e.g., idling in port, repairs, or maintenance), it filters out gaps occurring during port calls, isolating those more likely to reflect unauthorized behavior.

Next, the algorithm identifies particularly long AIS data gaps, defined as those exceeding the 99th percentile of time differences between consecutive signals for each vessel. These gaps are marked by start and end times, allowing the algorithm to isolate unaccounted periods that may involve sanctions evasion. After detecting prolonged gaps, it calculates the geographic distance between the vessel and the nearest port in a sanctioned country listed in Table A.1. The Haversine formula in Equation (A.1) ensures accuracy (see Figure 2a and Algorithm A.1).

The algorithm then calculates the average speed required for a vessel to reach and return from the suspicious port within the duration of the gap. The suspicion score for each long AIS gap is defined as one minus the percentile (divided by 100) of the required speed in the historical speed distribution for all vessels in the sample year. Lower required speeds make a visit to the suspicious port more plausible, and thus yield higher suspicion scores.

Finally, the algorithm assigns a suspicion score (S^{Port}) to each trip, based on the highest suspicion score from any long AIS gap within that trip. This score reflects the likelihood that the vessel transported oil for a sanctioned country while its AIS transceiver was off.

Algorithm A.1 Calculation of port-based trip suspicion scores

Inputs: $\boldsymbol{t}_j$: set of timestamps for ship $j \in \mathcal{J}$

$\left\{\left(lon_{j,t}^{Ship},\ lat_{j,t}^{Ship}\right)\right\}_{t\in\boldsymbol{t}_j}$: geographical coordinates of ship $j \in \mathcal{J}$

$\boldsymbol{s}_j = \{s_{j,t}\}_{t\in\boldsymbol{t}_j}$: speeds of ship $j \in \mathcal{J}$

$\boldsymbol{l}_j^{Trip} = \left\{l_{j,t}^{Trip}\right\}_{t\in\boldsymbol{t}_j}$: trip status labels for ship $j \in \mathcal{J}$

$\boldsymbol{l}_j^{Gap} = \left\{l_{j,t}^{Gap}\right\}_{t\in\boldsymbol{t}_j}$: long data gap status labels for ship $j \in \mathcal{J}$

$\left\{\left(lon_p^{Port},\ lat_p^{Port}\right)\right\}_{p\in\mathcal{P}}$: geographical coordinates of each port $p \in \mathcal{P}$

$\mathcal{P}^{Sanction} \subset \mathcal{P}$: set of ports in sanctioned countries

Outputs: $\boldsymbol{S}_j^{Port}$: set of port-based trip suspicion scores for each ship $j \in \mathcal{J}$

function PERCENTILE_OF_VALUE($\boldsymbol{s}$, $\bar{s}$)
  Sort $\boldsymbol{s}$ in ascending order
  $n \leftarrow$ length of $\boldsymbol{s}$
  $count \leftarrow$ number of elements in $\boldsymbol{s}$ where $s \leq \bar{s}$
  return $(count/n) \times 100$
end function
function CALCULATE_PORT_BASED_TRIP_SUSPICION_SCORES
  for all $j \in \mathcal{J}$ **do**
    for all long data gaps with start time t and end time $t^{\diamond}$ in $\boldsymbol{l}_j^{Gap}$ **do**
      Initialize $\boldsymbol{Dist} \leftarrow \{\}$
      for all $p \in \mathcal{P}^{Sanction}$ **do**
        $D_{j,t,p} \leftarrow \mathrm{D}\left[\left(lon_{j,t}^{Ship}, lat_{j,t}^{Ship}\right), \left(lon_p^{Port}, lat_p^{Port}\right)\right]$
        $D_{j,t^{\diamond},p} \leftarrow \mathrm{D}\left[\left(lon_{j,t^{\diamond}}^{Ship}, lat_{j,t^{\diamond}}^{Ship}\right), \left(lon_p^{Port}, lat_p^{Port}\right)\right]$
        $Dist_{j,p} \leftarrow D_{j,t,p} + D_{j,t^{\diamond},p}$
        $\boldsymbol{Dist} \leftarrow \boldsymbol{Dist} \cup \{Dist_{j,p}\}$
      end for
      $p^* \leftarrow \arg\min_{p\in\mathcal{P}^{Sanction}} \boldsymbol{Dist}$
      $\bar{s}_{j,t} \leftarrow Dist_{j,p^*}$/HOURS_DIFFERENCE$(t, t^{\diamond})$
      $S_{j,t} \leftarrow 1 -$ PERCENTILE_OF_VALUE $\left(\{\boldsymbol{s}_j\}_{j\in\mathcal{J}}, \bar{s}_{j,t}\right)/100$
      Store $S_{j,t}$
    end for
    for all trips with start time t and end time $t^{\S}$ in $\boldsymbol{l}_j^{Trip}$ **do**
      $S_{j,t^\star} \leftarrow \max_{t'\in[t,t^{\S}]} S_{j,t'}$
      for all $t' \in [t, t^{\S}]$ **do**
        $S_{j,t'}^{Port} \leftarrow S_{j,t^\star}$
      end for
    end for
  end for
end function

While prolonged AIS data gaps are central to our detection approach, relying solely on their frequency is insufficient to distinguish between white and dark ships. As shown in Figure A.2, the share of trips exhibiting such gaps does not differ significantly between the two groups across sample years. This highlights the importance of contextualizing AIS gaps, in particular, by incorporating geographic proximity to sanctioned ports and assessing the plausibility of a covert visit, as implemented in our algorithm.

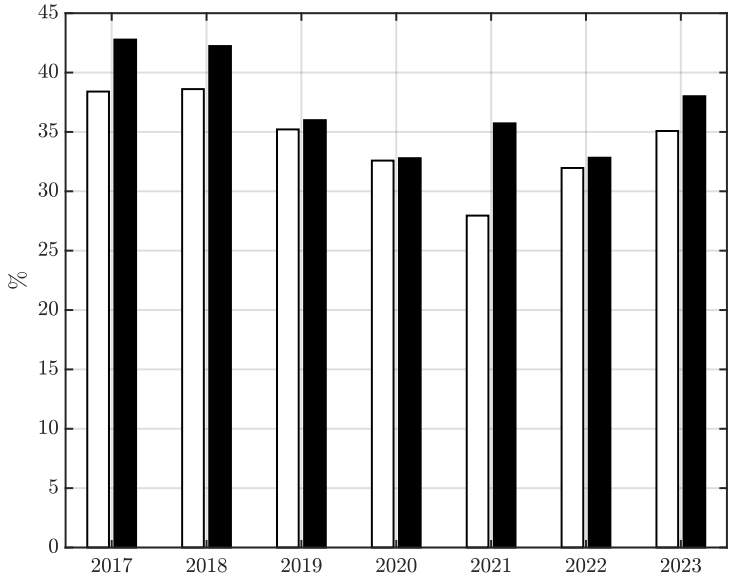


Figure A.2: Share of trips with prolonged AIS data gaps: White vs. dark ships

Notes. Shares of trips with prolonged AIS data gaps (defined as those exceeding the 99th percentile of time intervals between consecutive AIS signals for each vessel) undertaken by white and dark ships, as identified by our ship clustering model.

Ship-to-ship transfer. Identifying potential unauthorized ship-to-ship transfers during AIS data gaps involves several steps. The algorithm first converts each ship's heading, measured in degrees, into a vector.[9] This allows projection of the ship's travel path based on its coordinates and heading.

Next, the algorithm examines pairs of ships with overlapping AIS gaps to assess whether their paths could have intersected. It calculates the intersection point of their projected paths using the coordinates and headings recorded before signal loss (see Figure 2c and Algorithms A.2 and A.3). The intersection is considered valid only if both vessels could feasibly have reached it given their projected trajectories and speeds.

To refine the analysis, the algorithm calculates the temporal midpoint between overlapping AIS gaps for each ship pair. This midpoint helps determine the required average speed for each vessel to reach the intersection point from the last known location, potentially conduct an unauthorized ship-to-ship transfer involving sanctioned oil, and return to where its AIS signal reappears.[10]

[9] In AIS data, the heading indicates the direction of a vessel's bow relative to true north (0°).

[10] The algorithm assumes ships travel in straight lines and at constant speeds during AIS gaps, which may not reflect actual movements due to currents or operational changes. While effective at identifying potential intersection points, the method depends on the accuracy of pre-gap data. Incorporating models for path deviations or external data (e.g., satellite imagery) could improve detection. We leave these extensions for future work.

Algorithm A.2 Calculation of ship-to-ship transfer-based trip suspicion scores

Inputs: $\boldsymbol{t}_j$: set of timestamps for ship $j \in \mathcal{J}$
$\left\{\left(lon_{j,t}^{Ship},\ lat_{j,t}^{Ship}\right)\right\}_{t\in\boldsymbol{t}_j}$: geographical coordinates of ship $j \in \mathcal{J}$
$\boldsymbol{h}_j = \{h_{j,t}\}_{t\in\boldsymbol{t}_j}$: headings of ship $j \in \mathcal{J}$
$\boldsymbol{s}_j = \{s_{j,t}\}_{t\in\boldsymbol{t}_j}$: speeds of ship $j \in \mathcal{J}$
$\boldsymbol{l}_j^{Trip} = \left\{l_{j,t}^{Trip}\right\}_{t\in\boldsymbol{t}_j}$: trip status labels for ship $j \in \mathcal{J}$
$\boldsymbol{l}_j^{Gap} = \left\{l_{j,t}^{Gap}\right\}_{t\in\boldsymbol{t}_j}$: long data gap status labels for ship $j \in \mathcal{J}$

Outputs: $\boldsymbol{S}_j^{STS}$: set of ship-to-ship transfer-based trip suspicion scores for each ship $j \in \mathcal{J}$

function CALCULATE_STS_BASED_TRIP_SUSPICION_SCORES
  for all $j \in \mathcal{J}$ **do**
    for all long data gaps with start time t and end time $t^{\diamond}$ in $\boldsymbol{l}_j^{Gap}$ **do**
      Initialize $\bar{\boldsymbol{s}} \leftarrow \{\}$
      for all $j' \in \mathcal{J} \setminus \{j\}$ **do**
        for all long data gaps with start time $t^{\dagger}$ and end time $t^{\ddagger}$ in $\boldsymbol{l}_{j'}^{Gap}$ **do**
          if $t < t^{\ddagger}$ **and** $t^{\diamond} > t^{\dagger}$ **then**
            Compute intersection point $\left(lon^{Intersect}, lat^{Intersect}\right)$ of paths using positions at times t and $t^{\dagger}$, and headings $h_{j,t}$ and $h_{j',t^{\dagger}}$ ▷ *See Algorithm A.3*
            if intersection point exists **then**
              $t^{mid} \leftarrow \left(\max\{t, t^{\dagger}\} + \min\{t^{\diamond}, t^{\ddagger}\}\right)/2$
              Compute distances:
              $D_{j,t,Intersect} \leftarrow \mathrm{D}\left[\left(lon_{j,t}^{Ship}, lat_{j,t}^{Ship}\right), \left(lon^{Intersect}, lat^{Intersect}\right)\right]$
              $D_{j,t^{\diamond},Intersect} \leftarrow \mathrm{D}\left[\left(lon_{j,t^{\diamond}}^{Ship}, lat_{j,t^{\diamond}}^{Ship}\right), \left(lon^{Intersect}, lat^{Intersect}\right)\right]$
              Compute required average speed:
              $\bar{s}_{j,j'} \leftarrow \max\left\{D_{j,t,Intersect}/\left(t^{mid} - t\right),\ D_{j,t^{\diamond},Intersect}/\left(t^{\diamond} - t^{mid}\right)\right\}$
              $\bar{\boldsymbol{s}} \leftarrow \bar{\boldsymbol{s}} \cup \{\bar{s}_{j,j'}\}$
            end if
          end if
        end for
      end for
      if $\bar{\boldsymbol{s}} \neq \emptyset$ **then**
        $\bar{s}_{\min} \leftarrow \min \bar{\boldsymbol{s}}$
        $S_{j,t} \leftarrow 1 - \text{PERCENTILE_OF_VALUE}\left(\{\boldsymbol{s}_j\}_{j\in\mathcal{J}}, \bar{s}_{\min}\right)/100$
        Store $S_{j,t}$
      end if
    end for
    for all trips with start time t and end time $t^{\S}$ in $\boldsymbol{l}_j^{Trip}$ **do**
      $S_{j,t^{\star}} \leftarrow \max_{t'\in[t,t^{\S}]} S_{j,t'}$
      for all $t' \in [t, t^{\S}]$ **do**
        $S_{j,t'}^{STS} \leftarrow S_{j,t^{\star}}$
      end for
    end for
  end for
end function

The suspicion score is calculated as one minus the percentile (divided by 100) of the required average speed within the historical speed distribution for all vessels in the sample year. This score reflects the plausibility of the transfer: lower required speeds imply a higher likelihood of

Algorithm A.3 Calculation of intersection point of paths

Inputs: $\boldsymbol{t}_j$: set of timestamps for ship $j \in \mathcal{J}$
$\left\{\left(lon_{j,t}^{Ship},\ lat_{j,t}^{Ship}\right)\right\}_{t\in\boldsymbol{t}_j}$: geographical coordinates of ship $j \in \mathcal{J}$
$\boldsymbol{h}_j = \{h_{j,t}\}_{t\in\boldsymbol{t}_j}$: headings of ship $j \in \mathcal{J}$

Outputs: $\left(lon_{j,j'}^{Intersect},\ lat_{j,j'}^{Intersect}\right)$: intersection point of paths for ships $j, j' \in \mathcal{J}$

function HEADING_TO_VECTOR($h_{j,t}$)
  $\theta \leftarrow h_{j,t} \cdot \pi/180$
  $dx \leftarrow \sin(\theta)$
  $dy \leftarrow \cos(\theta)$
  return (dx, dy)
end function
function FIND_INTERSECTION($\left(lon_{j,t}^{Ship}, lat_{j,t}^{Ship}\right), \left(lon_{j',t'}^{Ship}, lat_{j',t'}^{Ship}\right), h_{j,t}, h_{j',t'}$)
  $(dx_j, dy_j) \leftarrow$ HEADING_TO_VECTOR$(h_{j,t})$
  $(dx_{j'}, dy_{j'}) \leftarrow$ HEADING_TO_VECTOR$(h_{j',t'})$
  $\Delta t \leftarrow \left[\left(lat_{j',t'}^{Ship} - lat_{j,t}^{Ship}\right) \cdot dx_{j'} - \left(lon_{j',t'}^{Ship} - lon_{j,t}^{Ship}\right) \cdot dy_{j'}\right] / \left(dx_{j'} \cdot dy_j - dy_{j'} \cdot dx_j\right)$
  $\Delta t' \leftarrow \left[\left(lat_{j',t'}^{Ship} - lat_{j,t}^{Ship}\right) \cdot dx_j - \left(lon_{j',t'}^{Ship} - lon_{j,t}^{Ship}\right) \cdot dy_j\right] / \left(dx_{j'} \cdot dy_j - dy_{j'} \cdot dx_j\right)$
  if $\Delta t \geq 0$ **and** $\Delta t' \geq 0$ **then** ▷ *Check if the intersection point is within a valid range*
    $lon_{j,j'}^{Intersect} \leftarrow lon_{j,t}^{Ship} + \Delta t \cdot dx_j$
    $lat_{j,j'}^{Intersect} \leftarrow lat_{j,t}^{Ship} + \Delta t \cdot dy_j$
    return $\left(lon_{j,j'}^{Intersect}, lat_{j,j'}^{Intersect}\right)$
  end if
end function

an unauthorized ship-to-ship transfer, and thus a higher suspicion score.

Finally, the algorithm assigns a suspicion score (S^{STS}) to each trip, based on the highest score among overlapping AIS gaps within that trip. This score reflects the likelihood that the vessel engaged in a suspicious ship-to-ship transfer of sanctioned oil while its AIS transceiver was off.

K-means clustering of trips. After normalizing the port-based and ship-to-ship transfer-based suspicion scores, the algorithm applies k-means clustering to categorize trips. As described in Algorithm A.4, it begins by randomly initializing centroids for two clusters. Each trip is then assigned to the nearest centroid based on squared Euclidean distance between its normalized scores and the centroids. The algorithm updates the centroids based on the current cluster memberships and repeats this process until the assignments stabilize.

After clustering, the final assignments determine whether a trip is classified as suspicious based on its port-based and ship-to-ship transfer-based suspicion scores (S^{Port} and S^{STS}). Trips with higher values for both scores are grouped and assigned a clustering label (c^{Gap}) of 1, indicating a greater likelihood of suspicious activity when the vessel disables its AIS transceiver.

Algorithm A.4 K-means clustering of trips

Inputs: $\boldsymbol{t}_j$: set of timestamps for ship $j \in \mathcal{J}$

$\boldsymbol{l}_j^{Trip} = \left\{ l_{j,t}^{Trip} \right\}_{t \in \boldsymbol{t}_j}$: trip status labels for ship $j \in \mathcal{J}$

$\boldsymbol{S}_j^{Port} = \left\{ S_{j,t}^{Port} \right\}_{t \in \boldsymbol{t}_j}$: port-based trip suspicion scores for ship $j \in \mathcal{J}$

$\boldsymbol{S}_j^{STS} = \left\{ S_{j,t}^{STS} \right\}_{t \in \boldsymbol{t}_j}$: ship-to-ship transfer-based trip suspicion scores for ship $j \in \mathcal{J}$

Outputs: $\left\{ \boldsymbol{\mu}_1^{Gap}, \boldsymbol{\mu}_2^{Gap} \right\}$: cluster centroids

$\left\{ c_{j,t}^{Gap} \mid j \in \mathcal{J},\ t \in \boldsymbol{t}_j,\ l_{j,t}^{Trip} = \text{Trip start} \right\}$: cluster assignments

function NORMALIZE($\mathcal{X}$)
  $\underline{x} \leftarrow \min \mathcal{X}$
  $\bar{x} \leftarrow \max \mathcal{X}$
  for $x_n \in \mathcal{X}$ **do**
    $x_n^{norm} \leftarrow (x_n - \underline{x}) \,/\, (\bar{x} - \underline{x})$
  end for
  return $\{x_n^{norm}\}_{n=1}^{|\mathcal{X}|}$
end function
function K-MEANS($\mathcal{X}$, K, I)
  Randomly initialize centroids $\boldsymbol{\mu}_1, \ldots, \boldsymbol{\mu}_K$
  for $i = 1$ to I **do**
    for $k = 1$ to K **do**
      $\mathscr{C}_k \leftarrow \{\}$
    end for
    for all $\boldsymbol{x}_n \in \mathcal{X}$ **do**
      $k^* \leftarrow \arg\min_k \|\boldsymbol{x}_n - \boldsymbol{\mu}_k\|^2$
      $\mathscr{C}_{k^*} \leftarrow \mathscr{C}_{k^*} \cup \{\boldsymbol{x}_n\}$
      $c_n \leftarrow k^*$
    end for
    $\boldsymbol{\mu}_{\text{old}} \leftarrow (\boldsymbol{\mu}_1, \ldots, \boldsymbol{\mu}_K)$
    for $k = 1$ to K **do**
      if $|\mathscr{C}_k| > 0$ **then**
        $\boldsymbol{\mu}_k \leftarrow \sum_{\boldsymbol{x}_n \in \mathscr{C}_k} \boldsymbol{x}_n / |\mathscr{C}_k|$
      end if
    end for
    if $\boldsymbol{\mu}_k = \boldsymbol{\mu}_{\text{old}}$ for all k **then**
      break
    end if
  end for
  return $\{\boldsymbol{\mu}_k\}_{k=1}^{K}$, $\{c_n\}_{n=1}^{|\mathcal{X}|}$
end function
$\boldsymbol{S}^{Port} \leftarrow \text{NORMALIZE}\left(\left\{ S_{j,t}^{Port} \mid j \in \mathcal{J}, t \in \boldsymbol{t}_j, l_{j,t}^{Trip} = \text{Trip start} \right\}\right)$
$\boldsymbol{S}^{STS} \leftarrow \text{NORMALIZE}\left(\left\{ S_{j,t}^{STS} \mid j \in \mathcal{J}, t \in \boldsymbol{t}_j, l_{j,t}^{Trip} = \text{Trip start} \right\}\right)$
$\left\{ \boldsymbol{\mu}_1^{Gap}, \boldsymbol{\mu}_2^{Gap} \right\}, \left\{ c_{j,t}^{Gap} \mid j \in \mathcal{J}, t \in \boldsymbol{t}_j, l_{j,t}^{Trip} = \text{Trip start} \right\} \leftarrow \text{K-MEANS}\left(\left\{ \boldsymbol{S}^{Port}, \boldsymbol{S}^{STS} \right\}, 2, 300\right)$

Level 3: Kinematic Movements

In the third level of the trip classification process, the algorithm analyzes anomalies in a ship's kinematic movements to detect suspicious behavior. It begins by computing three key metrics for each trip: average speed, speed standard deviation, and detour factor. These metrics are widely

used in the literature to identify abnormal ship behavior (Ristic et al., 2008; Rong et al., 2024) because these patterns may indicate evasive maneuvers or other suspicious activity.[11]

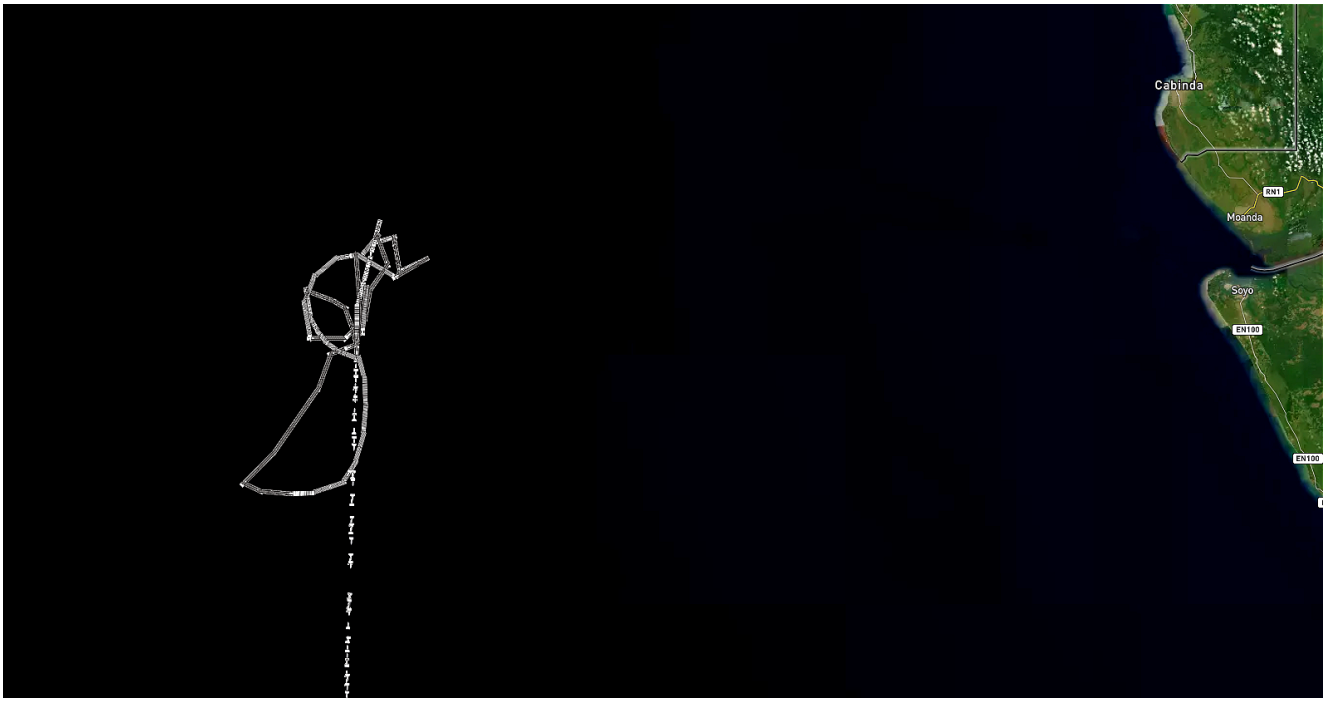


Figure A.3: Example of AIS spoofing

Notes. Trajectory of *Blazers* (IMO: 9307645), identified as a dark ship by our clustering algorithm. In early September 2023, the vessel spent an extended period drifting in ballast in international waters off the coast of Angola, indicating a high likelihood of AIS spoofing.

First, the algorithm calculates the vessel's average speed during each trip by summing recorded speeds and dividing by the number of measurements. Lower average speeds may indicate dark shipping activity, as vessels involved in covert operations often slow down to avoid detection or spend extended periods idling. This behavior may reflect waiting for favorable conditions or engaging in unauthorized ship-to-ship transfers.

Next, the algorithm calculates the standard deviation of the ship's speed, which captures the variability in velocity. A high standard deviation may reflect erratic movement, potentially signaling attempts to avoid detection or engage in unauthorized activity.

In addition to these speed metrics, the algorithm computes the detour factor (DF^{Trip}), which compares the actual path taken by the vessel to the direct route between the trip's start and end

[11] These features also help detect AIS spoofing, as spoofed signals often exhibit inconsistencies in movement (Triebert et al., 2023; Lloyd's List Intelligence, 2024a,b). For example, abnormal speed variation or unusual detours from typical routes (Figure A.3) can suggest data manipulation.

points, as defined in Equation (A.2):

$$DF_j^{\text{Trip}} = \frac{\sum_{n=1}^{N-1} D\left[\left(lon_{j,n}^{\text{Ship}}, lat_{j,n}^{\text{Ship}}\right), \left(lon_{j,n+1}^{\text{Ship}}, lat_{j,n+1}^{\text{Ship}}\right)\right]}{D\left[\left(lon_{j,1}^{\text{Ship}}, lat_{j,1}^{\text{Ship}}\right), \left(lon_{j,N}^{\text{Ship}}, lat_{j,N}^{\text{Ship}}\right)\right]}, \tag{A.2}$$

where $\left(lon_{j,n}^{\text{Ship}}, lat_{j,n}^{\text{Ship}}\right)$ are the n-th coordinates of ship j in radians. The Haversine formula is used to calculate the geographical distance between each pair of coordinates. A detour factor greater than one indicates that the vessel deviated from the direct route, which may be consistent with deceptive shipping practices (U.S. Department of State, 2020; Rong et al., 2024).

After computing these metrics, the algorithm normalizes the values to place them on a comparable scale. The normalized metrics are then input into a k-means clustering algorithm, which groups the trips into two clusters: one representing typical kinematic behavior and the other representing anomalous behavior. The algorithm iteratively updates the clusters until the centroids converge, ensuring stable and accurate classification.

Subsequently, clustering labels ($c^{\text{Kinematic}}$) are reassigned to reflect the level of suspicion associated with each trip based on kinematic patterns. Trips with lower average speeds, greater speed variability, and larger detour factors are grouped and assigned a label of 1, indicating potential involvement in dark shipping activity.

Finally, the clustering results from the second and third levels of the trip classification process allow us to assign categorical suspicion scores (S^{Trip}) to each trip based on anomalies identified in both prolonged AIS data gaps and kinematic movements. For each vessel, the algorithm checks whether any of its trips exhibit anomalies in both dimensions.[12]

If both clustering levels flag a trip as abnormal (i.e., $c^{\text{Gap}} = 1$ and $c^{\text{Kinematic}} = 1$), the trip is assigned a suspicion score of 1, indicating a high likelihood of dark shipping activity. If neither level detects anomalies, the trip receives a score of 0. If only one level flags an anomaly, a moderate score of 0.5 is assigned to reflect partial abnormality.

After assigning suspicion scores to individual trips, the algorithm computes the average trip suspicion score ($\bar{S}^{\text{Trip}}$) for each vessel by summing the scores across all trips and dividing by the total number of trips. This average provides an overall measure of the vessel's involvement in the dark shipping of sanctioned oil.

[12] Trip suspicion scores are assigned only to trips that were not already flagged. As noted earlier, trips that start or end at a port in a sanctioned country receive a suspicion score (S^{Trip}) of 1 in the first classification level.

A.4. Dark Ship Identification

The three-level trip classification process provides a comprehensive analysis of vessel travel patterns and movement dynamics. The resulting average trip suspicion score and idle trip ratio, defined as the fraction of trips classified as idle, serve as key indicators for identifying dark ships.[13]

Additional vessel-specific indicators are incorporated to capture vessel characteristics more comprehensively. We consider three key features: the vessel's years in service, the number of vessels owned by its commercial operator, and its flag state ranking, as defined in the Paris MoU List (Paris MoU, 2018).

Older vessels are more likely to engage in dark shipping, as they are typically near the end of their service life and hold lower residual value for operators (Miller, 2023). This reduces the financial risk associated with seizure or decommissioning, making such vessels more attractive for unauthorized activity. Likewise, ships owned by smaller commercial operators may face less regulatory scrutiny and possess fewer compliance resources, increasing the likelihood of participation in dark shipping (Lloyd's List Intelligence, 2023). In contrast, larger operators face greater reputational and financial exposure, which discourages their involvement.

A vessel's flag state ranking also provides insight into its regulatory environment, as ships registered under higher-risk flags are more likely to engage in non-compliant activities, as discussed in Section 2.4 of the main text.

After normalizing the five selected features, the algorithm applies the k-means clustering method to classify vessels into two groups: those with a higher likelihood of engaging in dark shipping and those with lower risk. The algorithm then reassigns clustering labels, adjusting the weight assigned to the number of vessels an operator owns. A smaller fleet size is associated with a higher suspicion, ensuring that vessels operated by entities with fewer compliance resources or facing less scrutiny are more likely to be flagged as high risk. Vessels in the high-suspicion cluster are labeled as dark ships, while those in the lower-risk cluster are classified as white ships.

[13] The idle trip ratio functions similarly to average vessel speed in detecting anomalies in kinematic movements. Dark ships often remain idle for extended periods to facilitate unauthorized ship-to-ship transfers, evade detection, or operate beyond regulatory oversight.

B. Predictive Performance of the Ship Clustering Model

In this appendix, we evaluate the predictive performance of our clustering model by comparing its identification of dark ships with external classifications across different years. As shown in Table B.1, our model agrees with these external classifications 83.3% of the time. Of course, there is no guarantee that these external classifications are more accurate than ours. In fact, our method may outperform them by relying on systematic, reproducible criteria rather than fragmented or proprietary information.

In any case, this result demonstrates that vessel-specific characteristics, combined with AIS-derived travel patterns and movement dynamics, can effectively identify dark ships without requiring proprietary or high-cost data sources such as insurance records (Lloyd's List Intelligence, 2023), ownership structures (S&P Global Market Intelligence, 2023), or satellite imagery (Triebert et al., 2023).

We also compare the performance of our model to that of a naive benchmark, which relies solely on vessel-specific characteristics —years of usage, the number of vessels owned by the ship's commercial operator, and its flag state ranking— to classify dark ships. A comparison of the last two columns in Table B.1 reveals that incorporating trip-level AIS data improves identification accuracy by more than 28%.

Additionally, we validate our approach using the Technique for Order Preference by Similarity to Ideal Solution (TOPSIS), developed by Hwang and Yoon (1981), to rank oil tankers based on the same features used in our clustering model. This method offers a more granular assessment of each vessel's likelihood of engaging in dark shipping. Rankings are available upon request and provide strong support for our findings.

Table B.1: Evaluation of model performance against external sources and a naive model

IMO	Source	Suspicion Years	Model Predictions	
			Full Model	Vessel-Specific Features Only
9182291	Lloyd's List Intelligence (2023)	2022, 2023	2022, 2023	2022, 2023
9224271	Lloyd's List Intelligence (2023)	2022, 2023	2022, 2023	N/A
9176993	Lloyd's List Intelligence (2023)	2021, 2022, 2023	2021	2021
9131357	Lloyd's List Intelligence (2023)	2022, 2023	2022, 2023	2022, 2023
9183295	Lloyd's List Intelligence (2023)	2021, 2022, 2023	2021, 2022, 2023	2021, 2022, 2023
9258521	Lloyd's List Intelligence (2023)	2022, 2023	2022, 2023	2022, 2023
9230969	Lloyd's List Intelligence (2023)	2022, 2023	2022, 2023	N/A
9307645	Lloyd's List Intelligence (2024a)	2023	2023	2023
9242118	Lloyd's List Intelligence (2024b)	2021, 2023	2021, 2023	N/A
9251274	S&P Global Market Intelligence (2023)	2022, 2023	2022, 2023	2022, 2023
9310147	S&P Global Market Intelligence (2023)	2022, 2023	2022, 2023	2022, 2023
9410870	S&P Global Market Intelligence (2023)	2022, 2023	N/A	N/A
9322827	S&P Global Market Intelligence (2023)	2021, 2022, 2023	2022	N/A
9235892	Triebert et al. (2023)	2023	2023	N/A
9249324	Triebert et al. (2023)	2023	2023	N/A
9259745	Triebert et al. (2023)	2023	2023	2023
9259733	Triebert et al. (2023)	2023	2023	2023
9157765	Meade (2023)	2021, 2022, 2023	2021, 2022, 2023	2021, 2022, 2023
9194127	Wijaya (2022)	2022	N/A	N/A
9304667	Wijaya (2022)	2022	2022	2022
9179701	Wijaya (2022)	2022	2022	2022
9255880	Wijaya (2022)	2022	2022	2022
9236353	Wijaya (2022)	2022	2022	N/A
9231767	Wijaya (2022)	2022	2022	N/A
9233208	Wijaya (2022)	2022	2022	N/A
		Summary		
		Total (Ship, Year)	42	42
		Identified (Ship, Year)	35 (83.3%)	23 (54.8%)
		Unidentified (Ship, Year)	7 (16.7%)	19 (45.2%)

Notes. The vessel with IMO number 9176993 lacks AIS data for 2022 and 2023, the years in which external sources classify it as a dark ship. "N/A" indicates instances where a vessel is not identified as dark in years when external sources do classify it as such. The vessel-specific features used in the analysis include years in service, the number of vessels owned by its commercial operator, and its flag state ranking.

C. Additional Dark Ship Identification Results

To show compelling validation of our model's effectiveness in detecting covert shipping activities, Figure C.1 presents three additional illustrations in which dark ships identified by our clustering algorithm are tracked using satellite imagery. These vessels either visited ports in sanctioned countries directly or conducted unauthorized ship-to-ship transfers during prolonged AIS data gaps.



(a) *C.Galaxy* (IMO: 9404924), Kharg Island (Iran), November 18, 2020

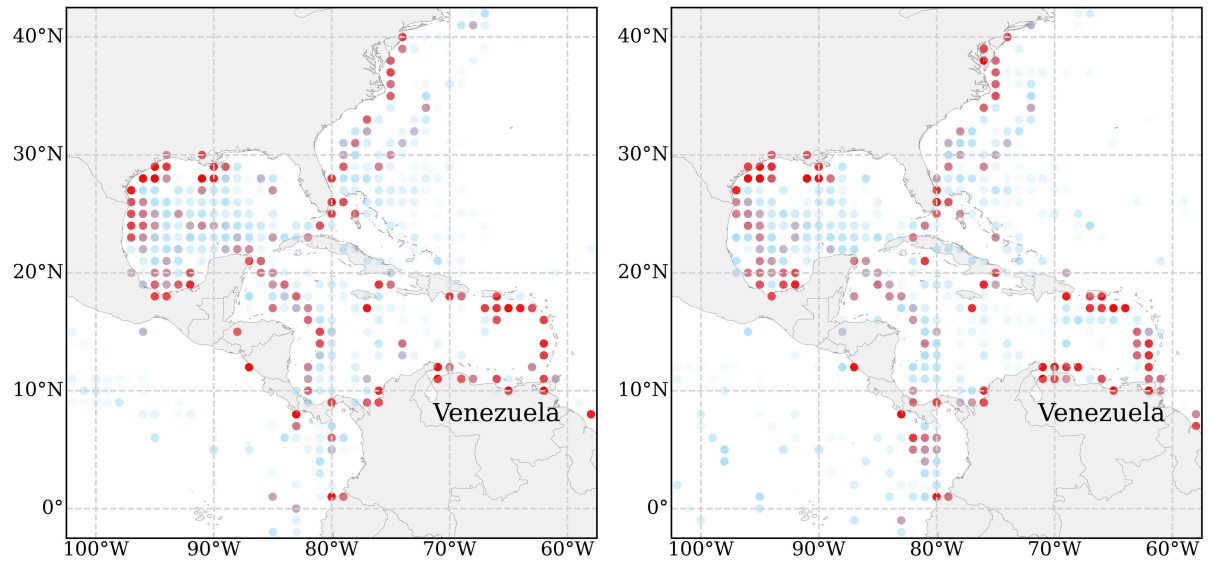
(b) *Azuron* (IMO: 9589750), Kozmino (Russia), December 7, 2023

(c) *Panda* (IMO: 9284582) & *Elka Parana* (IMO: 9625724), Gibraltar, March 15, 2023

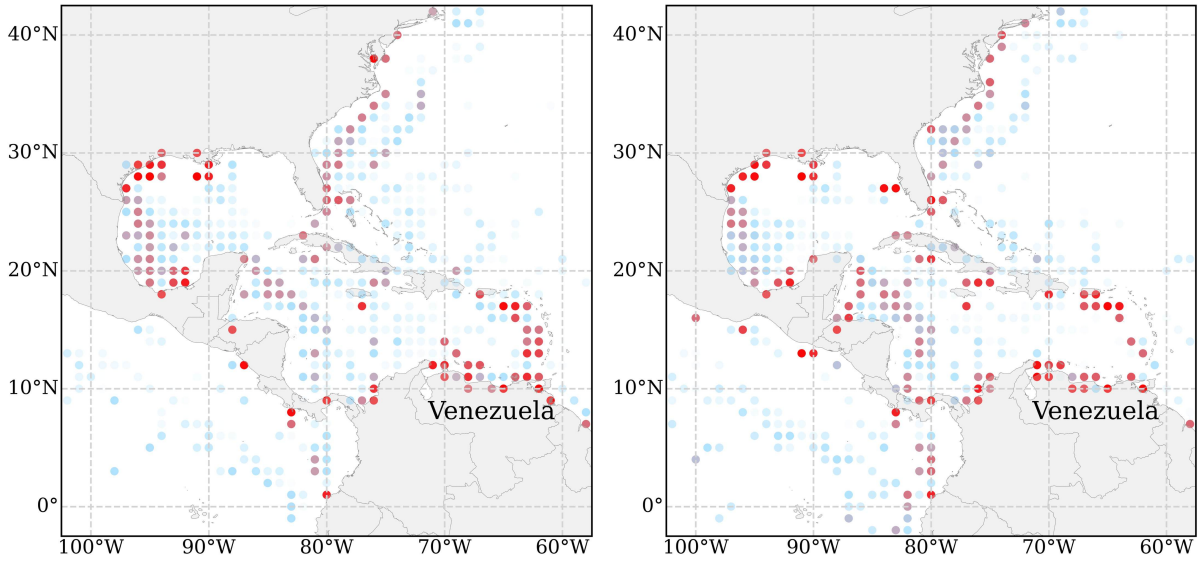
Figure C.1: Satellite imagery capturing dark ships during prolonged AIS data gaps

Notes. Panel C.1a shows satellite imagery of the identified dark ship *C. Galaxy* (IMO: 9404924) at Kharg Island, Iran, on November 18, 2020, during a period when its AIS transceiver was turned off. Panel C.1b presents imagery of the dark ship *Azuron* (IMO: 9589750) visiting Kozmino, Russia, on December 7, 2023, again while its AIS signal was disabled. Panel C.1c captures an unauthorized ship-to-ship transfer near Gibraltar on March 15, 2023, between *Panda* (IMO: 9284582) and *Elka Parana* (IMO: 9625724), both operating with their AIS transceivers turned off. The white dashed boxes highlight the identified dark ships.

Figures C.2 to C.4 illustrate the concentration of direct vessel visits to suspicious ports in Venezuela and in Russia near the Black Sea and the Baltic Sea during periods not covered in the main text.



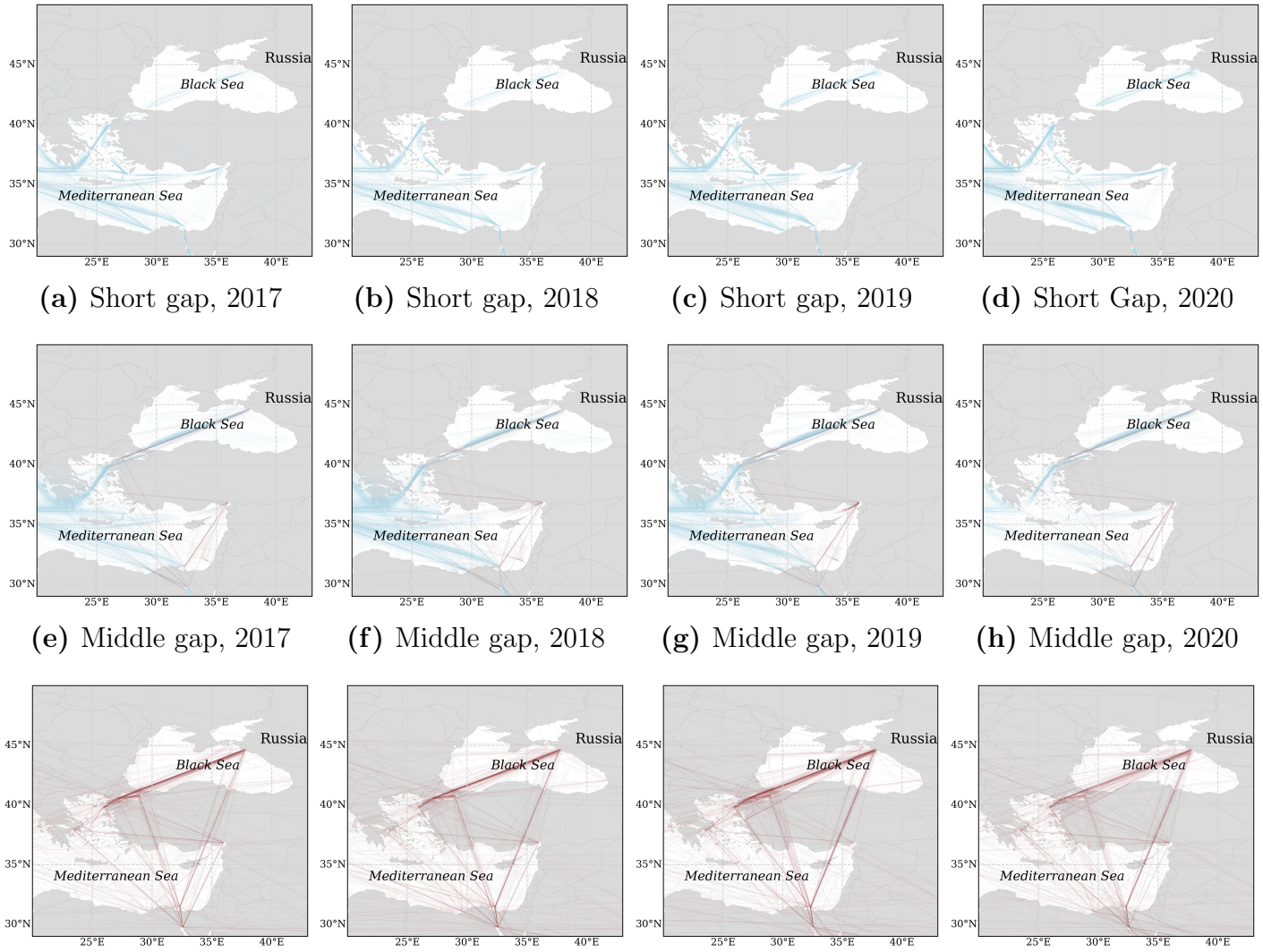
(a) 2020 **(b)** 2021



(c) 2022 **(d)** 2023

Figure C.2: Geographical concentration of dark shipping activities near Venezuela: 2020–2023

Notes. The color scheme and chromatic intensity are consistent with those used in Figure 5 of the main text.



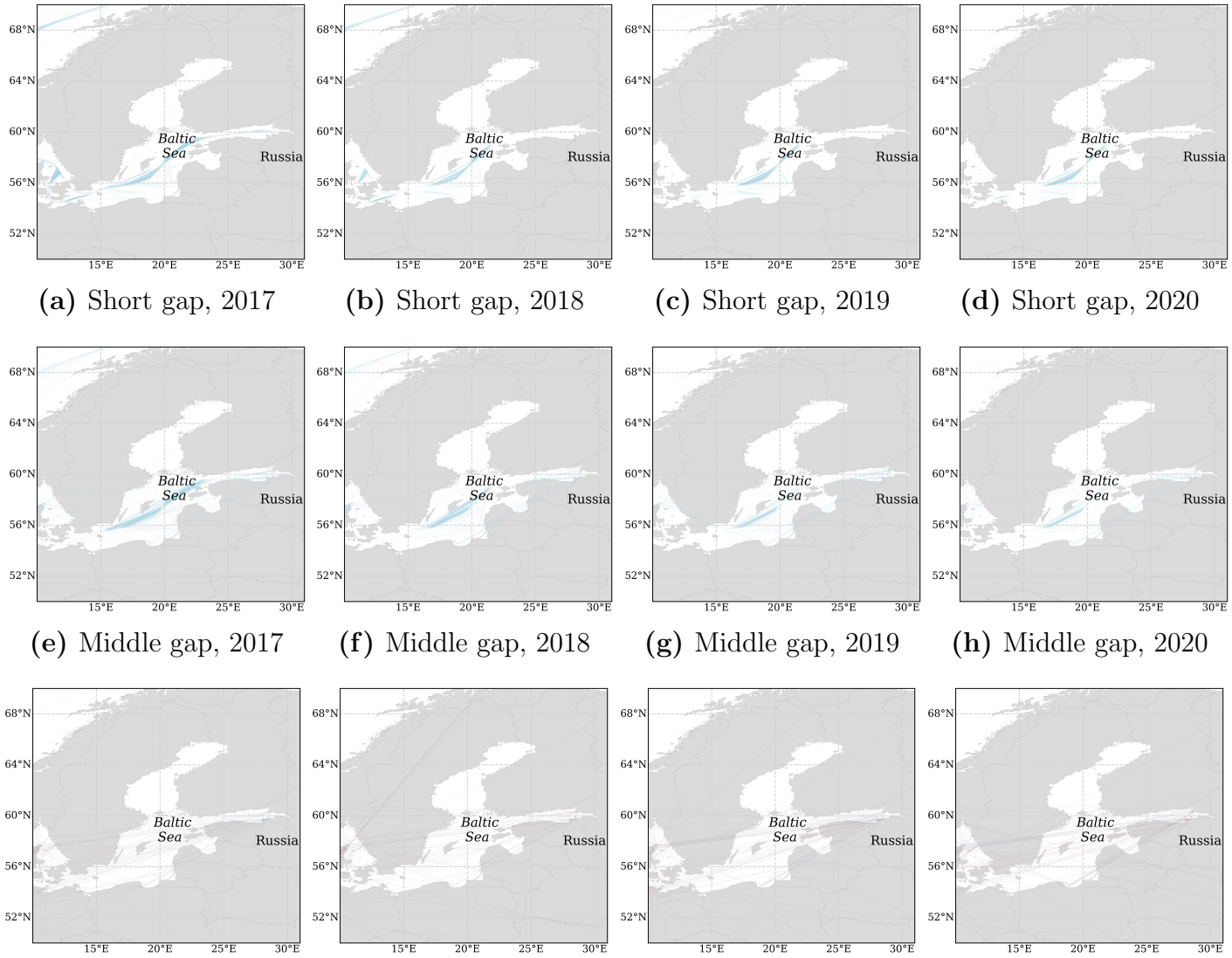
(a) Short gap, 2017 **(b)** Short gap, 2018 **(c)** Short gap, 2019 **(d)** Short Gap, 2020

(e) Middle gap, 2017 **(f)** Middle gap, 2018 **(g)** Middle gap, 2019 **(h)** Middle gap, 2020

(i) Long gap, 2017 **(j)** Long gap, 2018 **(k)** Long gap, 2019 **(l)** Long gap, 2020

Figure C.3: Geographical concentration of dark shipping activities in the Black Sea: 2017–2020

Notes. The color scheme and chromatic intensity are consistent with those used in Figure 6 of the main text.



(a) Short gap, 2017 **(b)** Short gap, 2018 **(c)** Short gap, 2019 **(d)** Short gap, 2020

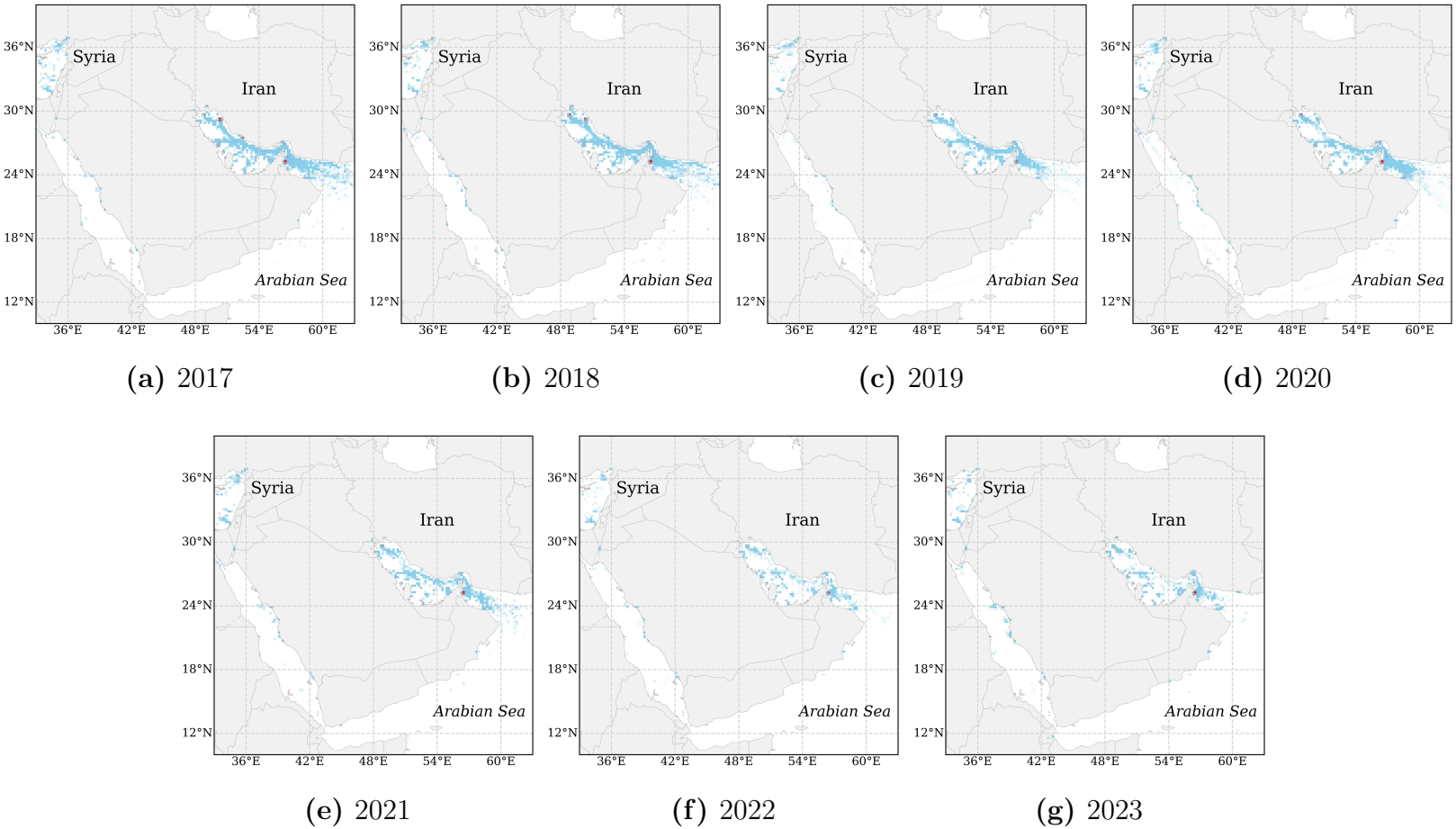
(e) Middle gap, 2017 **(f)** Middle gap, 2018 **(g)** Middle gap, 2019 **(h)** Middle gap, 2020

(i) Long gap, 2017 **(j)** Long gap, 2018 **(k)** Long gap, 2019 **(l)** Long gap, 2020

Figure C.4: Geographical concentration of dark shipping activities in the Baltic Sea: 2017–2020

Notes. The color scheme and chromatic intensity are consistent with those used in Figure 7 for the main text.

Figure C.5 shows dark shipping activity near Iran from 2017 to 2023. Notably, the number of trips with AIS gaps declined substantially after 2021, as indicated by the lower density of colored points, although suspicion scores remained high, particularly near the Strait of Hormuz.



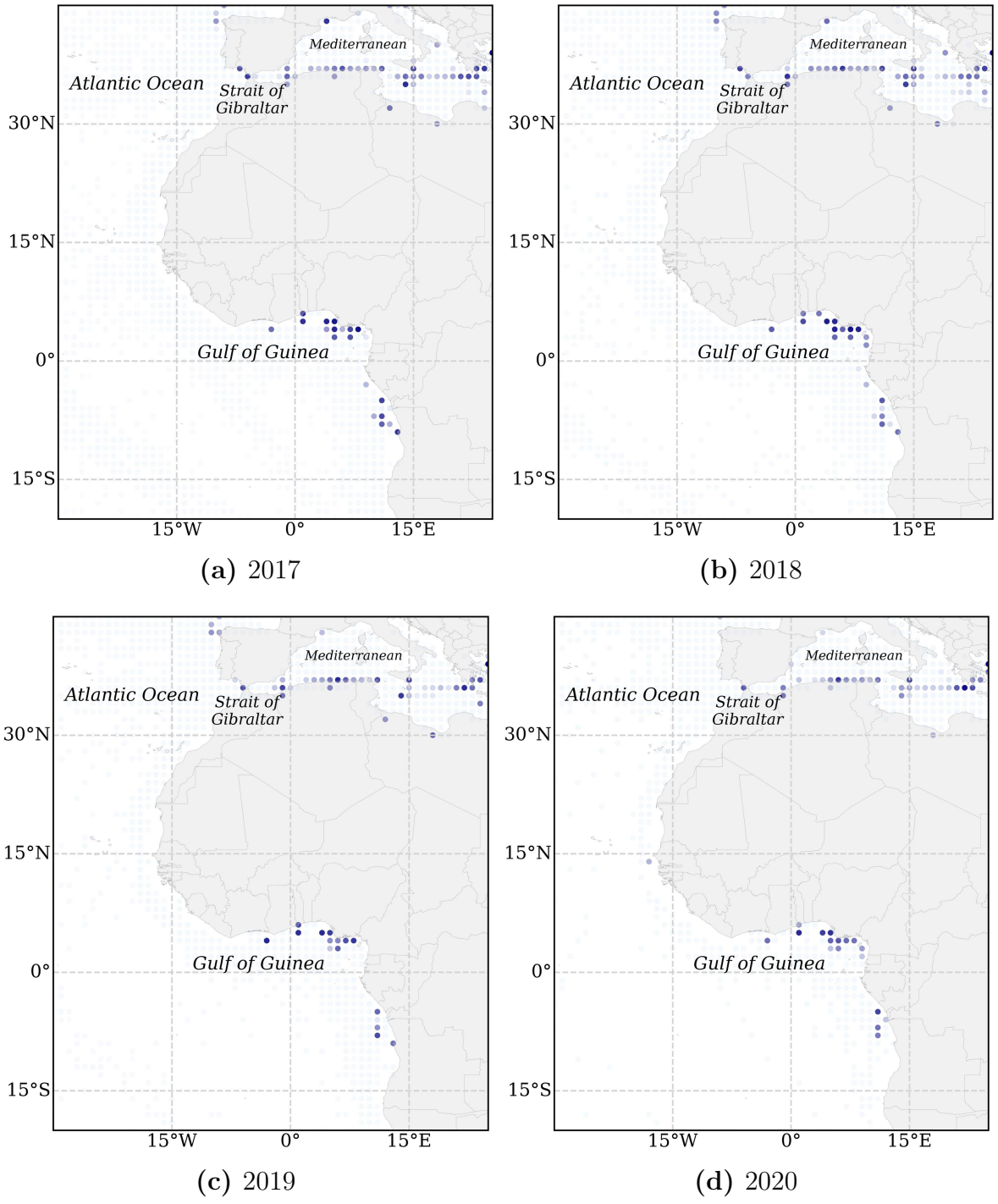
(a) 2017 **(b)** 2018 **(c)** 2019 **(d)** 2020

(e) 2021 **(f)** 2022 **(g)** 2023

Figure C.5: Geographical concentration of dark shipping activities near Iran: 2017–2023

Notes. Each colored point represents a 0.2-degree geographical square containing at least one last recorded data point before a vessel disables its AIS transceiver. The chromatic intensity reflects the cumulative port-based trip suspicion scores associated with these points within each square.

Figure C.6 presents the concentration of suspicious ship-to-ship transfers near West Africa and Gibraltar during years not covered in the main text.



(a) 2017 **(b)** 2018

(c) 2019 **(d)** 2020

Figure C.6: Geographical concentration of dark shipping activities near the Strait of Gibraltar and the Gulf of Guinea: 2017–2020

Notes. The colored points and chromatic intensity follow the same format as in Figure 8 of the main text.

D. Details of Oil Sanctions on Iran, Syria, Venezuela, and Russia in 2017–2023

Table D.1: Details of oil-related sanctions on Iran, Syria, Venezuela, and Russia during 2017–2023

Date	Sanctioning Parties	Sanctioned Party	Brief Details of the Sanction
May-17	European Union	Syria	Extended oil embargo and sanctions against Syria until June 2018 due to ongoing repression.
May-18	European Union	Syria	Extended oil embargo and sanctions against Syria until June 2019.
May-18	United States	Iran	Announced withdrawal from JCPOA; planned to reimpose sanctions on Iran's oil exports and energy sector.
Nov-18	United States	Iran	Re-imposed sanctions targeting Iran's oil exports, banking, and shipping; aimed to reduce Iran's oil revenue.
Nov-18	United States	Syria	Sanctioned entities involved in transporting Iranian oil to Syria.
Jan-19	United States	Venezuela	Imposed sanctions on PDVSA to cut off Venezuela's main revenue source.
Apr-19	United States	Venezuela	Expanded sanctions to entities transporting Venezuelan oil to Cuba; imposed restrictions on vessels and shipping companies.
May-19	European Union	Syria	Renewed oil embargo and sanctions against Syria until June 2020.
May-19	United States	Iran	Ended SREs allowing import of Iranian oil without sanctions; aimed to reduce Iran's oil exports to zero.
May-20	European Union	Syria	Extended oil embargo and sanctions against Syria until June 2021.
Jun-20	United States	Syria	Implemented Caesar Act; expanded sanctions on Syrian government and oil sector; targeted foreign entities aiding Syria's oil industry.
Aug-20	United States	Iran	Sanctioned entities facilitating oil shipments from Iran; aimed at disrupting Iran's oil exports.
Aug-20	United States	Syria	Sanctioned entities receiving oil shipments from Iran; intended to cut off oil supplies to Syria.
Mar-21	United States	Iran	Imposed sanctions on entities involved in sale and transport of Iranian petrochemical products, including companies in China and UAE.
May-21	European Union	Syria	Extended oil embargo and sanctions against Syria until June 2022.
Mar-22	United States	Russia	Banned imports of Russian crude oil, LNG, and coal in response to invasion of Ukraine.
Mar-22	United Kingdom	Russia	Announced phase-out of Russian oil imports by end of 2022.
May-22	European Union	Syria	Extended oil embargo and sanctions against Syria until June 2023.
Jun-22	United States	Russia	Imposed sanctions on Russian maritime entities to restrict transport of oil.
Jun-22	Canada	Russia	Banned imports of certain petroleum products; prohibited export of goods related to oil exploration and production.
Jun-22	European Union	Russia	Implemented ban on imports of Russian crude oil and refined petroleum products, with limited exceptions.
Oct-22	European Union	Russia	Adopted 8th sanctions package, including price cap on maritime transport of Russian oil.
Dec-22	EU, G7, Australia	Russia	Agreed on price cap of $60-per-barrel on Russian crude oil exports effective from 5 Dec 2022.
Jan-23	European Union	Russia	Prolonged economic sanctions, including ban on import or transfer of seaborne crude oil and certain petroleum products from Russia to EU.
Feb-23	EU, G7, Australia	Russia	Extended price cap mechanism to include Russian refined petroleum products, setting separate price caps.
Mar-23	United States	Iran	Sanctioned companies facilitating sale and shipment of Iranian petrochemical products and petroleum.
May-23	European Union	Syria	Extended oil embargo and sanctions against Syria until June 2024.
Jun-23	European Union	Russia	Adopted 11th sanctions package; prohibited transit of goods via Russia and tightened export restrictions on crude oil and petroleum products.
Sep-23	United States	Russia	Imposed sanctions on additional Russian energy companies and individuals involved in the energy sector.
Nov-23	United States	Iran	Escalated sanctions enforcement on unauthorized Iranian oil exports; lawmakers introduced 'SHIP Act' to strengthen measures.
Dec-23	United States	Russia	Imposed further sanctions on entities and vessels violating oil price cap, especially those engaging in deceptive practices.
Dec-23	European Union	Russia	Adopted 12th sanctions package; enforced oil price cap and prohibited import of liquefied propane from Russia.

Notes. We treat the European Union (EU) as a single sanctioning entity and count its measures accordingly. For the $60-per-barrel price cap on Russian crude oil exports introduced in December 2022, as well as the extended price cap mechanism implemented in February 2023, the sanctioning parties included the EU, Canada, Japan, the United Kingdom, the United States, and Australia. Accordingly, we assign a sanction intensity value of 6 to each of these two measures.

Table D.2: Status of oil-related sanctions as of December 2023

Sanctioned Country	**Updates Since Imposition**	**Still in Place as of 31 December 2023?**
Iran	2018 re-imposition of U.S. oil sanctions remained in force; no EU or UN sunset clauses were triggered during 2017–2023.	Yes
Syria	EU sanctions renewed annually in May; most recently extended to 1 June 2024.	Yes
Venezuela	Core PDVSA designation (E.O. 13857) was never revoked. A six-month General License 44 (October 2023) temporarily suspended parts of the oil and gas restrictions; it did not cancel the underlying sanctions and was explicitly time-limited.	Yes
Russia	Sanction packages from March 2022 to December 2023 were cumulative; none were repealed during 2023. EU and G7 reviews in 2023 confirmed continuation.	Yes

Notes. The sanction status information reflects public sources as of May 6, 2025. "Still in place" indicates whether the oil-related sanctions listed in Table D.1 remained formally in effect as of December 31, 2023, regardless of any temporary suspensions or exemptions.

E. Data Sources for LP Estimation

Table E.1 summarizes the data used in the LP estimation, including their sources and any construction or adjustment procedures. Additional datasets used for robustness checks are described later.

Table E.1: Data sources and description

Variable	Mnemonic/Series Key	Source	Notes on Construction/Adjustment
Global Oil Markets and Aggregate Dynamics			
Oil Sanction Intensity Index	N/A	Various Sources	Constructed from a dataset of oil-related sanctions (Table A.1).
Recorded World Seaborne Oil Exports	N/A	UN Comtrade	Extracted using HS code 2709 and manually seasonally adjusted.
Oil Exports by Dark Ships	N/A	AIS	Derived from dark ship identification and manually seasonally adjusted.
Brent Spot Price	MCOILBRENTEU	FRED	Manually seasonally adjusted.
WTI Spot Price	WTISPLC	FRED	Manually seasonally adjusted.
U.S. PPI Total	PPIFIS	FRED	Raw series obtained directly from FRED.
U.S. IP Total	INDPRO	FRED	Raw series obtained directly from FRED.
EU PPI Total	STS.M.I9.N.PRON.NS0020.4.000	Eurostat	Manually seasonally adjusted.
EU IP Total	STS.M.I9.Y.PROD.NS0020.4.000	Eurostat	Raw series obtained directly from Eurostat.
Propagation Channels			
U.S. PPI Energy	PPIDES	FRED	Raw series obtained directly from FRED.
U.S. IP Energy	IPB50089S	FRED	Raw series obtained directly from FRED.
U.S. PPI Total Exl. Energy	WPSFD49107	FRED	Raw series obtained directly from FRED.
U.S. IP Total Exl. Energy	IPX5001ES	FRED	Raw series obtained directly from FRED.
China Oil Import Price	N/A	National Bureau of Statistics of China	Manually seasonally adjusted.
U.S. Import Price for China, NAICS 31	COCHNZ31	FRED	Manually seasonally adjusted.
U.S. Import Price for China, NAICS 32	COCHNZ32	FRED	Manually seasonally adjusted.
U.S. Import Price for China, NAICS 33	COCHNZ33	FRED	Manually seasonally adjusted.
EU PPI Energy	STS.M.I9.N.PRON.NS0090.4.000	Eurostat	Manually seasonally adjusted.
EU IP Energy	STS.M.I9.Y.PROD.NS0090.4.000	Eurostat	Raw series obtained directly from Eurostat.
EU PPI Total Exl. Energy	STS.M.I9.N.PRON.NS0021.4.000	Eurostat	Manually seasonally adjusted.
EU IP Total Exl. Energy	STS.M.I9.Y.PROD.NS0021.4.000	Eurostat	Raw series obtained directly from Eurostat.
EU Import Price for China	ext_st_eu27_2020sitc	Eurostat	Raw series obtained directly from Eurostat.
China IP Total	N/A	National Bureau of Statistics of China	Constructed from the month-on-month IP growth rate.
China Total Import Value From EU	N/A	General Administration of Customs of China	Manually seasonally adjusted.

F. Robustness of LP Results

F.1. Oil Market Variables Only

Figures F.1 to F.5 present impulse response functions (IRFs) to an unexpected oil sanction intensity shock on global oil exports and prices. The IRFs are estimated using the LP model in Equation (3) under five alternative specifications: (i) extending the lag length to four; (ii) including a linear trend; (iii) replacing the Brent spot price with the WTI spot price; (iv) restricting the sample to January 2017–November 2022, ending just before the $60-per-barrel price cap on Russian crude took effect; and (v) using a simplified sanction intensity index defined as:

$$SANCTION_t^{Simple} = \begin{cases} 1, & \text{if } N_t > 0; \\ 0, & \text{if } N_t = 0, \end{cases} \tag{F.1}$$

where N_t denotes the number of new oil-related sanctions imposed by Western authorities on Iran, Syria, Venezuela, or Russia in month t. Compared to the baseline results in Figure 11, the IRFs remain largely unchanged.

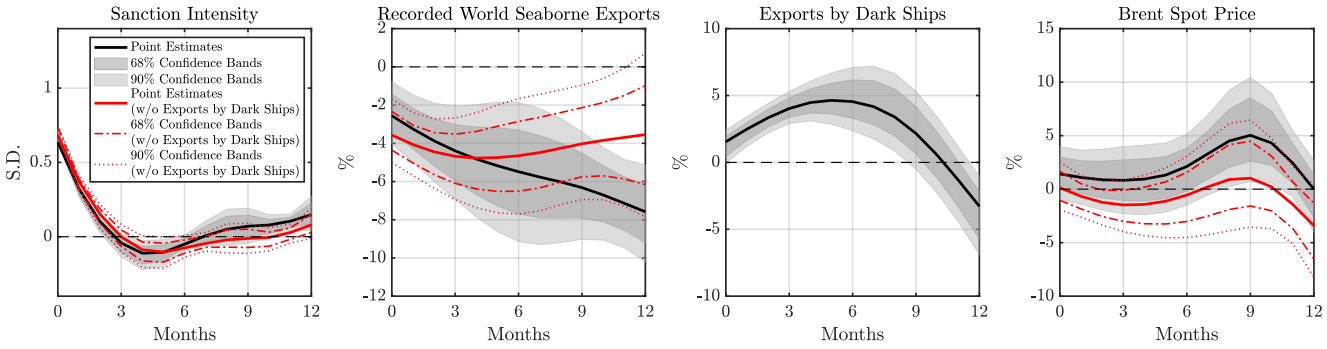


Figure F.1: IRFs to a one-standard-deviation oil sanction intensity shock for global oil exports and prices: $L = 4$

Notes. The IRFs are estimated using the same specifications as in Figure 11, except that the lag length is extended to 4. Black solid lines show the responses from the 4-variable LP model, with gray-shaded areas indicating the 68% and 90% confidence bands. Red solid lines represent the responses from the counterfactual 3-variable LP model, with red dash-dotted and dotted lines indicating the corresponding 68% and 90% confidence bands.

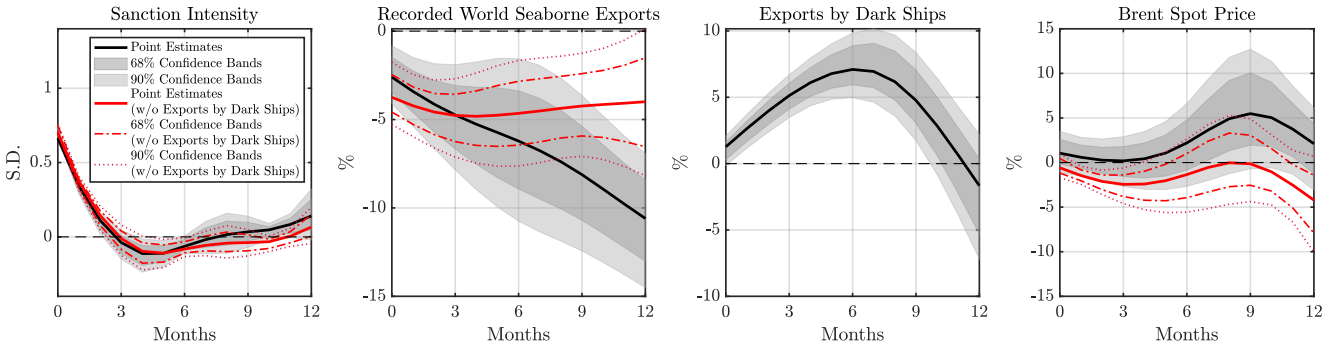


Figure F.2: IRFs to a one-standard-deviationa oil sanction intensity shock for global oil exports and prices: Linear trend

Notes. The IRFs are estimated using the same specifications as in Figure 11, except that a linear trend is included. Black solid lines show the responses from the baseline 4-variable LP model, with gray-shaded areas indicating the 68% and 90% confidence bands. Red solid lines represent the responses from the counterfactual 3-variable model, with red dash-dotted and dotted lines indicating the corresponding 68% and 90% bands.

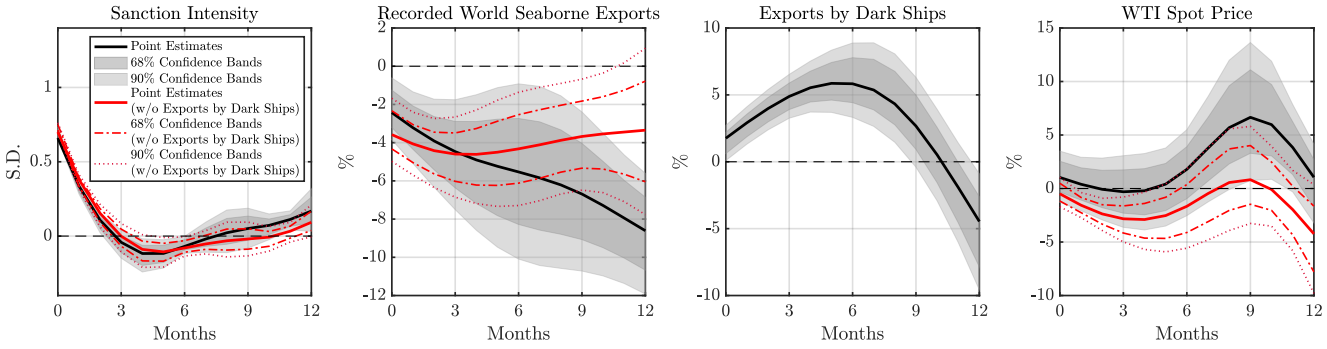


Figure F.3: IRFs to a one-standard-deviation oil sanction intensity shock for global oil exports and prices: WTI spot price

Notes. The IRFs are computed using the same specifications as in Figure 11, replacing the Brent spot price with the WTI spot price. Black solid lines show the responses from the 4-variable LP model, with gray-shaded areas denoting the 68% and 90% confidence bands. Red solid lines indicate responses from the counterfactual 3-variable model, with red dash-dotted and dotted lines marking the respective confidence bands.

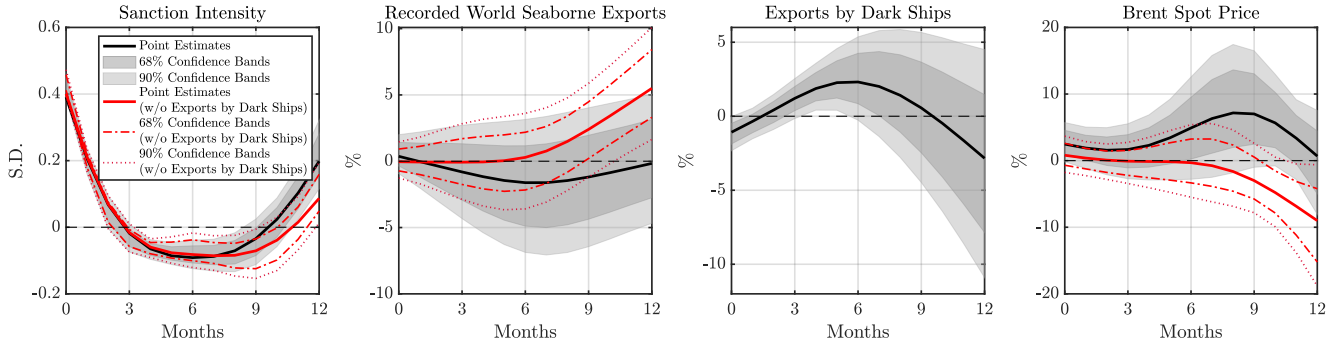


Figure F.4: IRFs to a one-standard-deviation oil sanction intensity shock for global oil exports and prices: January 2017–November 2022, before price cap on Russian oil

Notes. The IRFs are computed using the same specifications as in Figure 11, but restricting the estimation sample to January 2017–November 2022. Black solid lines show responses from the 4-variable LP model, with gray-shaded areas denoting the 68% and 90% confidence bands. Red solid lines represent responses from the counterfactual 3-variable model, with red dash-dotted and dotted lines indicating the respective confidence bands.

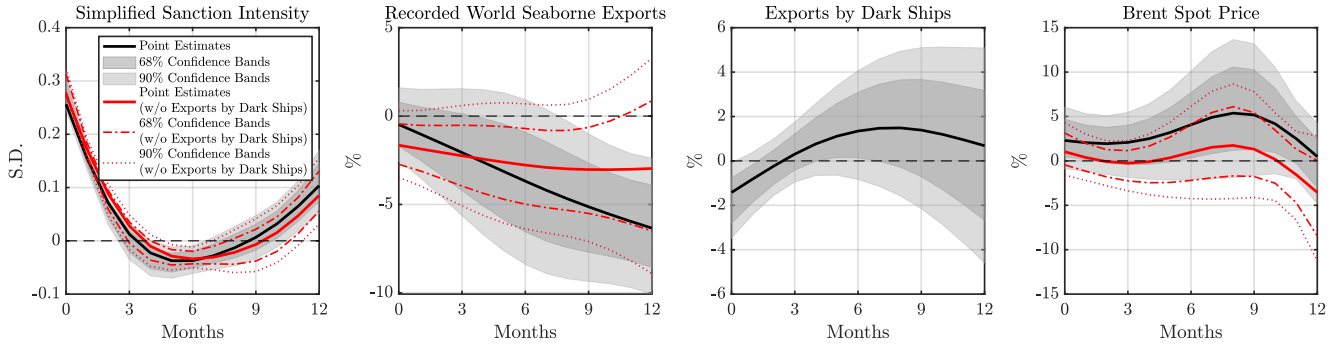


Figure F.5: IRFs to a one-standard-deviation oil sanction intensity shock for global oil exports and prices: Simplified sanction intensity index

Notes. The IRFs are computed using the same specifications as in Figure 11 for both the baseline 4-variable and counterfactual 3-variable LP models, except that a simplified sanction intensity index (defined in Equation (F.1)) is used. Black solid lines show responses from the 4-variable model, with gray-shaded areas denoting 68% and 90% confidence bands. Red solid lines represent the 3-variable model, with red dash-dotted and dotted lines indicating the respective confidence bands.

F.2. Aggregate Dynamics

Figures F.6 and F.7 present IRFs to an unexpected oil sanction intensity shock for the U.S. and EU economies, incorporating four lags of the endogenous variables in the LP specification. Figures F.8 and F.9 show IRFs estimated with both a constant and a linear trend. Figures F.10 and F.11 report results from a shorter sample ending in November 2022, just before the $60-per-barrel price cap on Russian crude. Finally, Figures F.12 and F.13 display IRFs using the simplified sanction intensity index defined in Equation (F.1).

Compared to the baseline results in Figures 14 and 15, the IRFs remain largely unchanged across these alternative specifications.

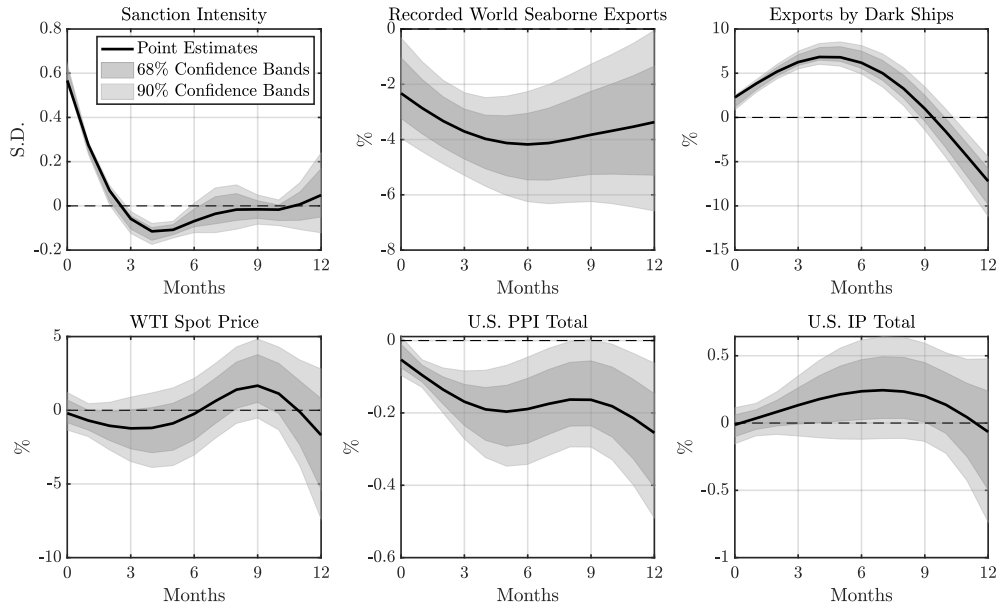


Figure F.6: IRFs to a one-standard-deviation oil sanction intensity shock for the U.S. economy: $L = 4$

Notes. The specification follows that of Figure 14, with the only difference being the inclusion of four lags of the endogenous variables. Black solid lines represent point estimates, and gray-shaded areas denote the 68% and 90% confidence bands.

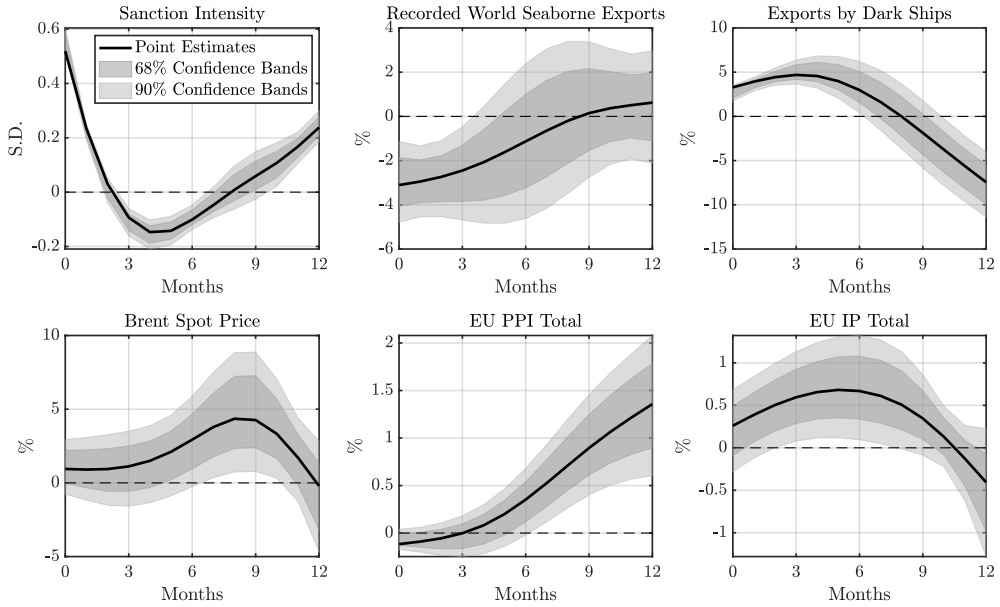


Figure F.7: IRFs to a one-standard-deviation oil sanction intensity shock for the EU economy: $L = 4$

Notes. Apart from incorporating four lags of the endogenous variables, the estimation follows the same specification as in Figure 15. Black solid lines represent point estimates, while gray-shaded areas indicate the 68% and 90% confidence bands.

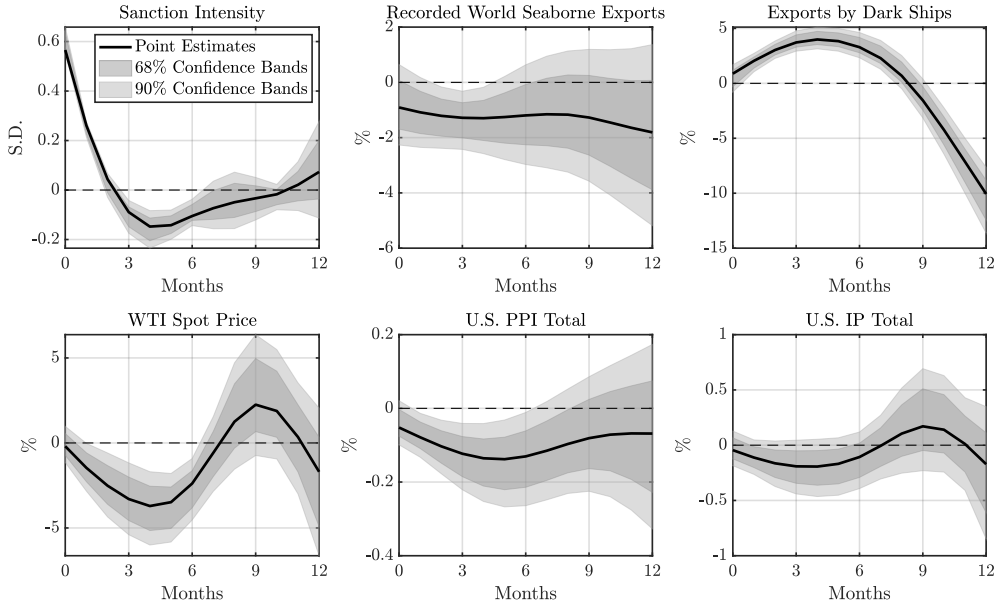


Figure F.8: IRFs to a one-standard-deviation oil sanction intensity shock for the U.S. economy: Linear trend

Notes. The specification is the same as in Figure 14, except for the inclusion of both a constant and a linear trend. Black solid lines represent point estimates, and gray-shaded areas indicate the 68% and 90% confidence bands.

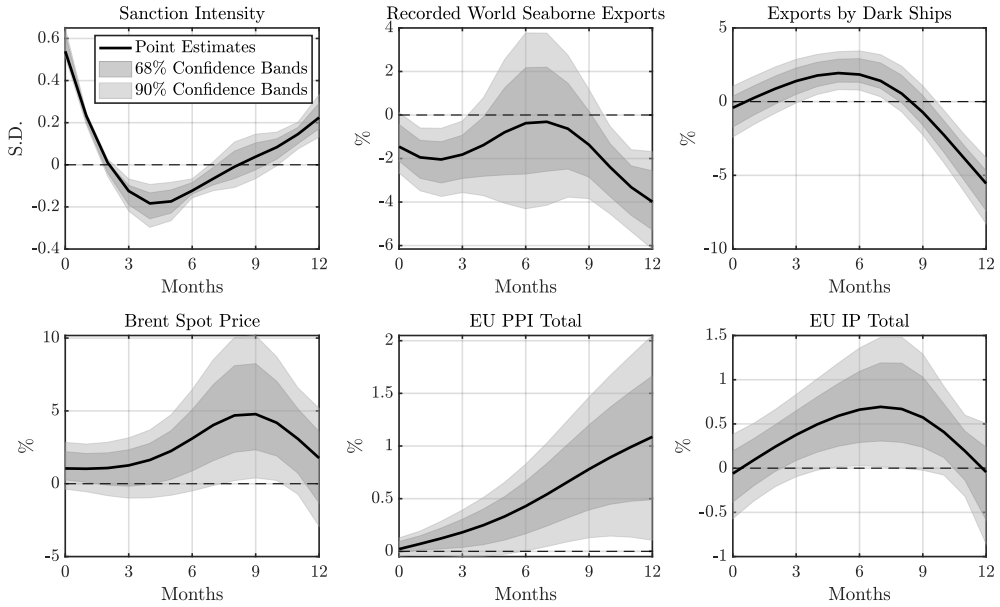


Figure F.9: IRFs to a one-standard-deviation oil sanction intensity shock for the EU economy: Linear trend

Notes. The specification is the same as in Figure 15, except for the inclusion of both a constant and a linear trend. Black solid lines represent point estimates, and gray-shaded areas indicate the 68% and 90% confidence bands.

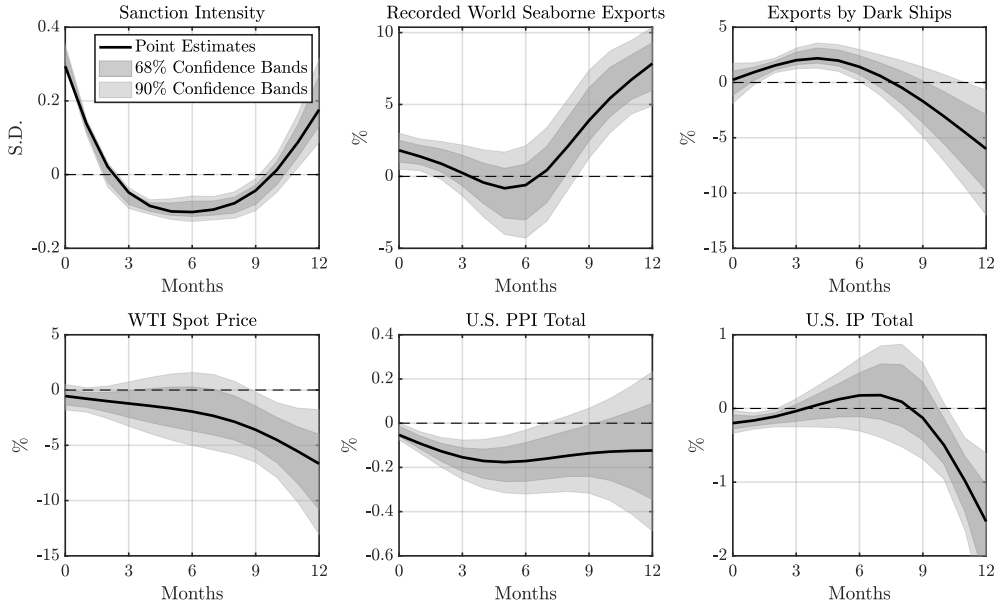


Figure F.10: IRFs to a one-standard-deviation oil sanction intensity shock for the U.S. economy: January 2017–November 2022, before price cap on Russian oil

Notes. The specification is the same as in Figure 14, except that the estimation sample is restricted to the period from January 2017 to November 2022. Black solid lines represent point estimates, and gray-shaded areas indicate the 68% and 90% confidence bands.

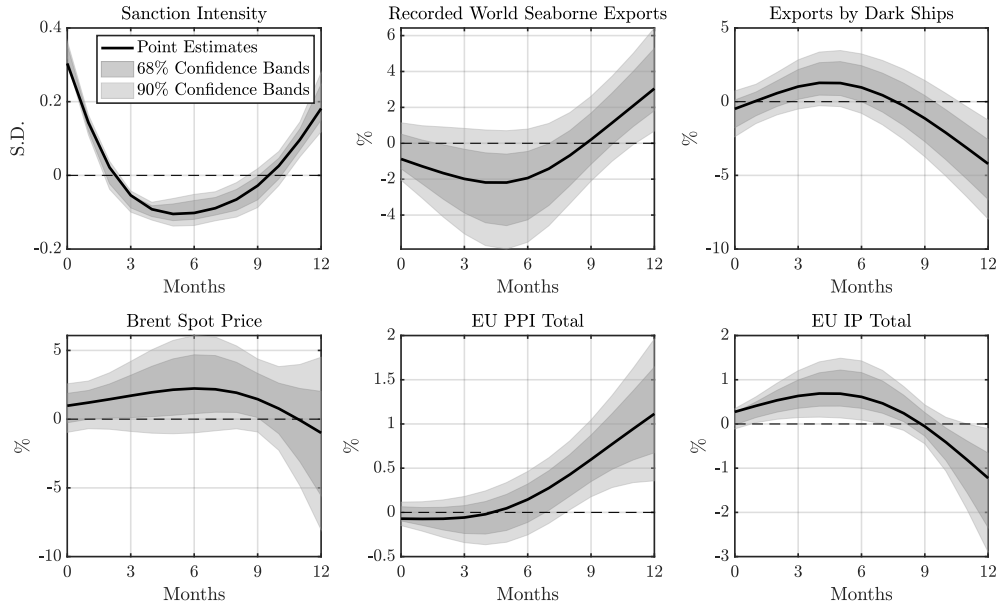


Figure F.11: IRFs to a one-standard-deviation oil sanction intensity shock for the EU economy: January 2017–November 2022, before price cap on Russian oil

Notes. The specification follows that of Figure 15, except that the estimation sample is restricted to the period from January 2017 to November 2022. Black solid lines represent point estimates, and gray-shaded areas indicate the 68% and 90% confidence bands.

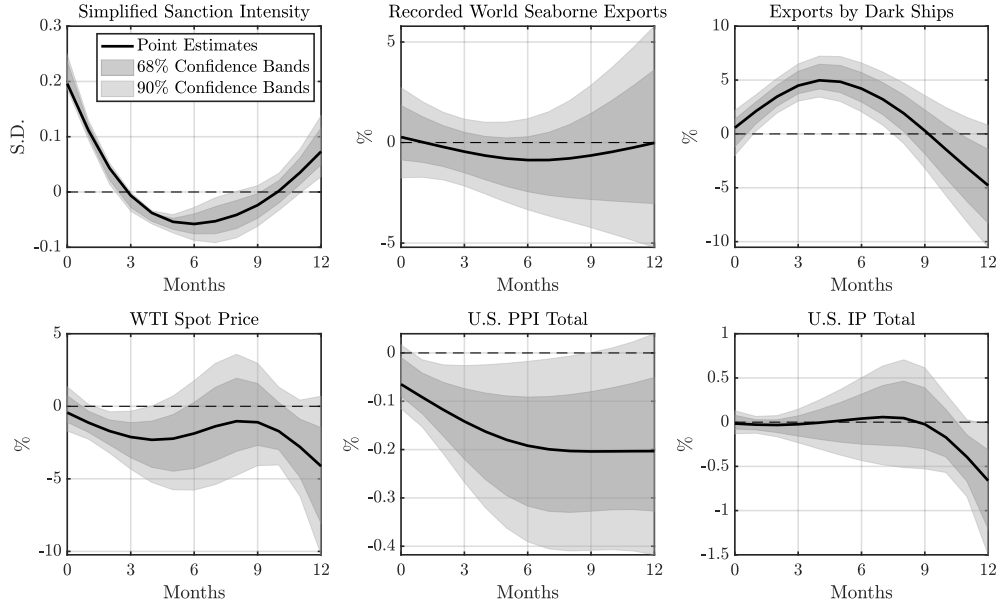


Figure F.12: IRFs to a one-standard-deviation oil sanction intensity shock for the U.S. economy: Simplified sanction intensity index

Notes. The estimation follows the same specification as in Figure 14, except that it incorporates the simplified sanction intensity index defined in Equation (F.1). Black solid lines represent point estimates, while gray-shaded areas indicate the 68% and 90% confidence bands.

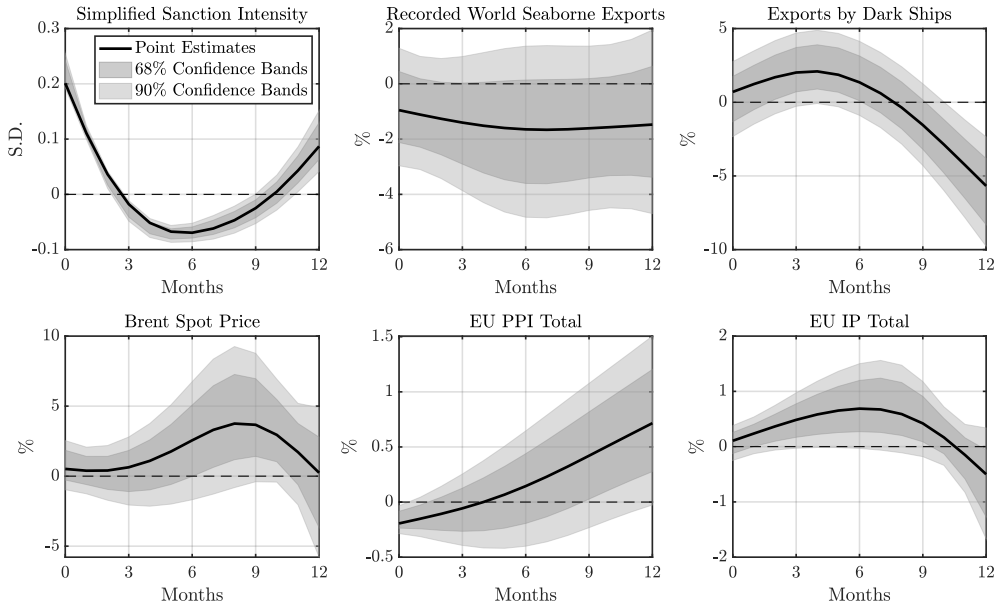


Figure F.13: IRFs to a one-standard-deviation oil sanction intensity shock for the EU economy: Simplified sanction intensity index

Notes. The estimation follows the same specification as in Figure 15, except that it incorporates the simplified sanction intensity index defined in Equation (F.1). Black solid lines represent point estimates, while gray-shaded areas indicate the 68% and 90% confidence bands.

Figures F.14 and F.15 present IRFs to an unexpected oil sanction intensity shock for the U.S. and EU economies, estimated using a Cholesky-ordered SVAR model. The endogenous variables are ordered as follows: the oil sanction intensity index, world seaborne crude oil exports (UN Comtrade), crude oil exports from sanctioned countries transported by dark ships, the WTI/Brent spot price, U.S./EU IP, and U.S./EU PPI.

This ordering assumes that an unexpected oil sanction intensity shock contemporaneously affects all subsequent variables. In contrast, shocks to recorded world seaborne and dark-shipped exports are assumed not to affect the sanction intensity index within the same period.

While the overall dynamics resemble those reported in Figures 14 and 15, some differences emerge. In the U.S., the WTI spot price remains persistently below its pre-shock level, and the initial rise in industrial production fades, turning negative after four months. In the EU, the Brent spot price increases over the first three months following the shock, whereas the PPI response remains subdued throughout the horizon.

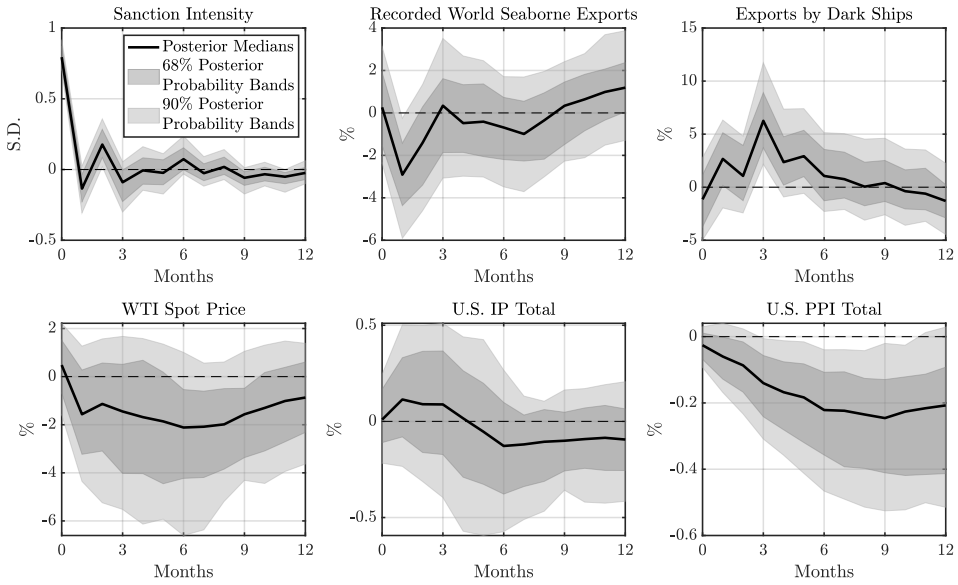


Figure F.14: IRFs to a one-standard-deviation oil sanction intensity shock for the U.S. economy: Cholesky-ordered SVAR

Notes. The IRFs are computed using a Cholesky-ordered SVAR model with three lags. The model is estimated using a Bayesian approach, following Antolín-Díaz and Rubio-Ramírez (2018). The solid line depicts the point-wise posterior medians, while the shaded areas indicate the 68% and 90% point-wise posterior probability bands.

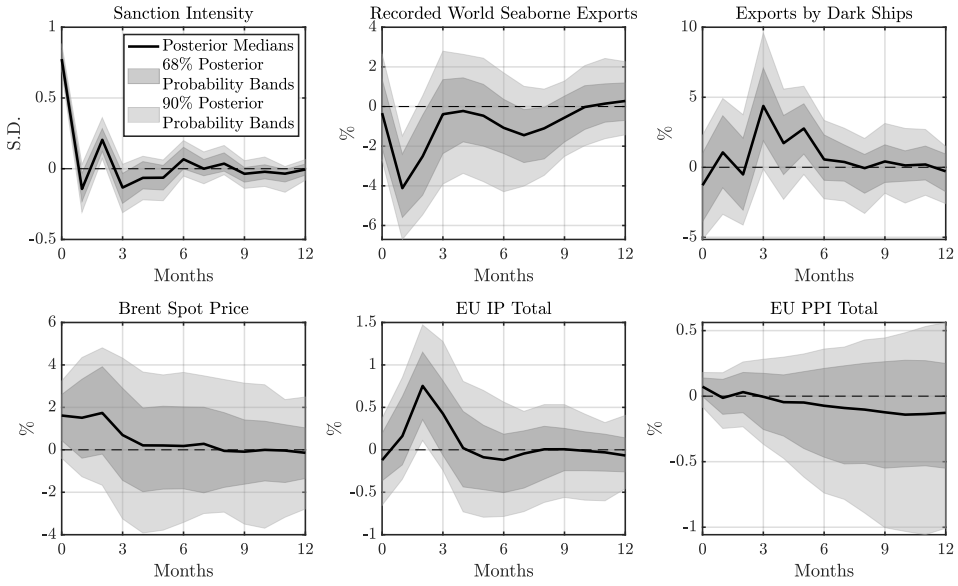


Figure F.15: IRFs to an oil sanction intensity shock for the EU economy: Cholesky-ordered SVAR

Notes. The IRFs are computed using a Cholesky-ordered SVAR model with three lags. The model is estimated using a Bayesian approach, following Antolín-Díaz and Rubio-Ramírez (2018). The solid line depicts the point-wise posterior medians, while the shaded areas indicate the 68% and 90% point-wise posterior probability bands.

F.3. Propagation Channels

To complement Figures 16 and 17 in the main text, Figures F.16 and F.17 present the full IRFs to an unexpected oil sanction intensity shock for the U.S. and EU economies, respectively.

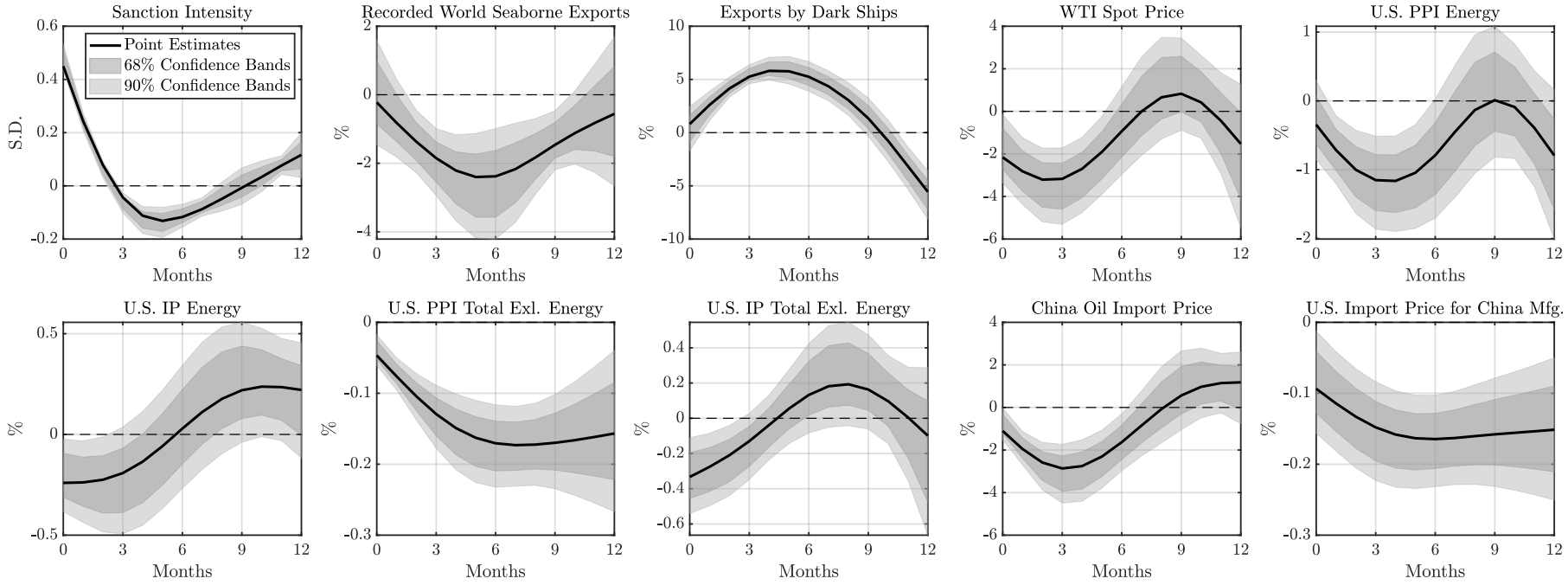


Figure F.16: IRFs to a one-standard-deviation oil sanction intensity shock for the U.S. economy: Propagation channels (full IRFs)

Notes. The estimation specifications follow the LP model outlined in Section 6.1 of the main text, with two modifications: (i) two additional variables —China's crude oil import price and the U.S. import price for manufacturing goods from China, averaged across NAICS sectors 31 to 33— are included; and (ii) the total PPI and IP for the U.S. economy are replaced by the PPI and IP for the energy and non-energy sectors. Black solid lines represent point estimates, while gray-shaded areas indicate the 68% and 90% confidence bands.

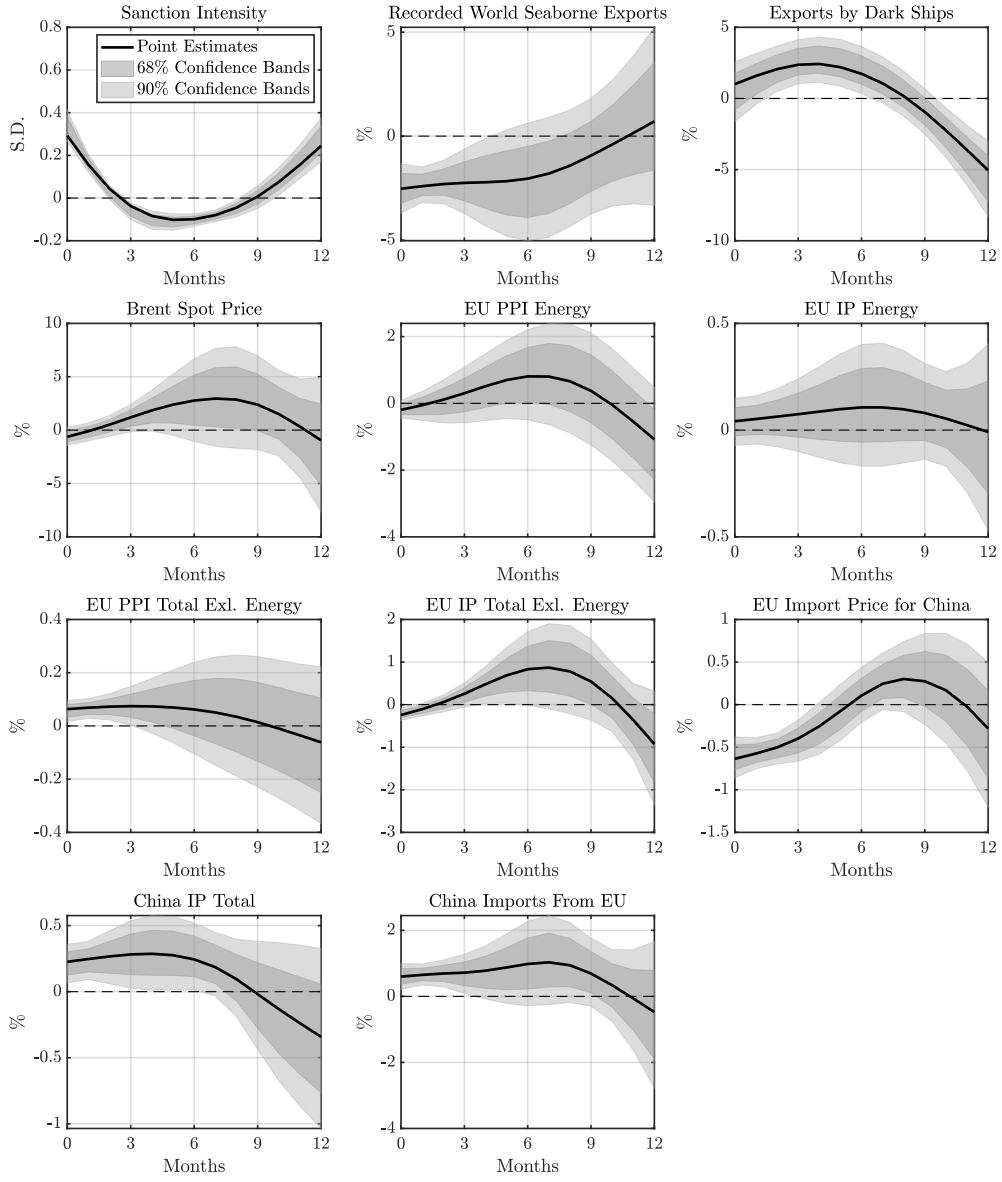


Figure F.17: IRFs to a one-standard-deviation oil sanction intensity shock for the EU economy: Propagation channels (full IRFs)

Notes. The estimation specifications follow the LP model outlined in Section 6.1 of the main text, with two modifications: (i) three additional variables —the EU import price for Chinese goods, China's total IP, and its total import value from the EU— are included; and (ii) the total PPI and IP for the EU economy are replaced by the PPI and IP for the energy and non-energy sectors. Black solid lines represent point estimates, while gray-shaded areas indicate the 68% and 90% confidence bands.

Figure F.18 presents the IRFs to an unexpected oil sanction intensity shock for the U.S. economy, using the same model specification as in Figure 16, except that China's oil import price is replaced with its total PPI. The monthly series for China's total PPI is sourced from the National Bureau of Statistics of China and has been seasonally adjusted.

The substitution has little impact on the results, as China's total PPI shows a consistent decline across all forecast horizons.

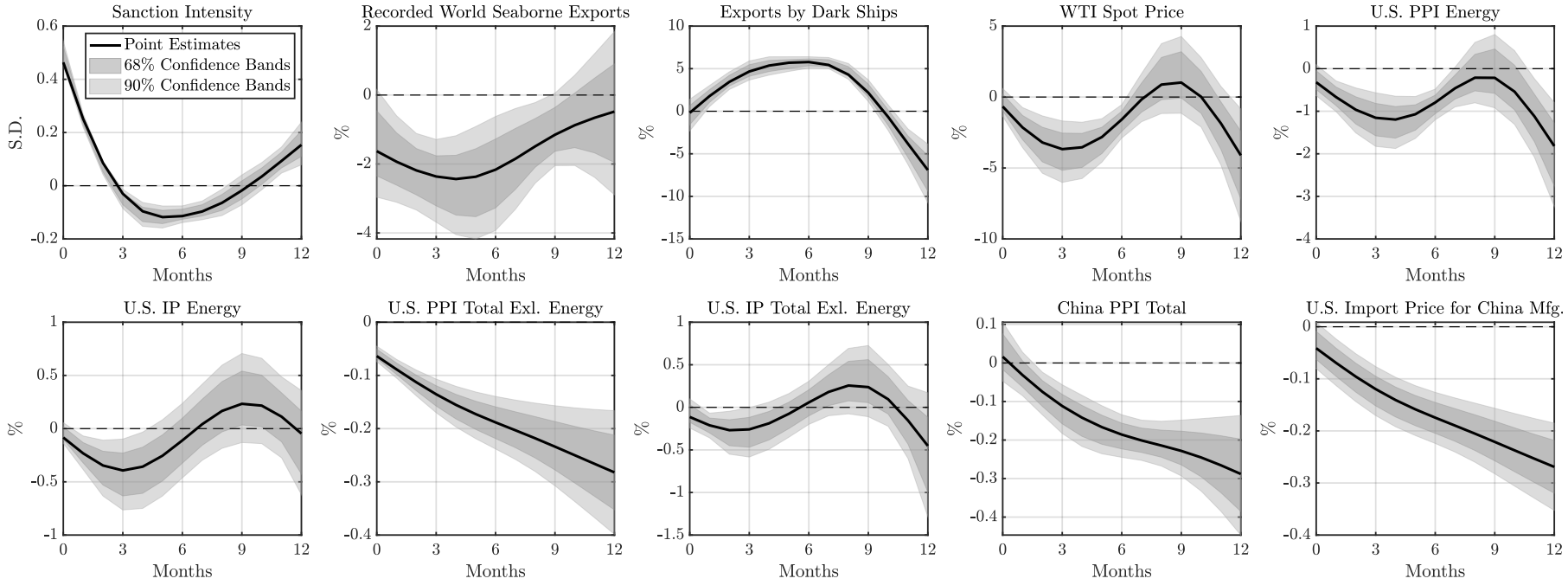


Figure F.18: IRFs to a one-standard-deviation oil sanction intensity shock for the U.S. economy: China's total PPI

Notes. The IRFs are computed using the same LP model specification as in Figure 16, except that China's oil import price is replaced with its total PPI. Black solid lines represent point estimates, while gray-shaded areas indicate the 68% and 90% confidence bands.

Figure F.19 presents the IRFs to an unexpected oil sanction intensity shock for the U.S. economy, using the same model specification as in Figure 16, except that the U.S. import price for manufactured goods from China is replaced with the import price for all Chinese products. The monthly series for the U.S. import price of all Chinese products is sourced directly from FRED (`CHNTOT`) and has been seasonally adjusted. As before, the results appear largely unaffected by this variable substitution.

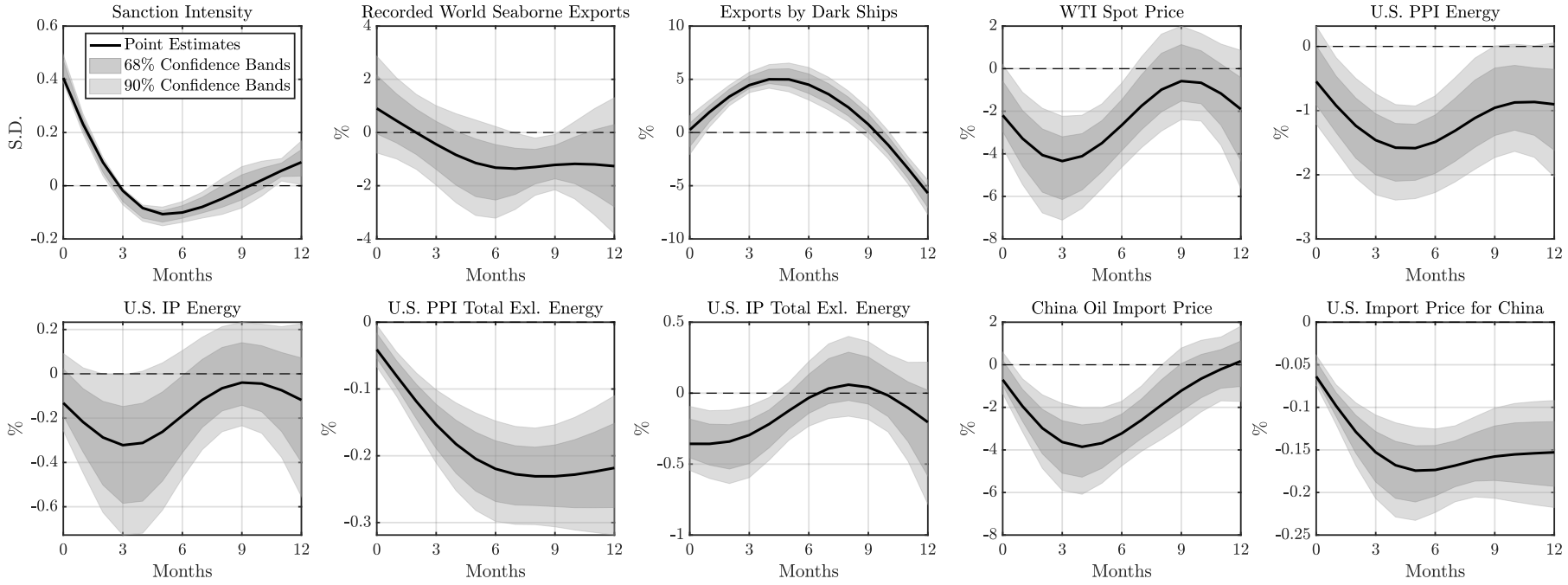


Figure F.19: IRFs to a one-standard-deviation oil sanction intensity shock for the U.S. economy: U.S. import price for China

Notes. The IRFs are computed using the same LP model specification as in Figure 16, except that the U.S. import price for manufactured goods from China is replaced with the import price for all Chinese goods. Black solid lines represent point estimates, while gray-shaded areas indicate the 68% and 90% confidence bands.

Figure F.20 presents the IRFs to an unexpected oil sanction intensity shock for the U.S. economy, estimated using an 11-variable LP model. This model extends the ten-variable specification from Figure 16 by including U.S. crude oil exports. The monthly data on U.S. crude oil exports are obtained from the U.S. Energy Information Administration and have been seasonally adjusted.

The responses of the original ten variables closely mirror those reported in Figure 16. U.S. crude oil exports decline markedly during the first six months following the shock and then partially recover, stabilizing at approximately -0.5%.

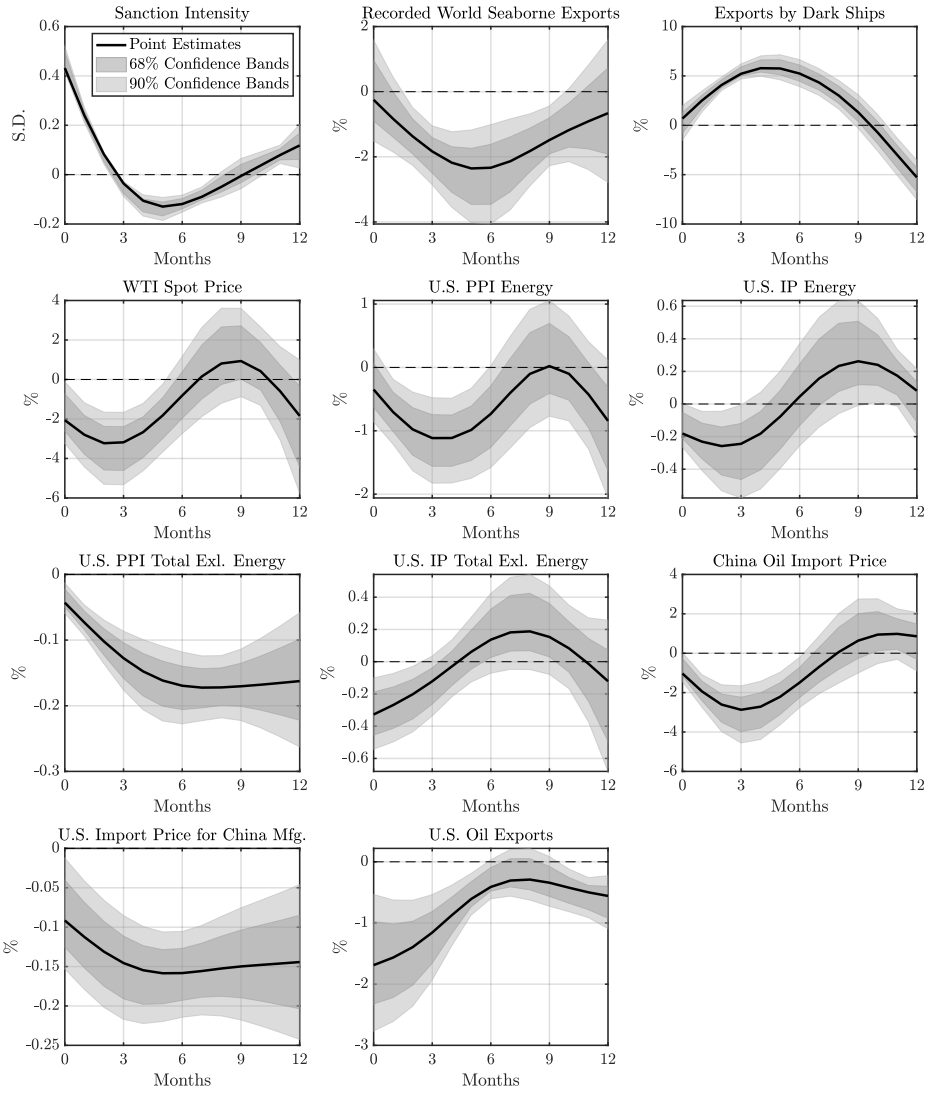


Figure F.20: IRFs to a one-standard-deviation oil sanction intensity shock for the U.S. economy: U.S. oil exports

Notes. The IRFs are computed using an 11-variable LP model, which augments the ten endogenous variables from Figure 16 of the main text with U.S. crude oil exports. Black solid lines represent point estimates, and gray-shaded areas indicate the corresponding 68% and 90% confidence bands.

Figure F.21 compares the IRFs for the U.S. economy estimated with and without two China-related variables —China's oil import price and the U.S. import price for Chinese manufactured goods. In the first three months, the responses of U.S. energy and non-energy IP are closer to the zero-response lines than in Panels 16b and 16d of the main text. This pattern suggests a positive omitted variable bias: lower Chinese import prices may help sustain short-term U.S. production.

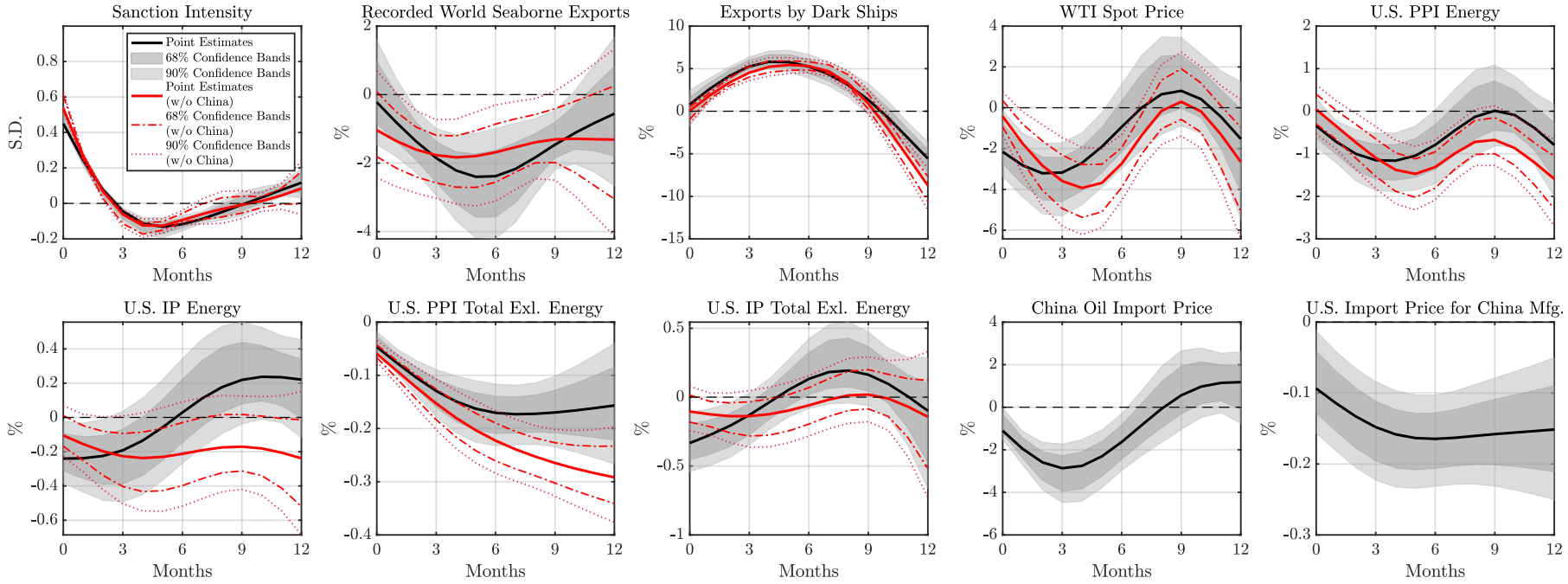


Figure F.21: IRFs to a one-standard-deviation Oil Sanction Intensity Shock for the U.S. economy: With and without China-related variables

Notes. The IRFs are computed using both a 10-variable LP model —as in Figure 16— and a counterfactual 8-variable LP model that excludes the two China-related variables: China's oil import price and the U.S. import price for Chinese manufactured products. Black solid lines represent the responses estimated from the 10-variable model, with gray-shaded areas indicating the 68% and 90% confidence bands. Red solid lines show the responses from the counterfactual 8-variable model, with red dash-dotted and dotted lines denoting the respective confidence bands.

G. Further Details on the Oil Market Model

Data on oil exports. We obtain monthly data on crude oil export volumes from Russia (S) and OPEC (NS) to the EU (E) and China (C), denoted by $Q_{E,S,t}$, $Q_{C,S,t}$, $Q_{E,NS,t}$, and $Q_{C,NS,t}$, covering the period from January 2017 to December 2023.

We compute the total volume exported by each supplier over the sample and normalize it by global oil exports. Let:

$$\begin{aligned}
\overline{Q}_{global} &\equiv 1, \\
\overline{Q}_{k,s} &\equiv \frac{\sum_t Q_{k,s,t}}{\sum_{k\in\{E,C\}}\left[\sum_{s\in\{S,NS\}}\left(\sum_t Q_{k,s,t}\right)\right]}, \\
\overline{Q}_{k} &\equiv \sum_{s\in\{S,NS\}} \overline{Q}_{k,s}, \\
\overline{Q}_{s} &\equiv \sum_{k\in\{E,C\}} \overline{Q}_{k,s}.
\end{aligned}$$

Data on oil prices. We measure the prices of Russian crude oil sold to the EU and China using the monthly capped Urals and ESPO prices, denoted by $P_{E,S,t}$ and $P_{C,S,t}$, respectively.[14] For OPEC crude oil exports to the EU and China, we use the Brent and Dubai benchmarks, denoted by $P_{E,NS,t}$ and $P_{C,NS,t}$, respectively.

Calibration. We normalize all prices (including FOB oil prices $P_{k,s}$, marginal costs Φ_s for both suppliers, and oil prices in both markets P_k) to one.[15]

We calibrate the demand intercepts α_k in Equation (8) of the main text to match $\overline{Q}_k$ and set $\beta_k = 1$ for all markets k. The steady-state share of supplier s' oil exports to market k, $\Omega_{k,s}$, is calibrated to $\overline{Q}_{k,s}/\overline{Q}_s$.

To calibrate the convexity parameter ρ_s in the CES oil supply cost function —which governs the degree of supply reallocation across markets— we estimate the following monthly time-series regression for Russia and OPEC over the period from March 2022 to December 2023:

$$d\ln\left(\frac{Q_{E,s,t}}{Q_{C,s,t}}\right) = \beta_{\rho,s}\, d\ln\left(\frac{P_{E,s,t}}{P_{C,s,t}}\right) + \epsilon_{s,t},$$

[14] The capped Urals crude oil price is based on reported Urals quotes. From December 2022 onward, any price above \$60 is replaced with \$60 to reflect the G7/EU price cap on Russian oil exports.

[15] We assume no sanctions in the steady state, i.e., $\delta_{k,s} = 0$, $\forall k, s$.

where $s \in \{S, NS\}$ and $d\ln(\cdot)$ denotes year-over-year growth. Based on Equation (7) in the main text, we set $\rho_s = 1/\widehat{\beta}_{\rho,s} + 1$, which yields values of 1.3 for Russia and 1.8 for OPEC.

References for Appendices

Adland, R., Cariou, P., and Wolff, F.-C. (2020). Optimal Ship Speed and the Cubic Law Revisited: Empirical Evidence From an Oil Tanker Fleet. *Transportation Research Part E: Logistics and Transportation Review*, 140:101972.

Androjna, A., Pavić, I., Gucma, L., Vidmar, P., and Perkovič, M. (2024). AIS Data Manipulation in the Illicit Global Oil Trade. *Journal of Marine Science and Engineering*, 12(1).

Antolín-Díaz, J. and Rubio-Ramírez, J. F. (2018). Narrative Sign Restrictions for SVARs. *American Economic Review*, 108(10):2802–29.

Ballinger, O. (2024). Automatic Detection of Dark Ship-To-Ship Transfers Using Deep Learning and Satellite Imagery. *arXiv preprint*.

Bernabé, P., Gotlieb, A., Legeard, B., Marijan, D., Sem-Jacobsen, F. O., and Spieker, H. (2024). Detecting Intentional AIS Shutdown in Open Sea Maritime Surveillance Using Self-Supervised Deep Learning. *IEEE Transactions on Intelligent Transportation Systems*, 25(2):1166–1177.

Chupilkin, M., Javorcik, B., Peeva, A., and Plekhanov, A. (2024). Decision to Leave: Economic Sanctions and Intermediated Trade. Working paper, European Bank for Reconstruction and Development.

Hwang, C.-L. and Yoon, K. (1981). *Multiple Attribute Decision Making: Methods and Applications A State-Of-The-Art Survey*. Springer Berlin Heidelberg.

Li, Y., Bai, X., Wang, Q., and Ma, Z. (2022). A Big Data Approach to Cargo Type Prediction and Its Implications for Oil Trade Estimation. *Transportation Research Part E: Logistics and Transportation Review*, 165:102831.

Lloyd, S. (1982). Least Squares Quantization in PCM. *IEEE Transactions on Information Theory*, 28(2):129–137.

Lloyd's List Intelligence (2023). Shifty Shades of Grey: The Different Risk Profiles of the Dark Fleet Explained. Technical report, Lloyd's List Intelligence.

Lloyd's List Intelligence (2024a). Understanding AIS Spoofing: The Case of the Blazers. Seasearcher Advanced Risk & Compliance.

Lloyd's List Intelligence (2024b). Understanding AIS Spoofing: The Case of the Shanaye Queen. Seasearcher Advanced Risk & Compliance.

MacQueen, J. B. (1967). Some Methods for Classification and Analysis of Multivariate Observations. In Cam, L. M. L. and Neyman, J., editors, *Proceedings of the Fifth Berkeley Symposium on Mathematical Statistics and Probability*, volume 1, pages 281–297, Berkeley, CA. University of California Press.

Meade, R. (2023). Euronav Investigating Claims It Unwittingly Stored Sanctioned Iranian Oil. Lloyd's List Intelligence.

Miller, G. (2023). Welcome to the Dark Side: The Rise of Tanker Shipping's 'Shadow Fleet'. FreightWaves.

Paris MoU (2018). Explanatory Note – "White," "Grey" and "Black List". Technical report, Paris Memorandum of Understanding on Port State Control.

Ristic, B., La Scala, B., Morelande, M. R., and Gordon, N. (2008). Statistical Analysis of Motion Patterns in AIS Data: Anomaly Detection and Motion Prediction. In *2008 11th International Conference on Information Fusion*, pages 1–7, Cologne, Germany.

Rodger, M. and Guida, R. (2022). Mapping Dark Shipping Zones Using Multi-Temporal SAR and AIS Data for Maritime Domain Awareness. In *2022 IEEE International Geoscience and Remote Sensing Symposium*, pages 3672–3675, Kuala Lumpur, Malaysia.

Rong, H., Teixeira, A., and Guedes Soares, C. (2024). A Framework for Ship Abnormal Behaviour Detection and Classification Using AIS Data. *Reliability Engineering & System Safety*, 247:110105.

S&P Global Market Intelligence (2023). Russia's Shadow Fleet – Understanding Its Size, Activity and Relationships. Technical report, S&P Global Market Intelligence.

Triebert, C., Migliozzi, B., Cardia, A., Xiao, M., and Botti, D. (2023). Fake Signals and American Insurance: How a Dark Fleet Moves Russian Oil. The New York Times.

U.S. Department of State (2020). Sanctions Advisory for the Maritime Industry, Energy and Metals Sectors, and Related Communities. Technical report, U.S. Department of State, U.S. Department of the Treasury's Office of Foreign Assets Control, and U.S. Coast Guard.

Wijaya, M. (2022). Palau Cancels Sanctioned VLCC Young Yong's Insurance Certificate. Lloyd's List Intelligence.

Yan, Z., Xiao, Y., Cheng, L., Chen, S., Zhou, X., Ruan, X., Li, M., He, R., and Ran, B. (2020). Analysis of Global Marine Oil Trade Based on Automatic Identification System (AIS) Data. *Journal of Transport Geography*, 83:102637.